DYNAMICS OF MOLECULAR COMMUNICATION IN BACTERIA WITHIN MICROFLUIDIC ENVIRONMENTS

A Dissertation
Presented to
The Academic Faculty

by

Caitlin Marie Austin

In Partial Fulfillment
of the Requirements for the Degree
Bioengineering in the
Woodruff School of Mechanical Engineering

Georgia Institute of Technology
December 2016

DYNAMICS OF MOLECULAR COMMUNICATION IN BACTERIA WITHIN MICROFLUIDIC ENVIRONMENTS

Approved by:

Dr. Craig Forest, Advisor
School of Mechanical Engineering
Georgia Institute of Technology

Dr. Mark Styczynski
School of Chemical and Biomolecular Engineering
Georgia Institute of Technology

Dr. Brian Hammer
School of Biological Sciences
Georgia Institute of Technology

Dr. Peter Hesketh
School of Mechanical Engineering
Georgia Institute of Technology

Dr. Faramarz Fekri
School of Electrical and Computer Engineering
Georgia Institute of Technology

Date Approved: October 20, 2016

ACKNOWLEDGMENTS

There are several people who have had a significant impact on my graduate career and I want to thank them. First, my family has always been my most valuable asset due to the encouragement, guidance, and love they provide for me. To my husband for supporting me every step of the way, for guiding me through the overwhelming and stressful days, and for celebrating even the smallest of my accomplishments, your love has strengthened me. To my mother for her determination and hard work she instilled in me through example, and for always having confidence I could succeed. To my father for always encouraging me to be my own person, to stand strong for myself, and to go after any goal I set. Thank you to my younger sister, Brenna, for the endless laughter and time together.

Thank you to the past and present members of the Precision Biosystems Laboratory. To my advisor, Craig Forest, for creating a unique lab space that encourages collaboration and innovation. His drive is infectious and promotes a motivational environment that has allowed me to thrive. His encouragement to take ownership of my project with the freedom to develop my undergraduate has allowed me to develop leadership skills. To my lab mates, I am incredibly thankful. Each of you have provided encouragement, guidance, and friendship. To Melissa Li, for being my go to person for questions, and for being my guide to handling the stress of graduate school. To William Stoy, for critical research collaborations, and support. To Sitara Sankar for unbelievable support, friendship and research collaboration. To Tim Lee, for the ability to always lighten the mood and create positive vibes in the lab. And to the many other lab members who have helped along the way, including Greg Holst, Ilya Kolb, and Chris Phaneuf.

A huge thank you to the amazing team of undergraduate studies who placed a critical role in the success of this work. To Marie Harber, for working tirelessly always with a smile and my original undergrad. To Peter Su, and Lucy Hu, for accomplishing an amazing amount of significant work in such a short summer period. To Jorge Perdomo, David Caro, and Sagar Patel for being the hardest working undergrads who cultivated a true research team. To Will Penniman and Xiebin Gu for jumping in with both feet and exceling in the crunch time at the end.

Thanks also to the many collaborators who contributed to the technical aspects of this work. First to Dr. Brian Hammer, for not only the genetically engineered bacteria expertise, but also for the mentorship, guidance and encouragement throughout this project. To the members of the Hammer Lab, Patrick Bardill, Samit Watve, and Jacob Thomas for genetically engineering the bacteria for this work, and for furthering the biological knowledge of this research team. To the Molecular Nano-Communication Network Team, Dr. Faramarz Fekri, Dr. Raghupathy Sivakumar, Dr. Ian Akylidiz, Arash Einolghozati, Bhuvana Krishnaswamy, and Ozan Bicen for a unique collaboration team that worked together and for expanding my knowledge in new fields.

Finally, to our funding support we thank. To the National Science Foundation (CISE 1110947), National Science Foundation Graduate Fellowship Program, and the National Science Foundation's National Nanotechnology Infrastructure Network (NNIN) Summer Research Experience for Undergraduates program.

TABLE OF CONTENTS

LIST OF TABLES

LIST OF FIGURES

LIST OF SYMBOLS AND ABBREVIATIONS

PDMS	Polydimethylsiloxane
QS	Quorum sensing
GI	Gastrointestinal
GMA	General mass action
GFP	Green fluorescent protein
MoNaCo	Molecular Nano-Communication Networks
V. fischeri	*Vibrio fischeri*
AHL	Acyl homoserine lactone
VI	Virtual instrument
AU	Arbitrary units
SNR	Signal-to-noise ratio
OOK	On-off keying
TEC	Time-elapse communication
TEC-SMART	Smart time elapse communication
SSE	Sum of square errors
DMPAP	2'-dimethoxy-2-phenylacetophenone
MMA	Methyl methacrylate
EDA	Ethylene diacrylate
BuMA	Butyl methacrylate
EDMA	Ethylene dimethacrylate
EGMP	2-(methacryloxy)ethyl phosphate
BAA	N,N'-methylenebis(acrylamide)
DMPA	2,2-dimethoxy-2-phenylacetophenone
DMF	N,N-dimethylformamide
DDC	1-dodecanol
DMSO	Dimethylsulfoxide
DI	Deionized
LC-MS	Liquid chromatography mass spectrometry
MRM	Multiple reaction monitoring

SUMMARY

Biosensors exploiting communication within genetically engineered bacteria are becoming increasingly important for monitoring environmental changes. Recently these sensors have miniaturized towards microfluidics due to the greater control they provide over things such as the population density and dynamic inputs. These genetically engineered bacteria can be used for a wide range of applications from monitoring environmental toxins in water or soil, to studying the complex communication networks in the human digestive system. Although great strides have been made to study a single strain of bacteria in a microfluidic device, there is still a need to be able to study two populations of bacteria communicating with one another.

Currently, there are a variety of mathematical models for predicting how bacteria respond to molecular stimuli in bulk culture, but when applied to microfluidics and to complex time-varying inputs, the shortcomings of these models have become apparent. The effects of microfluidic environments such as low oxygen concentration, strongly affect rate constants for gene expression not accounted for in previous models.

In this work we developed a microfluidic platform capable of housing two bacteria populations to study the bacterial communication with dynamic control of inputs, long-term experimentation, and no cross contamination. We also developed a mathematical model that accurately predicts the biological response of the bacteria populations communicating in the microfluidic environment. This work can serve as a valuable tool in understanding genetically engineered bacteria and improving biosensor design capabilities, opening the door for sensors that adapt to environmental dynamics and communicate with each other.

CHAPTER I

INTRODUCTION

Using synthetic biology to genetically engineer bacteria that are responsive to molecular cues has enabled a variety of sensing applications. For example, engineered bacteria have been used as toxicology biosensors to detect the presence of pollutants including metals [1] and arsenic pollution [2], and to monitor membrane biofouling [3]. These sensors are typically housed in flasks, wells, or agar plates [1-3], but miniaturization is becoming increasingly common and important because it enables one to minimize reagents and to have greater control over stimuli, population size, density, flow rate, temperature, and other factors. As noted by van der Meer, and Belkin, "owing to their small size, bacterial bioreporter cells are highly suitable for incorporation into microengineered platforms, transforming such devices into whole-cell biosensors [4]." Additionally polydimethylsiloxane (PDMS) is emerging as the material of choice for the design and fabrication of three-dimensional microfluidic networks of bacterial-cell arrays [4]. This shift to bacteria biosensors in microengineered platforms comes with many challenges, such as impact on bacterial communication, ability to house stable bacteria populations for an extended amount of time, and the ability to monitor bacterial communication. In this work, we address these concerns by examining bacterial communication in PDMS microfluidic devices capable of housing either one or two bacteria types independently.

1.1 Quorum Sensing

Quorum sensing (QS) is a naturally occurring communication mechanism found in bacteria populations that regulates gene expression in response changing local concentrations of chemical signaling molecule (autoinducers). These concentration changes are directly tied to changes in population density. Since individual bacteria cells can only produce a small amount of autoinducers, the collective bacterial population density must increase to raise the autoinducer concentration to a detectible level. Once the population density and the autoinducer concentration reach a threshold level, then gene expression can proceed. QS is a key survival tool that enables bacteria to coordinate their behavior in response to unfavorable environmental conditions, such as lack of nutrients, toxic compounds, and a competitive species. Bacteria use the QS communication to regulate numerous physiological activities such as symbiosis, virulence, competence, conjugation, antibiotic production, motility, sporulation, and biofilm formation [5].

Quorum sensing was first observed in two luminous marine bacterial species, *Vibrio fischeri* and *Vibrio harveyi* [6]. It was found that the bacteria light emission only occurred at high cell population density and high secreted autoinducer concentration. *Vibrio fischeri* has a symbiotic relationship inside of the Hawaiian bobtailed squid. The squid is at risk from predators below, that would normally be able to spot them easily due to the shadow the squid produces from the light above from the moon at night. The bacteria collect in a light organ and emit light that allow the squid to eliminate their shadow by counter illumination and blend in the light coming from above. This makes it much more difficult for predators to see the squid. In turn the squid provides the *V. fischeri* with a nutrient-rich environment to thrive in.

As *V.fischeri* replicates in the light organ, each continually produce auto inducers to a critical level that collects in the microenvironment of the organ. As the autoinducer concentration increases, it signals to the bacteria that they are in the light organ verses the open ocean, and leads to them activating the cascade that results in the emission of light [7]. When the sun rises, it signals to the squid to rid itself of 95% of the bacteria, and the remaining bacteria begin the process of building the population and autoinducer concentration again.

1.2 Genetically Engineered Bacteria

The natural quorum sensing communication methods can be adapted and engineered for specific purposes. To do this a desired DNA sequence that codes for a particular action, such as protein production, is integrated in the bacteria cell via a plasmid. Plasmids are small self-replicating circular sequences of DNA that occur naturally in bacteria. The plasmid is a vessel to ensure the survival and replication of the desired DNA sequence.

Plasmids are composed of several sections, but there are three main areas that make them ideal for genetically engineering bacteria. To maintain the plasmid number in the bacteria population, the plasmid contains an origin of replication, a section of the DNA, that ensures the plasmid is replicated by the bacteria. Bacteria prefer not to keep unnecessary plasmids because it is energetically taxing, but one method to ensure the bacteria preferentially keep the desired plasmid is to make it necessary for the bacteria to survive their environment. Some bacteria naturally are antibiotic resilient, and this naturally ability makes plasmid selection possible. An antibiotic resistance marker can be

integrated into the plasmid to ensure the bacteria will preferentially keep the plasmid when they are placed in an environment containing that same antibiotic. Finally, a promoter sequence on the plasmid allows for gene expression that can lead to several outcomes via the construction, such as light production, biofilm formation, or protein production.

Figure 1 illustrates the general process for integrating a desired strain of DNA into a plasmid. Restriction enzymes cut the DNA sequence and the plasmid. This cutting leave sticky ends of the DNA and plasmid exposed. These ends can then be joined using DNA ligase, which closes the circular plasmid with the integrated DNA sequence.

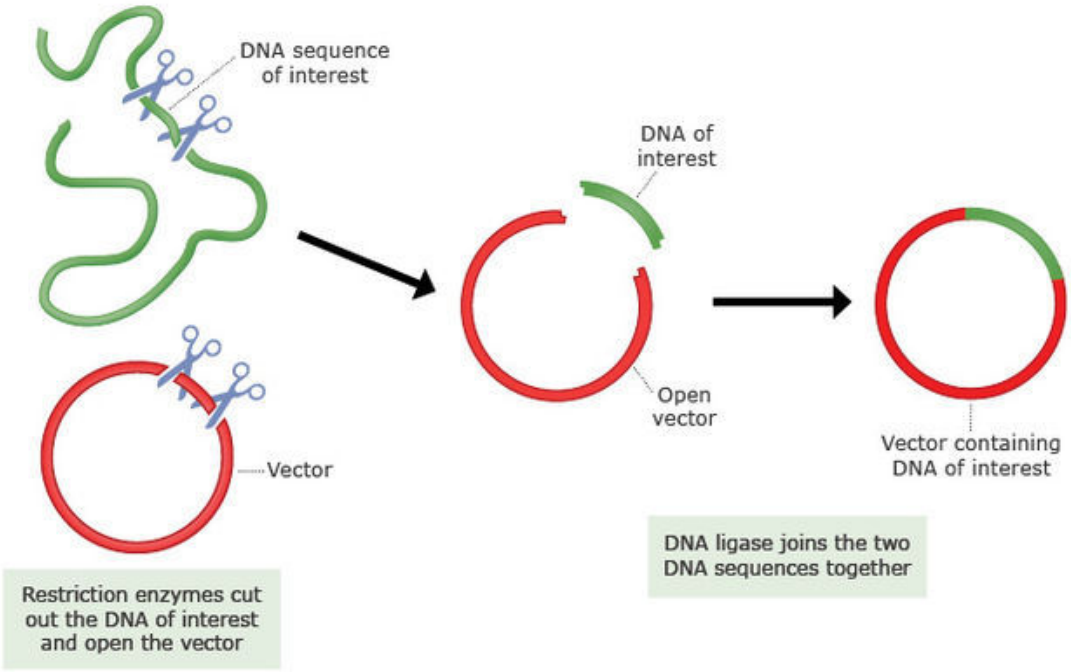

Figure 1: To clone a stretch of DNA (such as a gene) into a vector, restriction enzymes are used to cut out the DNA of interest and to open up the vector. The DNA is added to the vector by mixing the two together in the presence of the enzyme DNA ligase. Copyright University of Waikato.

Now with a complete plasmid, the process of integrating it into a cell can begin. Figure 2 demonstrates the general process for inserting the plasmid vector into the bacteria cell. The bacteria are either rapidly heated for a short period of time, or electrically shocked. This rapid change with either method causes the bacteria to have small pores that open briefly. The plasmid can the pass through the bacterial membrane and enter the cell. After the initial shock, the pores close and the cell resumes its previous state. The cell containing the plasmid is now free to replicate. The plasmid is passed on to daughter cells the same as the bacteria's DNA, due to the origin of replication. The bacteria are then cultured in a media containing the specific antibiotic the plasmid codes for to ensure a uniform population containing the correct plasmid.

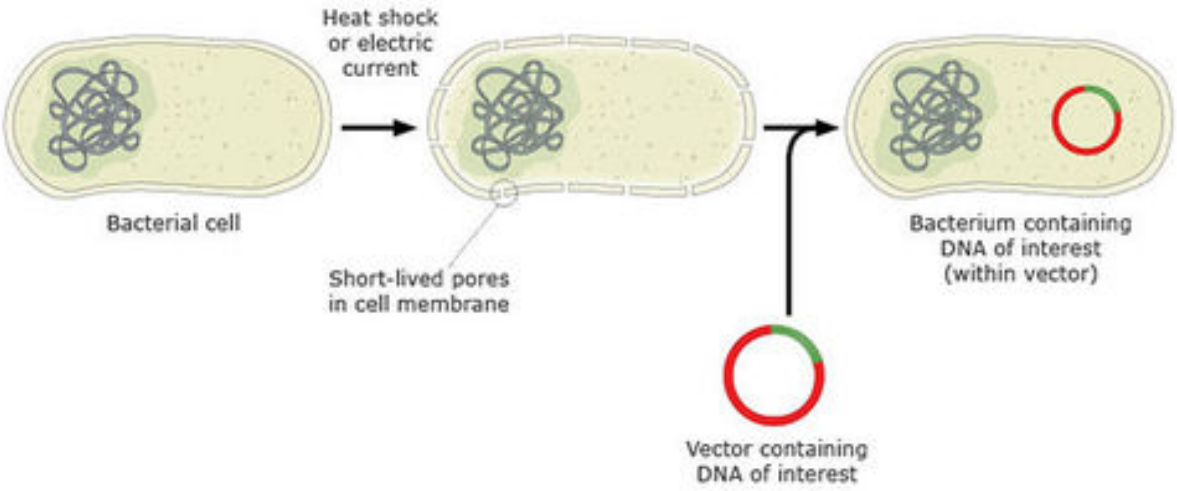

Figure 2: To introduce a cloning vector into bacteria, scientists cause pores to form for a short time in the bacterial cell membrane. The vector enters through the pores before they close. Copyright University of Waikato.

1.3 Bacterial Biosensors

Generally speaking, a bacterial biosensor is a device that combines a sensing bacteria, which produces a signal output proportional to the local analyte concentration, with an output detecting method. Bacteria are ideal sensors due to their ability to detect a diverse range of chemicals, capacity to survive in a wide range of temperatures and pH, and the ability to genetically engineer them to respond in a specific manor [8]

To understand and engineer bacteria for sensor applications, several groups have examined the response of engineered bacteria to stimuli, either in bulk culture or in a microfluidic environment [4]. Whitaker et al. [9] showed the effect of population density on the ability of bacteria to respond in microliter-scale volume wells. Further, the effects of flow on reporter bacteria have been examined in a microfluidic device [10]. Delivering a chemical stimulus to engineered bacteria in a microfluidic environment while monitoring fluorescent response, was done previously by Groisman et al. [11]. These studies provide a solid foundation for behavior of bacteria biosensors, which can be useful for application based sensors in the future. Although there are numerous applications for bacterial biosensors, we will look at two more relevant applications in the next sections.

1.3.1 Environmental Applications

Bacteria biosensors are advantageous for onsite environmental monitoring of water and soil, due to the low cost, sensitive detection limits, and reliable. Conventional methods for environmental monitoring are incredible accurate with low detection limits, but they require the sample to be collected and tested off sight in a facility. Additionally, the test requires highly trained personnel, extensive time to complete, and is very costly [12].

Bacteria biosensors can work with traditional methods to reduce overall costs and testing time. Onsite bacteria biosensors can be used as a method to screen a large number of samples and narrow down to only a few that need further off site testing, which would reduce the testing burden [13].

There are a wide range of bacteria biosensors being developed predominately for lab settings, with very few being developed commercially [14]. This is mainly due to extensive regulations surrounding environmental testing, but as biosensors become more reliable and accurate, this could change in the near future. The array of substances the bacteria can detect ranges from metal toxicity, benzene, toluene, phenol, and many more. For most studies, a single bacteria strain is used to detect a single component in the environment. If multiple components are of interest, then a separate bacteria strain is developed for each, and each bacteria population needs to be monitored over time. This can be seen in works like Charrier et al. with metal detection [1]. Furthermore, the output or response of the bacteria strains are often fluorescence, and can be difficult to discern from the noise of the system when analyte concentrations are extremely low.

These two issues, low signal to noise and multiple bacteria population monitoring, can be assisted by integrating a secondary bacteria population and utilizing true bacterial communication. One of the ways the issue of low signal to noise can be addressed is through amplification of the signal. Transmitter bacteria can be engineered to receive the low analyte concentration, and then produce a secondary chemical signal at a much higher concentration. This signal could then be transmitted to receiver bacteria, who would in turn produce an output, such as green fluorescent protein, that could be monitored. For the issue of multiple bacteria population monitoring, a secondary bacteria population can be used

again. With multiple transmitter bacteria populations each monitoring a specific analyte, a single receiver bacteria population can collect information from all transmitters and relay a single signal containing all the analyte readings. In order for these systems to be developed, fundamental studies of how bacteria population communicate, and how they can be contained in sustainable systems need to be conducted.

1.3.2 Health Applications

The human gastrointestinal (GI) tract maintains a large and diverse microbiome that plays a vital role in maintaining human health [15] . Gut microbiota are involved in essential processes including immune system development, nutrient synthesis, epithelial renewal, and antimicrobial secretion [16]. Dysregulation of GI tract bacterial populations has detrimental inflammatory and metabolic effects, leading to cardiovascular, neurodegenerative, and autoimmune disorders [17]. Although great advancements have been made in mapping the genetic diversity of this microbiome, we still lack a fundamental, scientific understanding of how this complex community of over 1000 bacterial species and 100 trillion individual cells in the human GI tract is able to maintain homeostasis within a living organism [18].

Current hypotheses suggest that GI tract bacterial species survey their microbiome and regulate their symbiotic relationships in response to stimuli such as pH, temperature, and molecular signals [5]. While the vast complexity of these species and stimuli is overwhelming, isolating and genetically engineering a few dominant species within a controllable, engineered environment (e.g., a microfluidic device) to monitor and perturb their molecular signals can yield fundamental insights on the network dynamics within the

human gut. Beyond elucidating the fundamental mechanisms in these physiological systems, understanding these communication signals could enable us to modulate, regulate, and even accelerate communication both for human health and engineered biosensors.

Advancements in microfluidic device fabrication could lead to the ability to take a subset of the vast GI tract microbiome and enable a fundamental understanding of the intercellular signaling between these bacterial populations (See Figure 3). This knowledge would be valuable to understanding how the symbiotic relationship between key GI tract bacterial species reaches stability or is disrupted. After understanding, fundamentally, the symbiosis of the GI tract bacterial subset, a synthetic bacterial modulator can be genetically engineered to disrupt the stability of the system (See Figure 4). This is advantageous because it is known that some bacterial strains are incredibly harmful to human health. Being able to regulate the population size or chemical output of a particular, harmful, bacterial species by manipulating its communication network to our advantage can change the balance of the microbiome. Ultimately, this can lead to personalized treatment for individuals suffering from GI tract disorders.

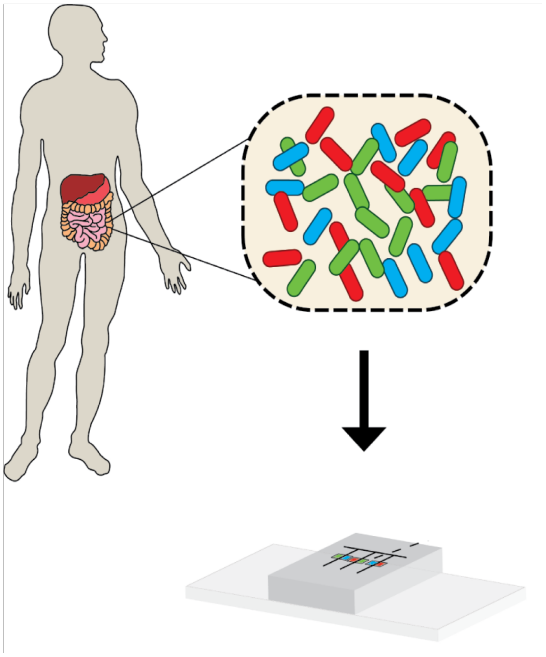

Figure 3: The gastrointestinal track microbiome is incredibly complicated, but to begin understanding this complex network, a small key subset could be studied using the advantages of microfluidics

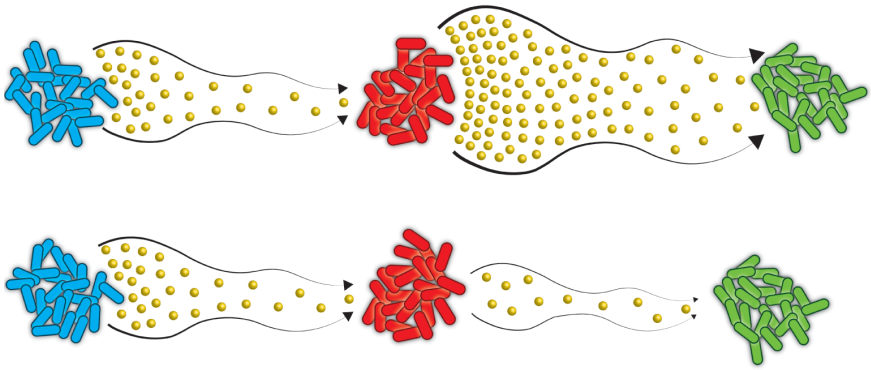

Figure 4: An intermediary bacteria population can act as a transmitter (red) and perturb the original molecular signals before the signal reaches the receiver bacteria (green).

1.4 Microfluidics

Microfluidics provide unique experimental conditions that make them ideal for housing bacteria populations for sensors. They provide a low cost, small volume environment that allows precise control over experimental conditions such as flow rates,

temperature nutrient levels, chemical stimulus delivery and removal, and ease of monitoring. In microfluidics, the small feature sizes combined with the low flow rates leads to low Reynolds number. This means that the viscous forces rather than the inertial forces dominate flow resulting in laminar flow. One outcome of this is no active mixing, and mixing only occurs through gradual diffusion.

Microfluidic environments affect bacterial populations most importantly by limiting molecular distribution to diffusion. Under shear stresses prevalent in microfluidic environments with constant flow, biofilm formation is increased relative to wells or flasks with low shear stress flow or no flow [19]. Additionally *Escherichia coli*, or *E.coli*, commonly used for genetically engineered sensors, increase biofilm production in stressful environments [20] (i.e,. low oxygen). Biofilm material slows diffusion of small molecules [21-23] such as oxygen and AHL. Polydimethyl siloxane (PDMS), a silicone elastomer often used for manufacturing microfluidic biosensors, is permeable to oxygen, yet the oxygen concentration in a PDMS microfluidic biosensor can be considered diffusion limited, in contrast with open wells or flasks [24]. The concentration of oxygen in a PDMS microfluidic biosensor is difficult to predict, but it is influenced by geometry, especially thickness to the external atmosphere, and the concentration of silicone elastomer to curing agent, which controls stiffness. Ultimately, oxygen concentration to the bacterial populations is influenced by biofilm, PDMS, atmospheric concentration, and oxygen dissolved in media. The expression of over 200 genes in *E.coli* can be affected by oxygen concentration [25].

Since the microfluidic environment can affect bacteria biosensors and their communication, there is still a great need to study these impacts to further develop bacteria

biosensors. If we can better understand how the communication changes, the detection limitations and the reliability of these test can improve making commercial applications more possible.

1.5 Modeling Bacterial Communication

A variety of models for chemical transduction that apply to genetically engineered bacteria sensors have been posed that rely on a combination of the Hill equation [26], Michaelis-Menten equation [27], and general mass action (GMA) equations [28]. The Hill equation quantifies the degree of cooperativity of the binding of a ligand (e.g., N-Acyl homoserine lactone, or AHL) to a receptor (e.g., LuxR). In particular, the Hill coefficient in the Hill equation describes the fraction of the receptor saturated by ligand as a function of the ligand concentration. n. The Michaelis-Menten equation is one of the best known models of enzyme kinetics that relates reaction velocity to substrate concentration for a system where a substrate binds reversibly to an enzyme, forming a complex. GMA equations describe the dynamics of chemical species arising from reactions with kinetic rates. The rate of a chemical reaction is directly proportional to the molecular concentrations of the reacting species. Thus a series of mass balances consisting of first-order differential equations can capture the dynamics between several chemical species that ultimately activate production of fluorescence (e.g., green fluorescent protein, or GFP).

Leveau and Lindow [29] made great strides towards modeling bacteria response by considering the activity of a promoter sequence as well as GFP maturation time and GFP degradation using such methods as Michaelis-Menten and a system of ordinary differential equations similar to GMA. This model has been utilized by many [30, 31] for non-

microfluidic environments. Since Leveau and Lindow's work, numerous attempts have been made to create a simplified model for reporter bacteria utilizing ordinary differential equations, the Hill equation, or Michaelis-Menten equation. Previously, a series of ordinary differential equations was derived for the quorum sensing signaling pathway in *Vibrio fischeri,* or *V. fischeri.* [32]. Michaelis-Menten has been used to model the quorum sensing regulatory system of the *Aeromonas hydrophila* [31]. Another group looked to characterize a promoter with a different number of DNA copies; with induction curves fitted with the Hill equation [30]. The use of this model is challenging because the necessary Hill coefficient varies widely between reports [30, 33], depends on specifics of the experimental system, and different forms of the Hill equation are often used as well. Both works were done in non-microfluidic settings.

In a previous study, the response of reporter bacteria to AHL was examined in microfluidic channels under flow and no-flow (quasi-static) conditions [10]. The Hill equation was used to predict the change in fluorescence over time using the input AHL concentration. Although the model included factors such as GFP degradation, the authors noted that "influences of a reduced oxygen concentration due to respiration, which might affect both the maturation of GFP and the cell physiology, were assumed to be negligible." This assumption, together with the over simplification of combining several chemical species and processes into a single equation, is limiting. In fact, the microfluidic environment, with time-varying inputs, exacerbates some of the shortcomings not only of the simplified models, but even the more encompassing and general Leveau and Lindow model. This can lead to a poor fit between model and experimental data in microfluidic biological sensor literature [10].

1.6 Bacterial Communication on Chip

These conditions in the microfluidic environment become increasingly more challenging when attempting to examine communication between two separate populations of bacteria. To do this, a microfluidic device must be able to house two separate populations of bacteria in the same device; meaning a transmitter population and a receiver population would be physically separated, but would still allow diffusion of small molecules between the populations. Additionally, careful consideration must be made with the design such as minimizing clogging due to excesses bacteria growth, duration of experiments, and the amount of small molecule to reach the receiver population. Communication between two bacterial populations over time has been examined through means of a micro-ratchet structure [34], microchambers [35], and chitosan membrane [36, 37].

Although the micro-ratchet structure [34] was able to house two separate populations of bacteria on chip, their experiments were limited to 8 hours due to contamination between populations in their design, seen in Figure 5. The microchambers shown in Figure 6, [35], where able to successfully keep the two population separate without contamination, but the chambers were very large, sealed off, and had no flow. This does not allow for dynamic experimentation with control of stimulants added or removed, population control, fresh nutrients, and removal of excess bacteria. The work done by Luo et al. [36, 37], made great strides in housing two populations of bacteria on the same microfluidic device. They housed bacteria in an alginate gel and separated them using chitosan membrane shown in Figure 7. They were able to have fluid flow over the bacteria, but were extremely limited in the flow rate. Additionally, the experiments were limited to 15 hours, after which the bacteria out grew the alginate gel and cross-contaminated the

populations, and clogged the device. The alginate gel used to mock the biofilm could potentially have negative effects on the bacterial growth and communication.

Since these are the only attempts to our knowledge thus far to have a two-node system in a microfluidic device, we look to be the first to dynamically control the inputs, allow long-term experimentation lasting two or more days, no cross contamination, two-node microfluidic system to examine bacterial communication.

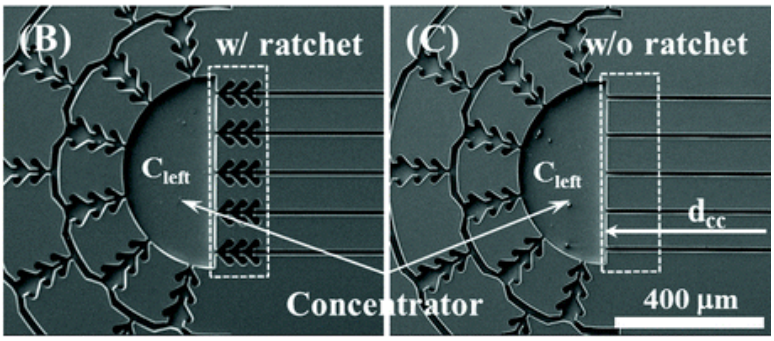

Figure 5: Microfluidic device with ratchet design to reduce contamination between 2 bacterial populations. Reproduced from Park 2012.

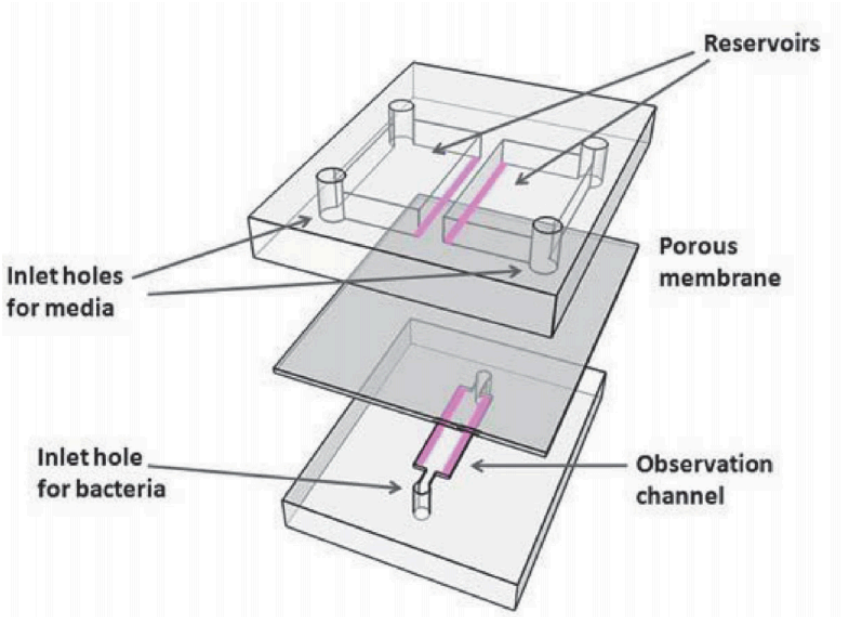

Figure 6: Microchambers on the mm scale were used to house two separated populations of bacteria while allowing diffusion of small molecules through the porous membrane. Reproduced from Nagy 2014.

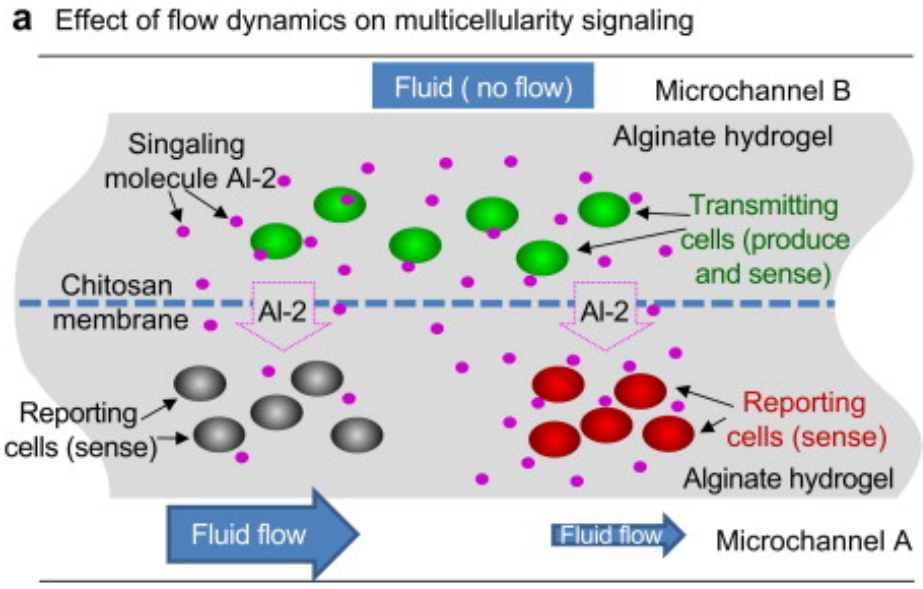

Figure 7: Alginate hydrogel house bacteria while the chitosan membrane separates the 2 populations while allowing diffusion. Reproduced from Luo 2012

1.7 Thesis Outline

This work has four primary aims:

- **Aim 1:** Design, fabricate, and test a microfluidic system to enable stimulation and measurement of discrete populations of bacteria.
- **Aim 2:** Model and validate receiver bacterial gene expression in microfluidic environments.
- **Aim 3:** Design, fabricate, and test a two-node microfluidic system to house both sender and receiver bacteria population
- **Aim 4**: Stimulation and measurement of communication between transmitter and receiver bacteria

This thesis outlines the design, fabrication, testing, and application of microfluidic systems that enable the stimulation and measurement of communication between the populations. Traditional network and communication methods are examined and tested within bacterial populations, and the fundamental limitations of the bacterial communication were explored. Our efforts on this project are in collaboration with four additional laboratories under the NSF funded project Molecular Nano-Communication Networks (MoNaCo). This collaboration spans from biology, mechanical engineering, electrical and computer engineering, and communications.

Chapter II

GENETICALLY ENGINEERED BACTERIA

This chapter describes the methods and construction of bacteria *E. coli* strains used to study bacterial communication. In collaboration with Dr. Brian Hammer's Lab, receiver and transmitter bacteria constructions were developed and tested. The transmitters receive a primary chemical stimulus, produce a secondary chemical stimulus, which then in turn causes them to produce green fluorescent protein. The receivers accept the secondary chemical stimulus and respond by producing green florescent protein.

2.1 Genetically Engineered Receiver *E. coli* Bacteria

Working with Dr. Brian Hammer's lab and their expertise in genetic engineering of bacteria, we set out to establish an experimental system for testing the foundations of molecular based communication in bacteria. To do this we utilized a marine symbiotic bacterium *Vibrio fischeri* (*V. fischeri*) that possesses a quorum sensing system called the LuxIR circuit. In standard laboratory conditions, the LuxIR circuit causes *V. fischeri* to generate light when a culture reaches an optical density 0.4 at 600 nM [38]. In the native system, the LuxI enzyme catalyzes the generation of a signaling molecule, Acyl homoserine lactone (AHL). Specifically, N-(3-oxohexanoyl) homoserine lactone, which is a homoserine lactone with a six-carbon acyl group (hexanoyl) attached to it, is the signaling molecule. The generic name for a family of compounds that are homoserine lactones with acyl groups of varying chain lengths is AHL.

This AHL diffuses freely into and out of the bacterial cell. In the bacterial cell,

AHL binds with a second component, the LuxR receptor. LuxR, in complex with AHL, binds specific DNA sequences and activates transcription of genes that are responsible for light production. In the native organism each individual cell serves as both a transmitter and receiver of signal. However, we ectopically expressed part of the LuxIR circuit in the model bacterial organism *E. coli* to engineer cells that only behave as receivers of signals. Specifically, we introduced into *E. coli* a plasmid that constitutively produced the LuxR receptor protein.

Standard microbiological techniques were used in the culturing of E. coli. All experiments were performed in 2xYT broth [39]. *E. coli* strain DH5α was used for all cloning. Receiver bacteria were derived from the fully sequenced K-12 strain MG1655 [40]. To generate the receiver plasmid, Biobrick BBa T9002 (partsregistry.org) was modified using PCR based methods to append a ssrA-degradation tag (ANDENYALAA) to the C-terminus of green fluorescent protein (GFP) [41]. The resulting plasmid was transformed into MG1655 to create the receiver bacteria. The resulting strain exhibits fluorescence upon the receipt of a specific signal molecule AHL, and is depicted schematically in Figure 8 (a). When AHL is added to the fluidic platform, it enters the receiver *E. coli* cells, LuxR complexes with AHL and then binds to DNA sequences that recruits RNA polymerase to the P_{Lux} promoter to induce transcription of an unstable variant of GFP (Figure 8(a)). A constitutive promoter (P_{on}) that is always on drives expression of the *luxR* gene that codes for the AHL receptor, LuxR. When the AHL signal reaches the receiver cells, it diffuses into the cell, and binds to LuxR. The LuxR/C6- HSL complex activates the lux promoter (P_{Lux}), resulting in expression of the *GFP* gene carrying a degradation tag, and production of green fluorescent protein (GFP). Engineered in this

manner, receiver cells will become fluorescent in response to AHL, and will stop being fluorescent when AHL is no longer present.

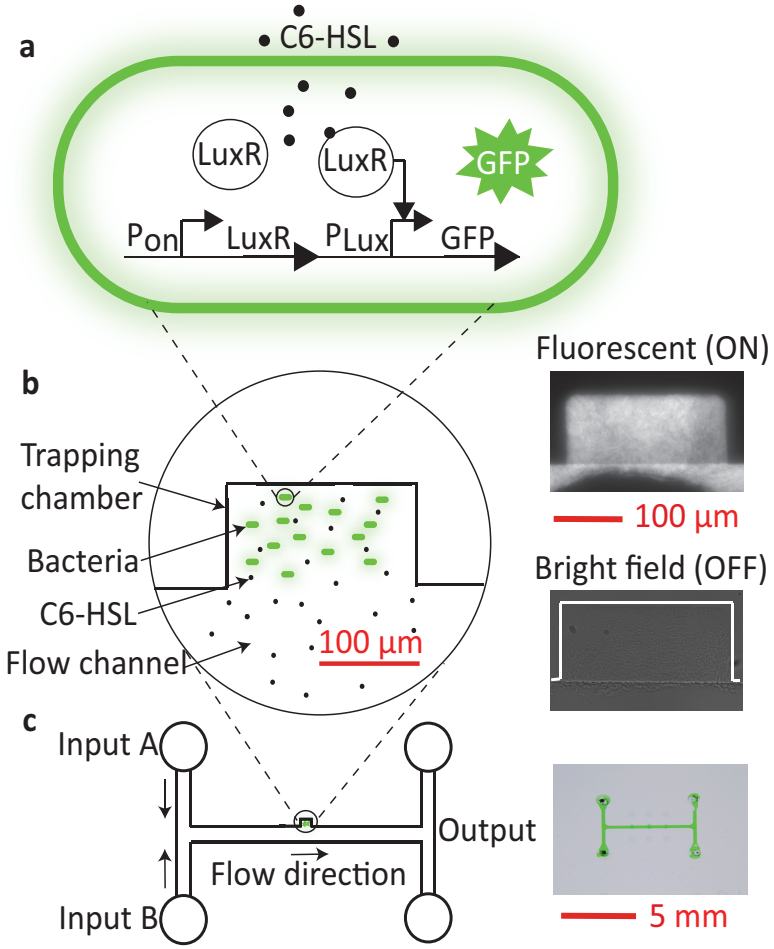

Figure 8: (a) Genetically Engineered *E. coli* Bacteria (b) Bacteria are housed in rectangular trapping chambers that are in fluidic contact to the main flow channel. As AHL(C6-HSL) flows through the main channel, the AHL diffuses across the trapping chamber, which leads to the fluorescent response in the bacteria (fluorescent image inset). In the absence of AHL, there is no fluorescence (bright field image).(c) Two inputs and two outputs are used in the microfluidic device adapted from Danino et al.[42]. (Photo of microfluidic device inset.)

Initial experiments were conducted on a plate reader to establish the receiver bacteria were functioning properly. This was done by inoculating bacteria cultures in a

plate well at the same density. A series of AHL (C6-HSL) concentrations were given to different wells. The bacteria plate well was then placed in a plate reader to record the optical density and relative fluorescence over time. Figure 9 indicates that the receiver bacteria will produce green fluorescent protein in response to AHL. As the concentration is increased, the fluorescence/OD increased. This showed the potential positive effect AHL concentrations can have on GFP output.

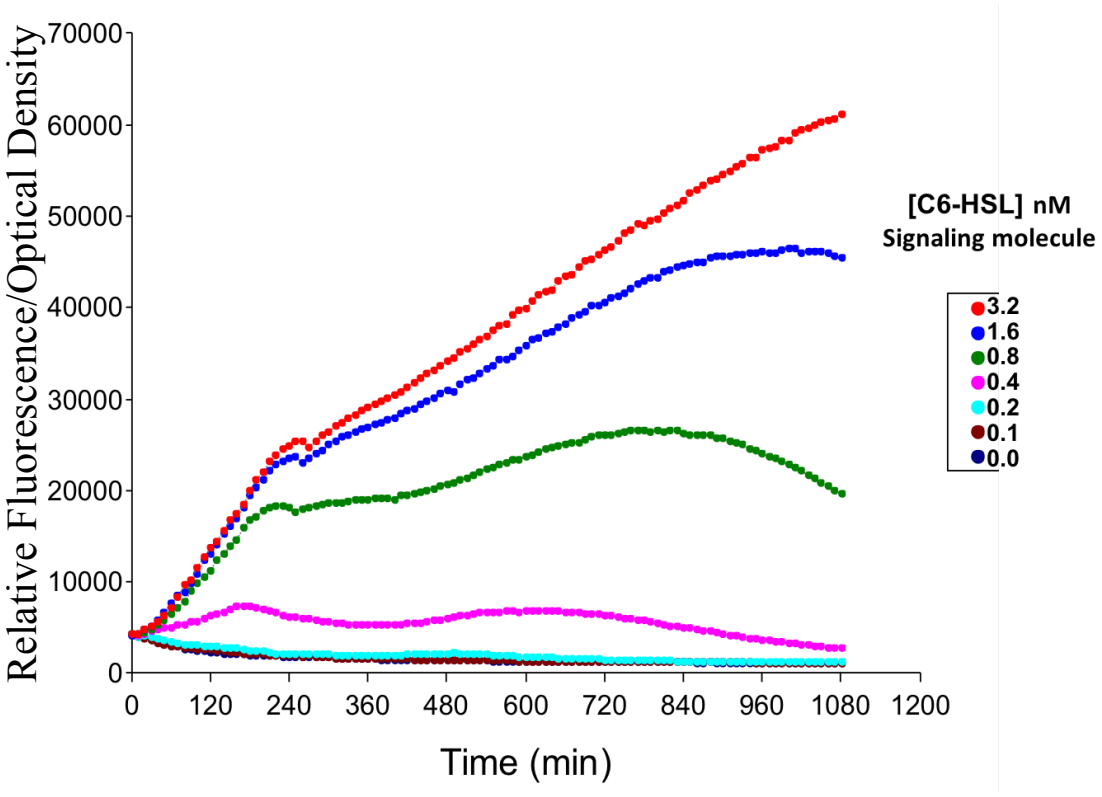

Figure 9: Response of receiver bacteria to AHL at varying concentrations over time.

2.2 Genetically Engineered Transmitter *E. coli* Bacteria

Once again working with Dr. Brian Hammer's lab and their expertise in genetic engineering of bacteria, a transmitter bacteria construction was developed to complete the

bacterial communications network. The key considerations during the development of the transmitter bacteria were as follows: stimulated via a small molecule, produced AHL, fluoresced in response to the stimulation molecule, contained an on and off state, and functioned properly in the microfluidic device. This list of requirements created several challenges, which resulted in several design attempts. Although the failed constructions are quite interesting, they will only be briefly mentioned, while the successful strain will be discussed in more detail.

All tested bacterial constructions were developed in *E. coli* strains. The first strain we tried, was integrated with a plasmid that would allow the production of AHL in presence of arabinose. Although this strain behaved as expected when tested in bulk on a plate reader, the strain did not fare well in the microfluidic environment. In our microfluidic device, the bacteria did not grow sufficiently for experimentation. To combat this issue, the plasmid was integrated in a new strain of *E. coli* that would better adapt to the adverse microfluidic conditions. This second attempt flourished when grown in the microfluidic device, but their growth rate was too unpredictable and often lead to overgrowth and clogging. This proved very difficult for future two node experimentation where this transmitter would grow at a rate up to five times the growth of the receivers. When both bacteria populations are grown in the same microfluidic chip, the temperature will be the same for both. If the transmitters grow five times faster, then they can potentially overgrow and clog the chip while the receiver population lags behind and attempts to fill the trapping chamber at a much slower rate. Since growth rates were an important aspect, the transmitter plasmid construction was moved into the same bacterial strain as the receivers. Ideally this would lead to the same growth rates for both the transmitters and the receivers.

With the issue of growth solved, we moved onto our next design trait. The plasmid that encoded the ability to produce AHL when given arabinose, did not provide us with an easy method of confirming the bacteria were receiving the arabinose and producing AHL. It will be discussed in chapter six that AHL is a very small molecule that cannot be easily fluorescently labeled or quantified. But as we have discussed with the receiver bacteria, we did have a plasmid construction that would produce GFP in the presence of AHL. Incorporating both the transmitter plasmid and the receiver plasmid into the transmitter bacteria, would create a method for monitoring the transmitter communication. The transmitter bacteria would receive arabinose, next AHL production would begin, then the bacteria would fluoresce with the production of GFP. Imaging of the transmitter bacteria would confirm the bacteria were producing the secondary chemical AHL.

Although this seemed like the perfect strain, there was one main flaw with the design. For bacteria to preferentially keep the plasmids, there needed to be a biological need for them to keep it. Normally when a particular plasmid is introduced in bacteria, there is a portion of the circuitry that codes for some antibiotic resistances. For example, if the plasmid contained an ampicillin resistance, then the bacteria would be grown in a media that contained ampicillin. This would ensure as the population develops, only the bacteria containing the desired plasmid would live.

Now with two integrated plasmids, this becomes more challenging. Since the ultimate goal is to have the transmitters and the receivers growing in the same microfluidic device where their media would be shared, using more than one antibiotic would not be possible. The transmitter with two plasmids would need to contain a different antibiotic resistance for each plasmid. If the same antibiotic resistance was used for both plasmids,

the bacteria would preferentially choose to only hold onto one plasmid since two can be taxing and one would be enough for them to survive the environment containing the antibiotic. If two different antibiotic resistances are used, this becomes problematic for the receiver bacteria population. Since the receivers only contain one plasmid with only one antibiotic resistance, they would not survive in the same media as the transmitters. With this in mind, it was concluded that only a single plasmid could be used for the transmitters, and the construction that was on the two separate plasmids needed to be combined.

To simplify the system, the same bacterial strain used for the receivers, was used for the transmitters with a new single integrated plasmid. The arabinose and AHL plasmid construction was developed from Schleif [43]. Similar experimental techniques were used in the plasmid construction and integration for the transmitter bacteria, as was used in the construction of the receiver bacteria. There are two states for the transmitter, on and off. In the on state arabinose is present in the bacteria's environment, while the off state means there is no arabinose present.

Native AraC protein has high affinity for binding to the inhibitory sites and low affinity for the active sites. In the off state, a dimer of AraC repressed gene expression by creating a loop in the DNA and binding to the I_1 (inhibitory site) and to O_2 (operator site) sites (one arabinose subunit per site) on the plasmid. The DNA looping prevents the RNA polymerase from binding and proceeding along the DNA. This theoretically would provide a tight off state, allowing dynamic control of the transmitter bacterial behavior. The off state is exhibited in Figure 10.

In this construction, the transmitter bacteria are stimulated by arabinose (a monosaccharide containing five carbon atoms). The arabinose transports across the

bacterial membrane by utilizing the electrochemical potential. Once the arabinose is in the bacterial cell, two arabinoses form a dimer and bind to the AraC dimer mentioned in the off state. This binding causes a change in protein conformation, and leads to the AraC subunit bound to the O_2 to fall off and rebind to the I_2 site. This leads to the unlooping of the DNA and allows gene expression by RNA polymerase. The CAP site on the DNA is integral for both the p_C and p_{BAD} promoters. The promoter for the synthesis of AraC, p_C, is stimulated by CAP and repressed in the absence of arabinose. When no arabinose is present, and the DNA is looped, the dimer of AraC binds to the O_1 pair of half-sites that partially overlaps the p_C RNA polymerase-binding region. This inhibits the production of AraC. The DNA unlooping and CAP stimulation allow the p_{BAD} promoter to synthesize AHL. This can be seen in **Figure 11**.

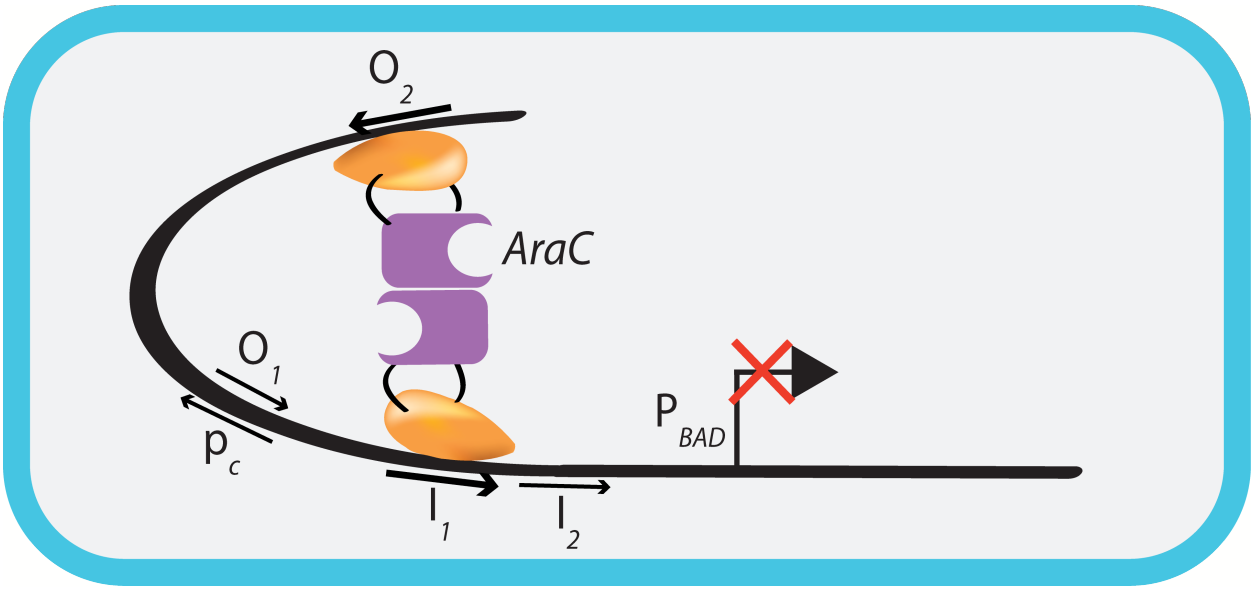

Figure 10: Transmitter off state. When no arabinose is present, the DNA is looped and no AHL is produced.

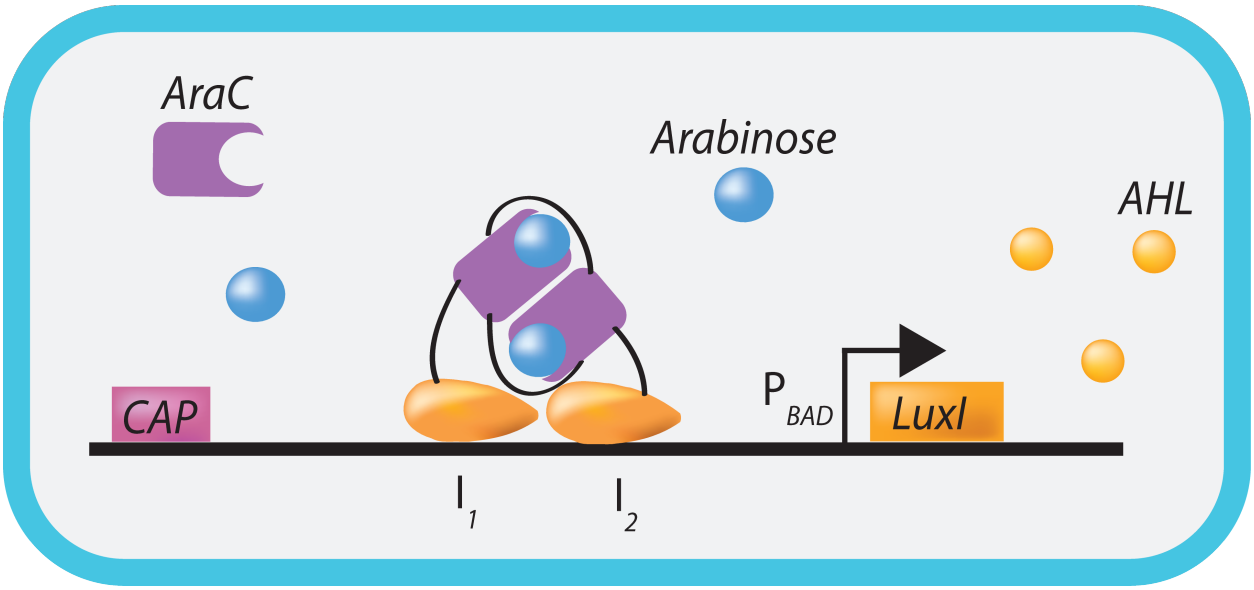

Figure 11: Transmitter on state. When arabinose is present, a dimer is formed with AraC and the P_{BAD} promoter is free to produce AHL.

Since the quantification of a small molecule like AHL is very difficult, we needed a visual cue for the transmitters to indicate they received the arabinose stimulus and were producing AHL. On the same plasmid construction, a similar AHL to GFP method was used from the receiver construction. As the p_{BAD} promoter synthesizes AHL, a constitutive promoter (P_{on}) drives the expression of the luxR gene. LuxR forms a dimer with the AHL to form a complex. That complex then activates the lux promoter (P_{Lux}), resulting in expression of the GFP gene carrying a degradation tag, and production of green fluorescent protein (GFP).

The transmitter bacteria strain was tested in bulk culture to validate AHL production when induced by arabinose. Concentrations of arabinose ranging from 2% to 0.002%, were given to bulk transmitter bacteria populations and allowed to sit for 24 hours. After the 24-hour time period, the supernatant was removed from the cultures and given to receiver bacteria populations. The populations were then placed on a plate reader which

recorded the relative fluorescent output of the receiver bacteria over time. For comparison a receiver bacteria population was also given 0.1 nM synthetic AHL. Figure 12 shows the results of this validation experiment. Higher concentrations of arabinose resulted in higher concentrations of AHL, which in turn caused the receiver bacteria to produce more GFP. This provided evidence that the transmitter bacteria were working as expected.

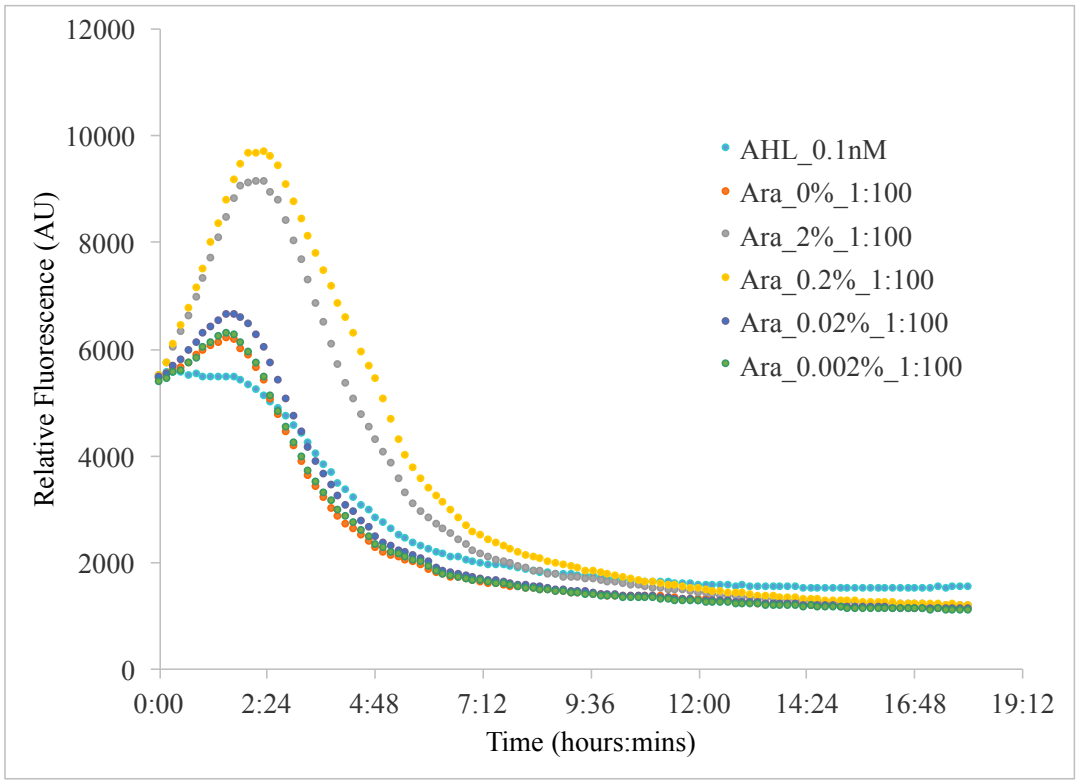

Figure 12: Transmitter bacteria AHL production. Transmitter bacteria were stimulated with varying concentrations of arabinose, and the output was given to the receiver bacteria to validate AHL production. The relative fluorescence as a function of time is the output of those receiver bacteria who were given AHL produced by the transmitter bacteria.

2.3 Conclusion

The transmitter and receiver bacteria strains were developed and tested. The transmitters respond in the presence of arabinose, by first producing AHL. That AHL then caused the transmitters to produce GFP. The receiver bacteria respond in the presence of AHL, by producing GFP. This GFP output will allow an effective means to monitor the bacteria communication, with the use of fluorescent imaging. The established concentration ranges for stimulating the two bacterial strains will provide a good starting biases for the microfluidic experiments to come.

Chapter III

SINGLE NODE MICROFLUIDIC DEVICE DESIGN AND TESTING

This chapter describes the design, fabrication, and testing of a microfluidic system to enable stimulation and measurement of discrete populations of receiver bacteria. Both receiver and transmitter bacteria are tested separately in this section. We were able to establish that the receiver bacteria response is effected by the duration of the AHL pulse input. The time of the receiver response was utilized to develop a new encoding method called time elapsed communication. Initial testing of the transmitter bacteria population was tested in the microfluidic system to establish their capabilities for monitoring bacterial communication

3.1 Single Node Device Design

Traditionally, bacterial studies rely on culturing bacteria in large bulk, for example petri dishes, test tubes, and micro wells. These bulk culturing methods are limited in the ability to study dynamic bacterial communication due to the inability to both add and remove stimulus dynamically. Additionally, since bacteria are constantly growing in an exponential phase the population size does not remain constant. This eventually leads to the complete depletion of all nutrients resulting in bacterial death, limiting experimentation time. Microfluidics allow increased control over experimental parameters such as nutrients, temperature, chemical stimulus, waste removal, population control, and allows long term experimentation. Because of the increased control, we chose to create a microfluidic device to house our receiver bacterial population to test the limitations of bacterial

communications. Careful consideration was given to the following during the designing process: oxygen permeability of the device, nutrient/stimulus delivery, removal of excess bacteria, ease of imaging, and biocompatibility. Traditional microfluidic devices are comprised of PDMS bonded to a glass slide. PDMS is a great tool when working with cells due to the biocompatibility and the fact it is oxygen permeable. This creates an environment for bacterial proliferation. PDMS is optically clear and the glass slide allows ease of imaging on a microscope. The fabrication is discussed further below, but briefly, the process of photolithography allows incredible flexibility in the design. Initially our first microfluidic chip design, illustrated in Figure 13, was adapted from the work done by Danino et al. [42].

In this design small areas, designated as trapping chambers, house the receiver bacteria populations for the duration of the experiment. This design consisted of three different trapping chamber widths (100 μm, 150 μm, and 200 μm), while the height (5 μm) and depth (100 μm) remained the same. The trapping chambers are in direct fluidic contact to the main channel (10 μm height), which allows the delivery of fresh nutrients and chemical stimulus. This allows control over the bacteria population size. As the bacteria continue to grow they eventually spill out of the chamber into the main channel. The excess bacteria are then washed out to the waste port from the constant flow. This provides a reliable control of the bacteria population not only during the duration of an experiment, but also provides consistency across all experiments. Although there is constant flow in the main channel, there is no flow in the trapping chambers once the bacterial populations are established. This limits the transfer of nutrients and small molecules to diffusion only.

To input nutrients or stimulants in the device, ports were integrated into the design. These are the large bulb shaped objects in Figure 13. One important factor considered during all microfluidic designing processes is the aspect ratio of all features. It was important not to have any areas in the device greater than a 25:1 ratio. If the ratio exceeds this limitation, the PDMS channels can collapse inwards causing blockage in the device. In areas that required wider features, such as the input ports, a trio of pillars were added for structural support to prevent collapsing.

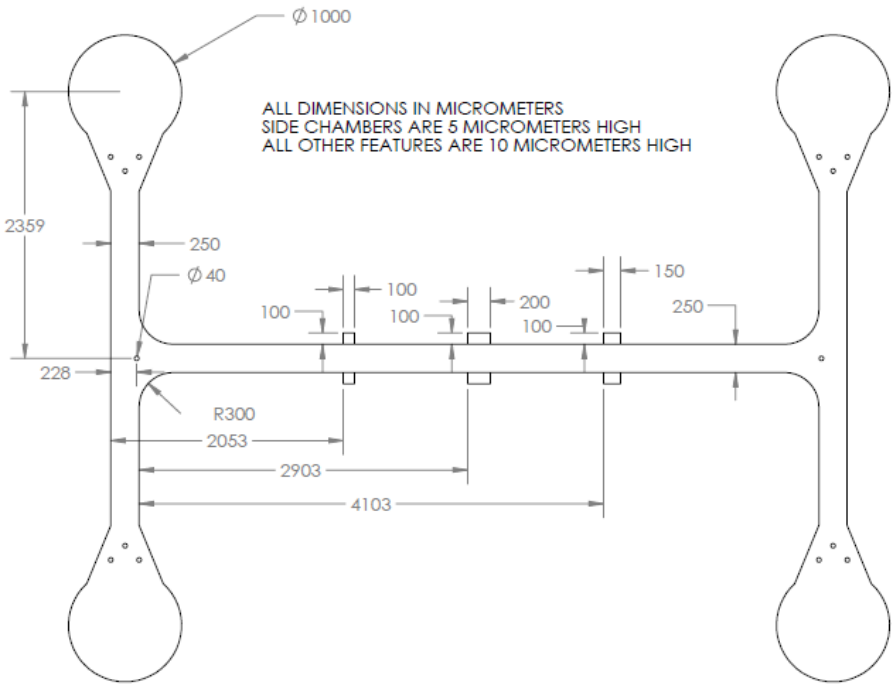

Figure 13: Single node microfluidic device design with three different chamber sizes, and four ports.

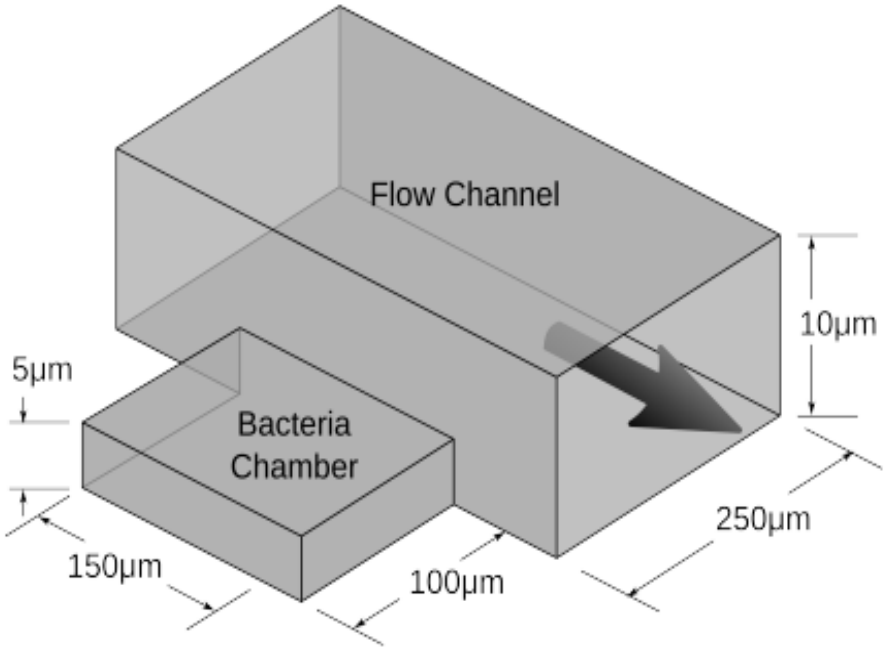

Figure 14: Rendering of the trapping chamber and flow channel interface.

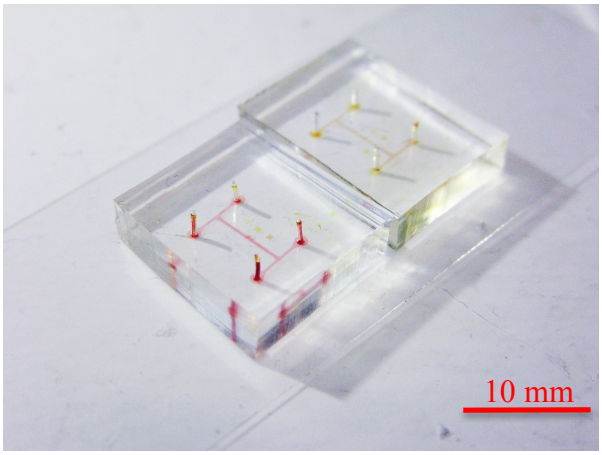

Figure 15: Photo graph of single node microfluidic device design with three different chamber sizes.

We first used the design shown in Figures 13, 14, and 15, to determine the effects of chamber size on the receiver bacterial response (results and discussion in section 3.3). These results governed our design decisions for our final one node microfluidic device. The final overall design for the single node chip can be seen in Figure 16. To increase our sample size per experiment, we increased the number of trapping chambers from 6 (3 per side) to 14 (7 per side). All trapping chamber were 100 μm x 100 μm x 5 μm and in direct fluidic contact to the main channel. Additionally, we reduced the number of outputs from 2 to 1, simplifying the experimental setup. In this design, input A and B provide a constant stream of nutrient and provide the chemical stimulus when needed, while the waste is collect via the output.

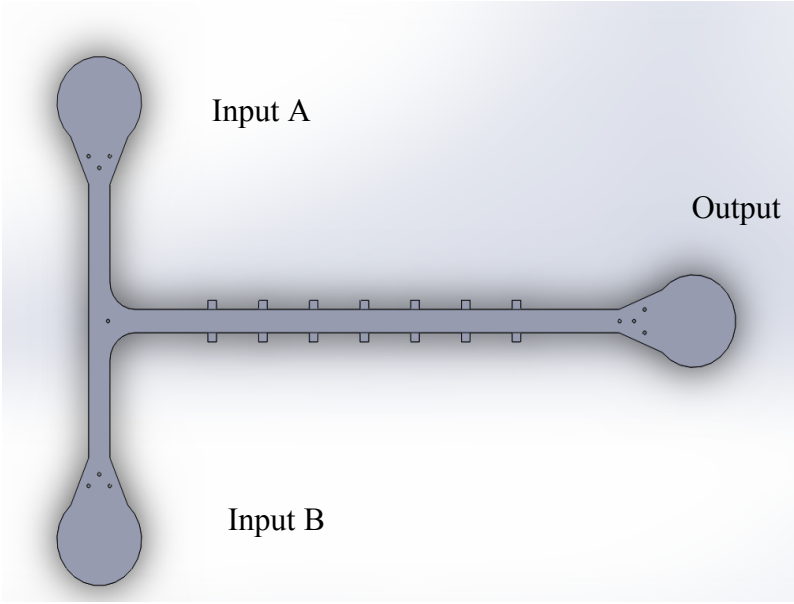

Figure 16: Single node microfluidic device design to house the receiver bacterial population.

3.2 Fabrication and Experimental Platform

To fabricate the microfluidic device we utilized standard soft lithography [44] to create a silicon (Si) wafer mold. Shown in Figure 17, SU-8 was spin coated onto a four inch Si wafer, soft baked, mask aligned and treated with UV light, developed, and then rinsed. Then transparent polymer polydimethylsiloxane (PDMS) (Sylgard 184, Dow Chemical) (1:10) was cast on the wafer. The poured polymer was then placed in a vacuum chamber at -15 to -25 psi gauge pressure to eliminate air bubbles. Degassed polymer was then cured at 70◦C for at least 4 hours, and the polymer gently peeled away from the mold. Devices were cast for uniform thicknesses of 3.2 mm–a height which allows firm anchoring of fluid interconnects from the device to Tygon tubing using small metal connectors. Next, the PDMS was then cut into individual chips and input and output interfacing holes were punched in PDMS using a 23 gauge Luer needle with a beveled edge. Use of a non-beveled needle would result in interfacing holes with small pieces of PDMS debris which may dislodge and occlude channels during testing. The PDMS chips were then plasma treated with the grade 1.1 coverslip for 1.5 min, and bonded immediately following.

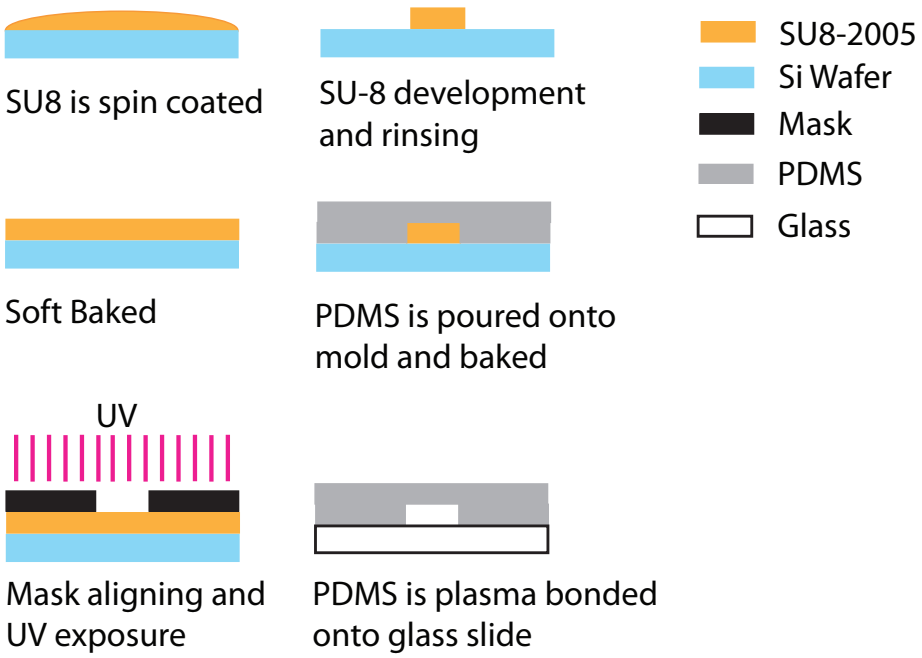

Figure 17: Fabrication process of the microfluidic device from soft lithography to PDMS bonding.

To properly image the bacteria and maintain experimental conditions, an experimental platform was developed. The platform consists of a Nikon microscope, stage control in the x and y direction, z-axis control, shutter control, CCD camera, syringe pumps, stage heater and controller, LabView virtual instrument (VI), and Matlab image processing. The stage heater with a thermal couple feedback was used to control the temperature of the chip, and subsequently the bacteria. This allowed us to adjust the temperature as need for the bacteria. The syringe pumps (Harvard Apparatus) were used to provide either the media or a chemical stimulus to the microfluidic chip. This was done by placing syringes, with Tygon tubing attached using a blunt tip 25 gage needle, on the syringe pump. On the opposite end of the tubing, a 25 gage blunt tip needle connectors were inserted into the inlet ports of the microfluidic chip. Additionally, a metal connector

and tubing were connected to the outlets, while the other end of the tubing was placed in a falcon tube to collect the waste. The chip was placed on the microscope stage for the duration of the experiment to allow imaging and temperature control.

A LabView VI was created to control several aspects of the experimental setup. The user first sets the shutter speed, number of images to capture, and the frequency of the imaging. Next the user can move the stage, via a joystick, to the desired x-y location and focus to the desired z. This position can then be added to the program and the xyz coordinates are recorded. This is continued to set all trapping chamber locations. Once the locations are set, the program can run autonomously. The program first moves the stage to the first set of xyz coordinates, opens the microscope shutter, tells the camera to take an image with the given shutter speed, and closes the shutter. The image is save to a designated folder, and the program continues the process with the remainder of the set trapping chamber positions. Once the experiment is completed, a Matlab code is used for all image processing. A region of interest is selected, the pixel values in that region are added and then averaged per pixel, finally the background is subtracted leaving the relative fluorescence. This image process was done for each chamber over the duration of the experiment. These values are then plotted with relative fluorescence with arbitrary units (AU) vs time (minutes).

3.3 Troubleshooting

Once this system was completed, there were many tests conducted to trouble shoot issues that arose. The main hurdles that we had to overcome were contamination, air bubbles, and overgrowth. To combat contamination, we added ampicillin to our media

solution to prevent the growth of any bacteria that did not contain our genetically engineered plasmid. In theory, this would prevent unwanted bacteria from populating the device. Unfortunately, some naturally occurring bacteria are ampicillin resilient which can lead to contamination of the device. We implemented sterile cell culture techniques and moved all experimental preparation into a sterile biosafety cabinet to limit exposure to unwanted bacterial strains. Since the microfluidic chip cannot be cleaned and sterilized, the microfluidic chips are singe use only.

A complication that can arise during experimental setup is the introduction of air into the microfluidic device. This creates air bubbles that can potentially lodge in the main channel, blocking the flow in the device leading to experimental failure. Although PDMS is permeable to oxygen, it can take up to 12 hours for a bubble to naturally dissipate. If a smaller air bubble enters the microfluidic device and does not lodge in the main channel, it can potentially flow through the device forcing all bacteria out of the chip (similar to a syringe plunger pushing fluid out). This can happen at any time throughout the experiment, and renders the experiment useless. There are two main instances where air bubbles can be introduced to the system. The first is at the interface between the tubing connectors and the ports in the microfluidic chip. As the connectors are pressed into the PDMS, a small pocket of air can become trapped leading to infiltration. To combat this issue, we integrated a new step in our procedure that required a small droplet of media to be placed on the port entrance before the connector was inserted. This ensured a fluid to fluid connection eliminating potential air bubbles. The other point of air bubble introduction occurs in the syringe and tubing apparatus. Unlike the first issue, this introduction of air bubbles could occur at any time during the experiment. To reduce this possibility, after filling the syringe

with media, we removed all air from the syringe before connecting the tubing. Next we connected the tubing to the syringe and then pushed excess media through the tubing, removing any latent air bubbles.

One of the most challenging complications that arose during experimentation, was the overgrowth of bacteria that clogged the device and prematurely ended the experiment. This required a more intensive approach. There are two factors that can greatly affect the growth of the bacteria, temperature and the flow rate in the main channel. Initially the bacteria were injected via one of the inlet ports with a syringe. During the injection process the bacteria flowed through the microfluidic device and seeded anywhere from 1 -100 bacteria per chamber. We then allowed the bacteria to grow and create a stable population in the trapping chambers over a 24-hour growth period.

Because of the variability of both starting bacteria count and the bacterial behavior, this growth period had to be carefully monitored and adjusted. The first tool used to impact the bacterial growth is the stage heater on the microscope that controls the temperature of the microfluidic device. If there is a low starting seed count, it is beneficial to increase the temperature by upwards of 2 degrees to stimulate an increase in growth rate. Similarly, decreasing the temperature, upwards of 2 degrees, can slow the slow the growth of bacteria.

The flow rate in the main channel during the growth period is also crucial. When bacteria are first seeded into the trapping chamber, they have not formed a biofilm to protect themselves against the fluid flow. This makes them exceptionally susceptible to washing out if the flow rate in the main channel is too great. Once the bacteria begin to grow and they start to form a biofilm, they become adhesive to the trapping chamber. in away creates a protected environment for the bacteria to grow unhindered by the flow

the main channel. At this point in time, the bacteria population is robust enough to withstand a higher flow rate in the main channel.

Figure **18** represents possible experimental conditions that would best control the bacterial growth as the experiment progressed.

These two adjustment tools are not independent from one another. While adjusting one the other must be considered at all times. For example, if there is a low starting seed count and the temperature is increased to help bacterial growth, the flow rate must be incrementally increased as the population grows. If the flow rate is not increased, the bacteria are free to populate not only the trapping chamber but the main channel leading to clogging. On the other hand, if the flow rate is stepped up too quickly and the bacteria are not properly anchored, all bacteria can be flushed out of the chamber. This is just a small subset of the challenges faced while optimizing the experimental procedure. This procedure was then tested and the results are discussed in the following 3.3 results sections.

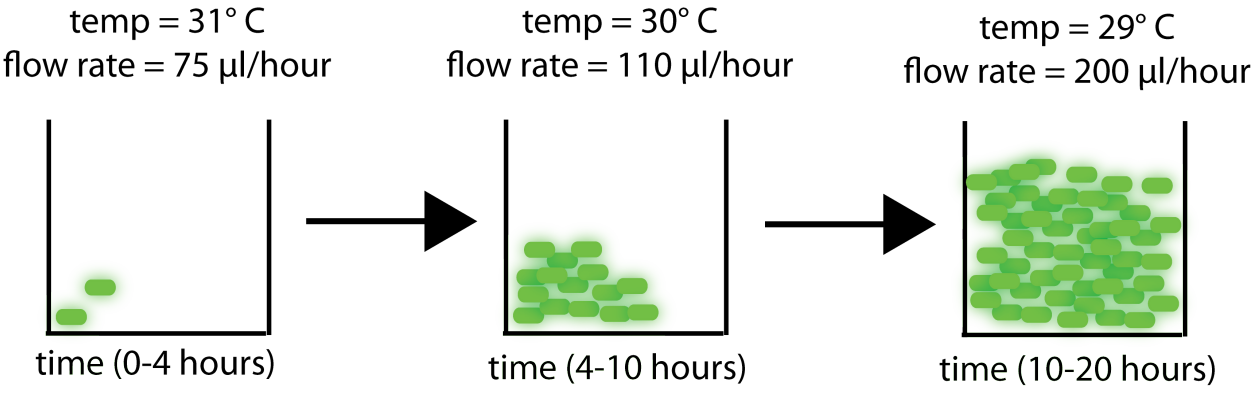

Figure 18: Representation of possible experimental conditions used during bacterial growth period. As time progresses, both the temperature and the flow rates must be adjusted to adapt to the bacterial colony formation.

3.3 Single Node Experimentation

Our studies showed that the microfluidic device was capable of housing the receiver or transmitter bacteria in trapping chambers for several days while supplying them with fresh nutrients. The microscope setup was able to capture images of the fluorescent green protein being produced by either the receiver bacteria, in response to the AHL, or the transmitter bacteria, in response to arabinose. The single node device designs were adapted from Danino et al. and is shown in Figure 13 and Figure 16.

3.3.1 Testing of Single Node Receivers

The first experiment conducted was to determine if the chamber size affects the fluorescent response of the receiver bacteria. The first generation single node microfluidic device, illustrated in Figure 13, contains three different chamber sizes. All chambers were 100 μm deep and 5 μm height while the widths were 100 μm, 150 μm and 200 μm. Experimentally, a single pulse of AHL (10 μM) was given to the receiver bacteria for a duration of 50 minutes followed by no AHL for the remainder of the experiment. The bacterial response from ten trapping chambers of each size were measured. To determine if there was a significant difference between chamber sizes, several factors were compared. Three relative fluorescence levels are notable: a "threshold fluorescence" at 5% of peak, 95% of peak, and peak. A variety of durations were determined from the three chamber sizes and compared. "Response delay" is defined as the time between the start of the AHL pulse and the time of threshold fluorescence. "Ramp-up time" is defined as the time between the threshold fluorescence and 95% of peak. "Peak time" is defined as the time between the start of the AHL pulse and the time of peak fluorescence. "Response duration"

is the duration that the response is above the threshold fluorescence. “Ramp-down time” is the time between the 95% of peak after achieving peak and threshold fluorescence. For each of these durations, both a student t-test and Bayesian statistical methods were used to evaluate the effects of chamber size. Our results showed no statistical differences between the different sized chambers having equal density of bacteria. For this reason, we choose the smaller 100 μm by 100 μm by 5 μm chamber size for the final single node design shown in Figure 16.

Using the genetically engineered bacteria in the final single node microfluidic system in Figure 16, we were able to elicit a fluorescent response to AHL and image it with the fluorescence microscope. At steady state (e.g., 1 hour) we were able to image fluorescent bacteria (number of experiments=10, SNR=20), and return them to non-fluorescing state by removing AHL from the flow channel (number of experiments=10, SNR< 1). We experimented with modulating the AHL input as a pulse with 10 μM concentration for a variety of durations. As shown in Figure 19, the bacteria responded differently to the varying input pulses with varying widths.

In order to select an appropriate input pulse width, an experiment was run with varying pulses of 10 μM AHL to determine the minimum pulse width that fit our requirements for a distinguishable signal. To be considered as a signal, we define a threshold signal-to-noise ratio (SNR) as ≥ 5, and a plateau region of sustained fluorescence above this SNR threshold of duration greater than 10% of the total signal time. Shown in Figure 19, the bacteria were exposed for 300, 200, 100, 50 and 30 mins with periods of pure media in between. The 50 min pulse was the shortest pulse that met these requirements, and was therefore used in the following experiments. The bacteria were

exposed to AHL for a 50 min pulse for all results shown in Figure 20. For ten samples, the average response time, defined as the time from when the bacteria begin to fluoresce until the time they stopped, was found to be 435 minutes with a standard deviation of 47. The average delay time, characterized as the time between when the bacteria start to receive the AHL until they begin to fluoresce, was 31 minutes with a standard deviation of 11. The average SNR was 7.9.

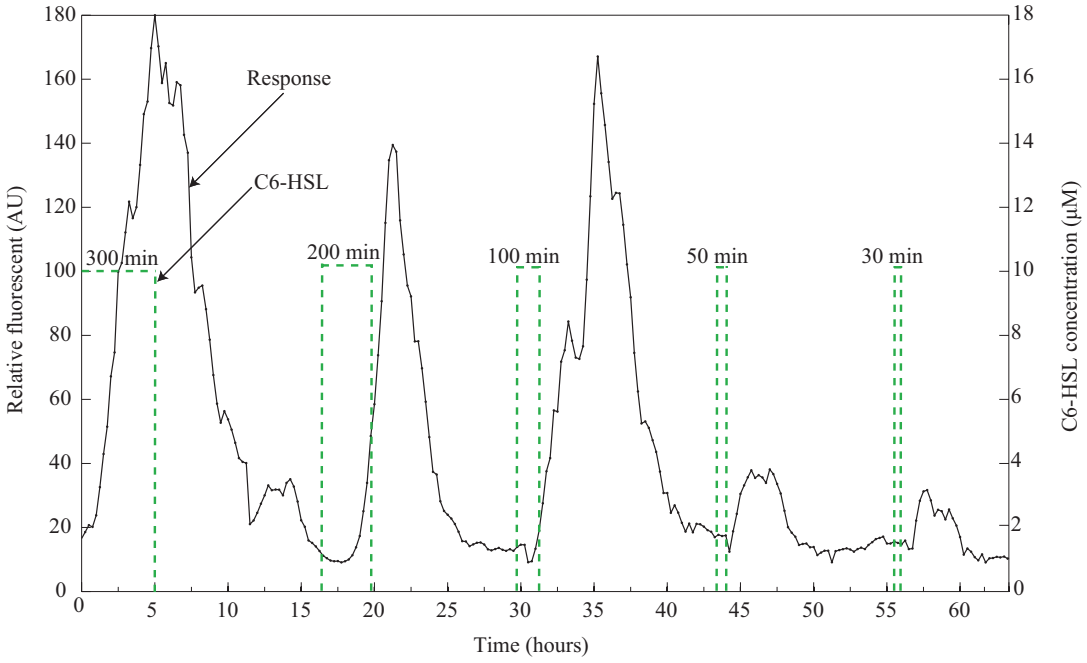

Figure 19: Bacteria relative fluorescence was measured in response to varying pulse inputs (300, 200, 100, 50 and 30 min) of AHL. A typical response is shown.

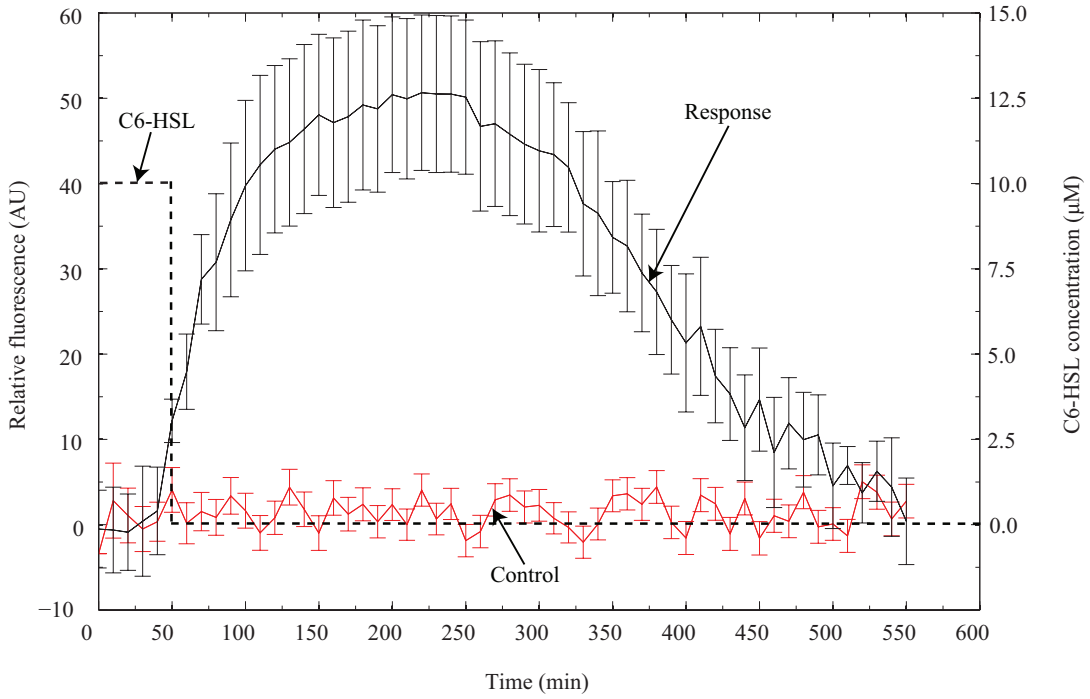

Figure 20: Bacteria relative fluorescence was measured in response to pulse input of duration 50 min of AHL (Number of experiments=10), as compared to a reference (Number of experiments=4). Error bars represent one standard deviation.

Additionally, we wanted to explore both theoretically and experimentally how the concentration of AHL varies spatially and temporally through the chamber. To model and validate this, we performed both COMSOL Multiphysics simulations and experimental validation of the concentration of AHL across a densely-packed bacteria chamber as a function of time. The model predicted a transient response time of approximately 3 seconds. In other words, 3 seconds after the concentration of AHL in the channel is changed at the start or end of a pulse, we would expect the AHL concentration in the chamber to reach steady-state. To experimentally verify this, we flowed fluorescently-labeled bovine serum albumin (Alexa Fluor 488) at 2 μM through the chip using 5 mL syringes with concurrent fluorescence CCD imaging. Results were compared against COMSOL

simulation, and confirmed the accuracy of the simulation's predictions of mass transfer, as seen in Figure 21 below.

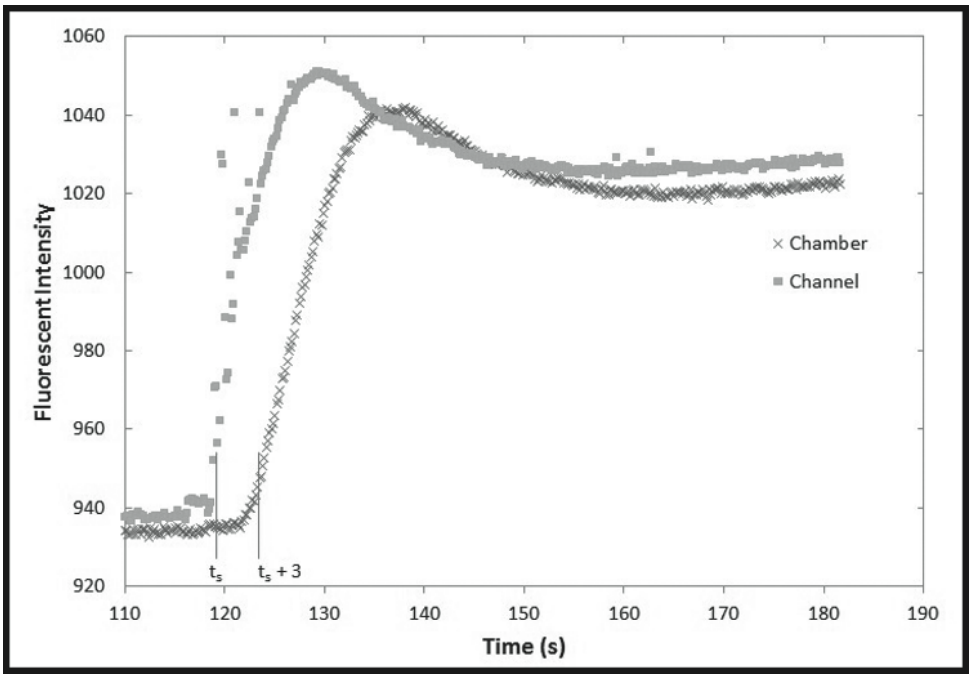

Figure 21: Experimental measurement of the transient temporal response of the microfluidic chamber to the flow of fluorescently labeled BSA in the main channel. The 3-second delay between channel and chamber agrees with COMSOL predictions.

At steady-state, the concentration of AHL will vary across the biofilm (chamber) spatially. This steady-state spatial variation can be assessed from Figure 21 after the transient behavior. To measure this, the average fluorescent intensity from time 160 to 170 seconds is 1027 units and 1031 for the channel and chamber, respectively. Therefore, the percentage drop from front to back of the chamber at steady-state is (1031-1027)/1031= 0.4%.

To assess the variation in GFP fluorescence measured across the chamber, we analyzed a sequence of fluorescent images of the chamber captured in one of our experiments. While the individual bacteria fluorescence varies considerably (i.e., some of the bacteria are dead), when averaging over a population of 50,000, we found that at most, the front of the chamber is 1% brighter than sub-populations at the rear, farthest from the AHL supplying channel.

3.3.2 Time Elapsed Communication

Bacterial populations housed in microfluidic environments can serve as transceivers for molecular communication, but the data-rates are extremely low (e.g., 10−5 bits per second.). In our work with collaborator's in Sivakumar's lab, genetically engineered *Escherichia coli* bacteria were maintained in a microfluidic device where their response to a chemical stimulus was examined over time. The bacteria serve as a communication receiver where a simple modulation such as on-off keying (OOK) is achievable, although it suffers from very poor data-rates. We explored an alternative communication strategy called time-elapse communication (TEC) that uses the time period between signals to encode information.

In this work, we explored the fundamental limits of pulse width. We modulated input signals using chemical cues to measure fundamental performance limits and ultimately to develop a new method of encoding molecular information. The simplest form of amplitude shift keying occurs in the presence of a signal (ON) represented as a 1, and the absence (OFF) represented as a 0. The new methods we will discuss surpassed previous data-rate limitations common with OOK.

During experiments, bacteria were maintained in chambers on the microfluidic device (see Figure 16) while bacterial growth medium (2xYT media containing ampicillin at 10 μg/ml) was delivered to flow channels alternatively with medium containing AHL signal (note inlet A and B in Figure 16). The central flow channel (250 μm wide x 10 μm high) is in direct fluidic contact with the chamber (150 μm x 100 μm x 5 μm high) as shown in Figure 14. In response to AHL, the bacteria fluoresce (see Figure 8(b)), as imaged on a fluorescent microscope (Nikon TE 2000), with stage heated to 30°C. The microfluidic system included the microfluidic device on the microscope stage, pumps and tubing. To initially load bacteria on the chip, cells were injected in media through one of the inlet ports using a syringe to fill the chip entirely. Excess bacteria were flushed away. Tygon tubing was attached between the chip and pumps using short metal tubes, and the chip was placed on the microscope stage. The bacteria were then allowed to populate the chamber for 24 hours until it reached capacity, ~10^5 bacteria per chamber, during which time both inlets were used to flow 2xYT media at 100 μl/hr using syringe pumps (Harvard Apparatus). This flow rate was empirically determined to allow the bacteria to successfully colonize the chambers without being washed away.

Once the bacteria had filled the trapping chamber, combined flow rate was increased to 360 μl/hr. Inlet B was used for 2xYT medium alone (at 350 μl/hr), while inlet A (10 μl/hr) was used to varying concentrations and durations of AHL as noted. Fluorescent images where captured during the course of the experiment (1 every 10 minutes) and were processed using MATLAB. The intensity of the pixels within the bacteria chamber was averaged and the background fluorescence was subtracted, yielding relative fluorescence (arbitrary units, or AU). The obtained signal strength is defined as the

relative fluorescence. The SNR was then computed as the signal strength divided by the standard deviation of the background noise (non fluorescent bacteria-filled chamber).

It can be seen that the receiver signals clearly follow the ON-OFF patterns at the sending side, albeit offset by the propagation delay in the environment (Figure 19 and Figure 20). While the above results demonstrate that OOK can indeed be relied upon for conveying information from the sender to the receiver, we proceeded to derive the achievable data-rates using OOK based on parameters extracted from the experiments. The key parameter of interest in determining the achievable data-rate is the bit period. The bit period at the receiver is greater than that at the sending side due to the biological processing at the receiver bacteria. We define the maximum of the two bit periods as the effective bit period t_b. Acceptable SNR threshold used was an empirical value based on visual observation. The condition on SNR threshold determines the effective bit period (t_b) of the system. Therefore, we analyzed different values of t_b in our numerical analysis. The data-rate of OOK is thus 1 t_b, which for a t_b of 435 minutes is 3.8×10^{-5} bps. In the following work, we introduce and describe strategies that are aimed toward improving the achievable data-rates in super-slow networks.

The data-rate performance of OOK in bacterial communication is low due to the exceedingly large bit period involved. Hence, in this work we explore a communication strategy called time-elapse communication (TEC), wherein information is encoded in the time period between two consecutive signals. A pictorial representation of TEC and OOK is presented in Figure 22 and Figure 23. The number of molecular signals generated always remains at two (the start and the stop) irrespective of the number of bits required to represent the information. TEC requires the clock rates at the sender and receiver to be the

same, although no clock synchronization is required. Intuitively, TEC improves the data-rate over OOK by reducing the number of communication signals that needs to be conveyed per unit of information.

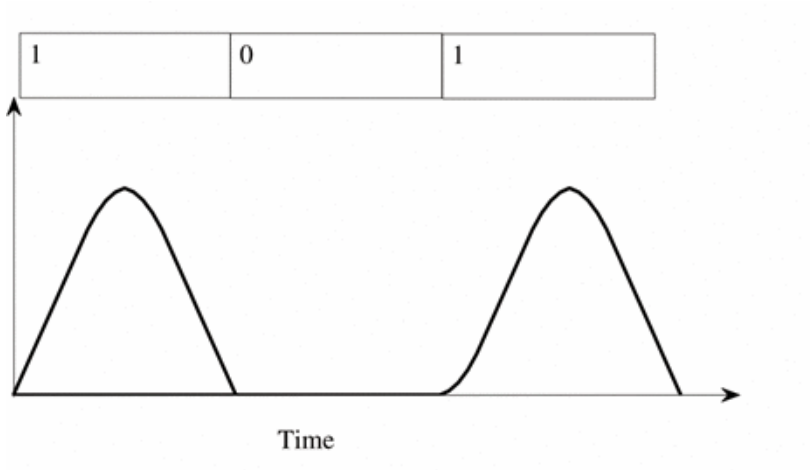

Figure 22: Illustration of modulation scheme for OOK.

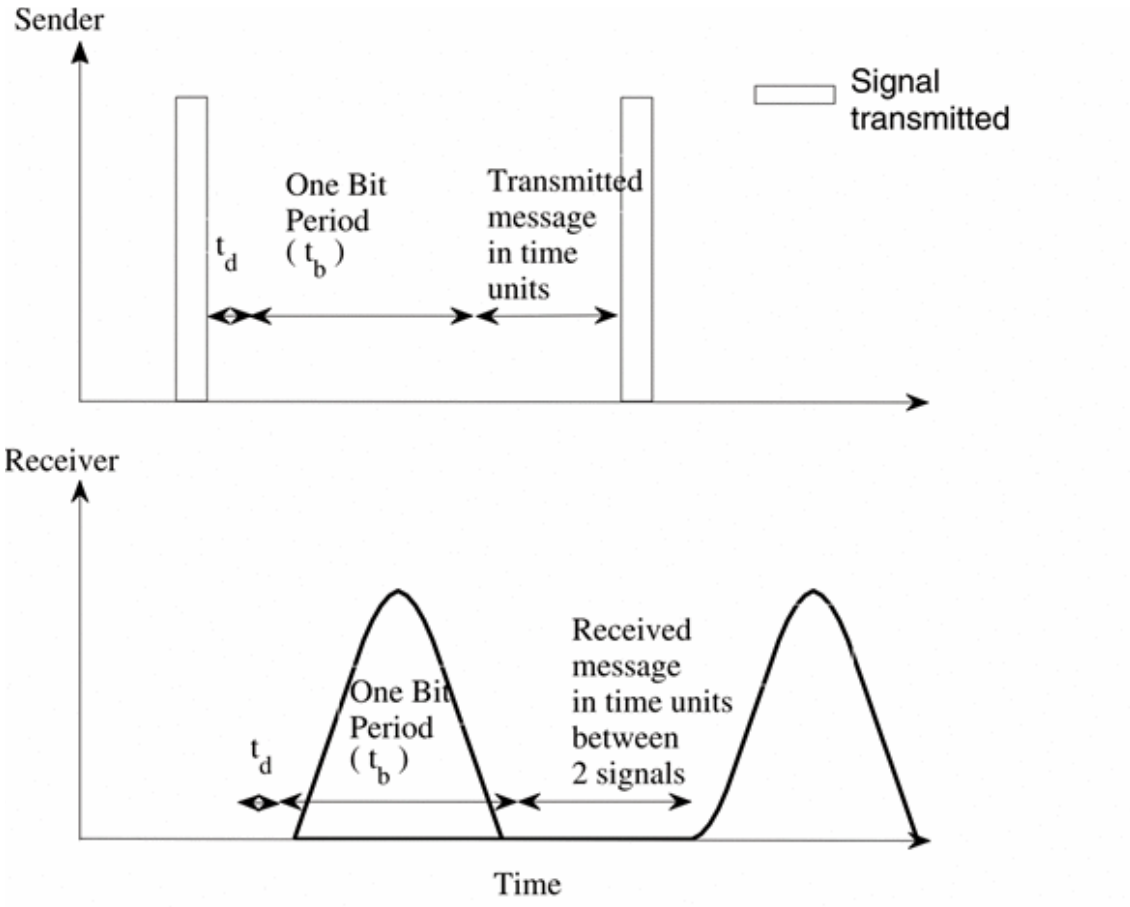

Figure 23: Illustration of modulation schemes for TEC with no error.

We then used numerical analysis of the data-rate equations of both OOK and TEC to study the ability of TEC, under various parameters, to improve the bit rate over OOK. Unless otherwise specified, we used a molecular signaling bit period t_b of 435 minutes based on the experimental results presented in section 3.3, and a clock rate of 1 Hz. The data-rates of OOK and TEC as a function of the bit period t_b is shown in Figure 24, while Figure 25 presents the relative performance improvement of TEC with respect to OOK. As t_b increased, TEC 's improvement over OOK increased. This was due to TEC's performance relative insensitivity to the parameter compared to OOK's sensitivity. Figure

26 presents the relative performance improvement of TEC with respect to the number of bits n. It can be observed that the relative performance varies with n. Thus, for a given set of t_b and f_c, there is an optimal value of n that should be used in TEC.

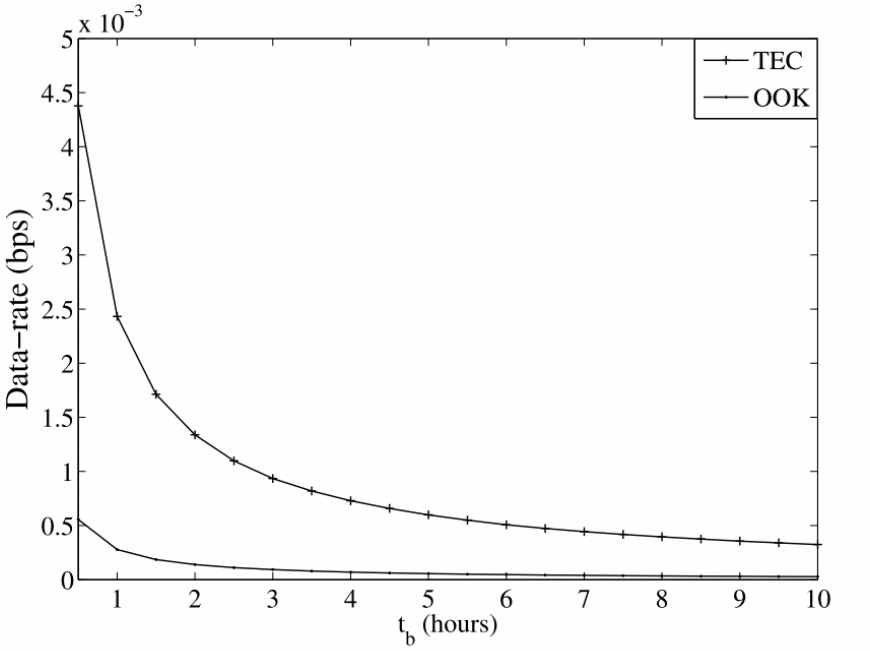

Figure 24: Performance of TEC under ideal zero error conditions. Data-rate as a function of effective bit period.

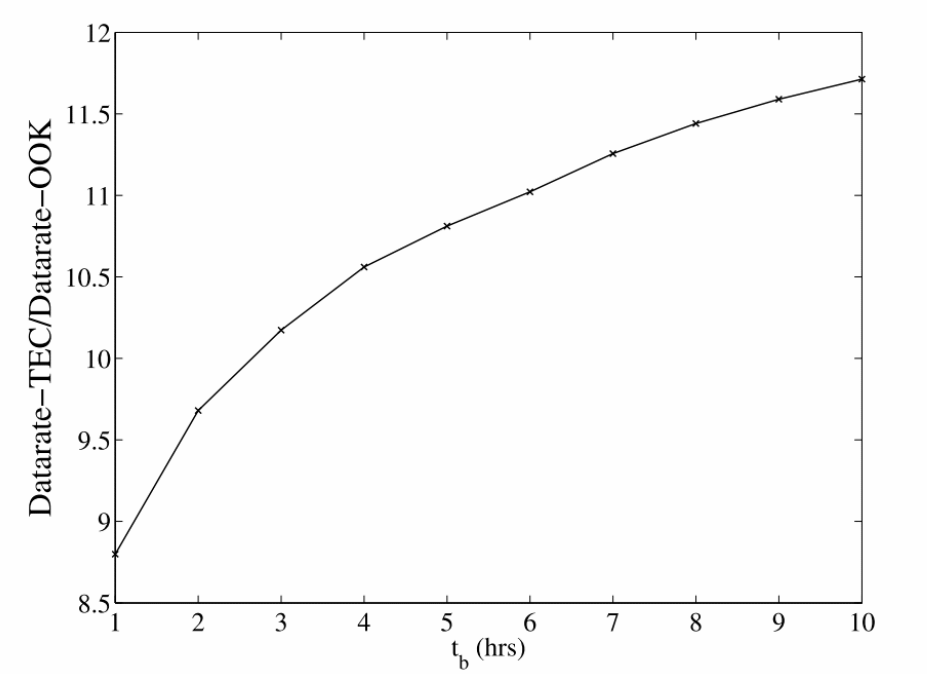

Figure 25: Performance of TEC under ideal zero error conditions. Data-rate TEC/ Data-rate OOK as a function of effective bit period.

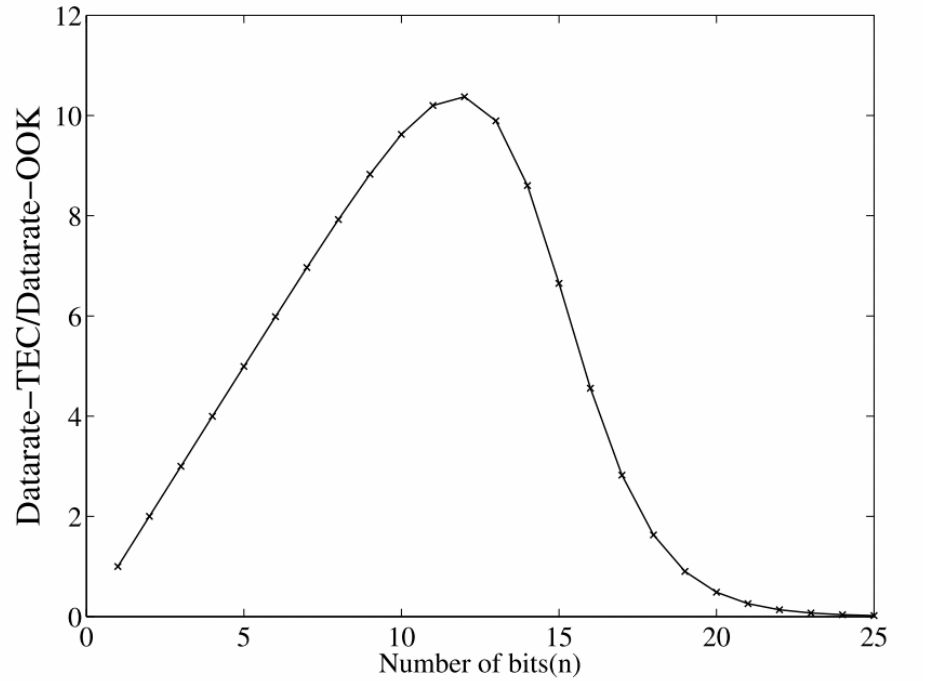

Figure 26: Performance of TEC under ideal zero error conditions. Data-rate TEC/ Data-rate OOK as a function of number of bits.

Thus far, we have explored the performance of TEC under idealized zero error conditions. In reality, the responses of biological systems will vary across time. Figure 27 illustrates a deviation from ideal behavior. The start signals in Figure 27 gets delayed and hence the time elapsed between the signals is different leading to bit errors. To the best of our knowledge, there has not been any work that models the statistical distribution of the delay in the response of bacteria to molecular signals. Hence, we consider a simple uniform distribution U (t_b -ε, t_b +ε) to model the real response time of receiver bacteria. On an average, one bit period is t_b with a bounded error that is uniformly distributed U(-ε,+ε) . Any deviation from the average is termed as error. The net error ε is the sum of all errors from the time of introduction of molecules into the medium to the detection of fluorescence output. Given that the error is bounded, it is possible for the receiver to decode with 100% accuracy by the simple technique of increasing the minimum distance between messages. A message is defined by both the start and the stop signals, and both these signals can be subject to an error of +/-ε. If the minimum distance between adjacent messages is at least 4ε, the receiver can decode messages correctly in spite of any errors. We refer to TEC with simple error correction as TEC-SIMPLE. We found the relative data rate performance of TEC-SIMPLE in a realistic system reduced to approximately 1.8 x OOK (for an error of 10% in t_b). Thus, the introduction of error in the system brought down the performance of TEC considerably.

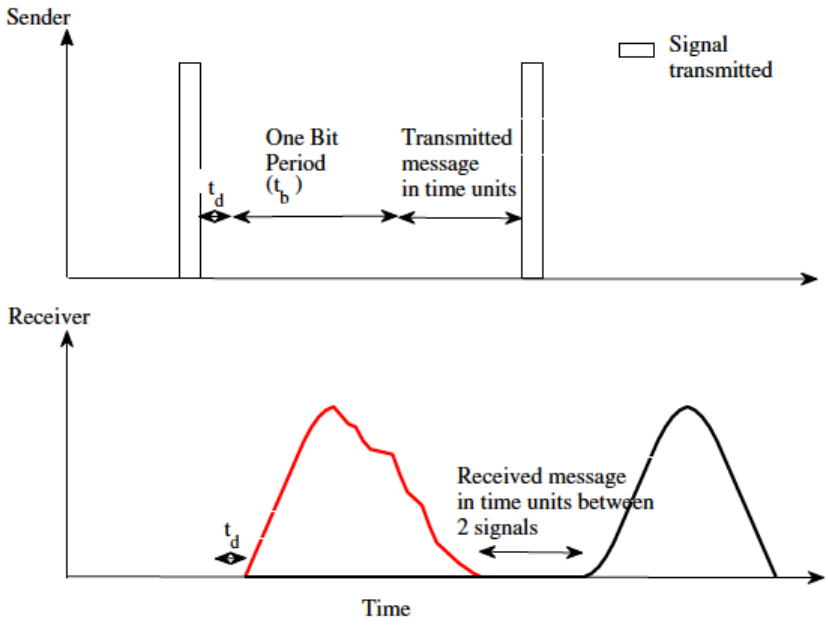

Figure 27: Illustration of modulation schemes for TEC with error

To combat these issues, our collaborators developed a new encoding method smart time elapse communication (TEC-SMART). The development of TEC-SMART utilized the data collected by our lab, but since the scope of the work lies outside the aims of this thesis, I will only briefly summarize the final findings. If interested further, the full methods and results can be found in [45]. We first used the microfluidic system to demonstrate that on-off keying is (a) achievable in the target environment; and (b) has a data-rate performance that is quite low. Dr. Sivakumar's lab was then able to use this data to develop a system to increase the data-rate performance of the bacteria by establishing a smart method of time elapsed communication. In this method, information is encoded in the time between signals, and achieves over a 10x improvement in data-rate compared to on-off keying.

3.3.3 Testing of Single Node Transmitters

In chapter two, several transmitter bacterial constructions were discussed. Although the single node chip design was used to test all generations of the transmitters, only the results of the final transmitter design will be discussed here. The transmitter experimental setup was very similar to the receiver setup. The final transmitter strain was injected into the single node microfluidic device via a syringe through an inlet port. Tubing was attached to the device utilizing metal connectors to provide fresh media and the primary chemical stimulus arabinose. The chip was placed on a heated microscope stage for the duration of the experiment, and fluorescent images were captured.

One of the key differences in the experimental setup was the waste collection. With the receivers, there was no need to collect the waste, and the solution was disposed of after every experiment. However, with the transmitters we are keenly interested in collecting the output of the bacteria. Since the transmitters produce the secondary chemical stimulus AHL, we collected the waste output of the device so AHL extraction and quantification could be conducted post experimentation. This post processing will be discussed in greater detail in chapter six. The waste tubing was attached to a syringe that was on a Harvard Apparatus syringe pump. The pump was run in the withdraw mode at the same rate as the combined inlet rates. The tubing was long enough to ensure the output remained in the tubing at all time and did not reach the syringe. This was done to allow time segmentation of the waste output. Although there would be some diffusion between time plugs, this was the most efficient way to collect the waste and keep everything sterile. To combat the growth of the excess bacteria being washed away through the output, and to slow AHL degradation, the waste tubing was kept on ice. After the experiment, the pump would run

in the infuse direction and the waste output could be segmented out for different time points.

In bulk cultures, the transmitter bacteria responded to arabinose in concentration ranging from 2% to 0.002%. To keep the experimental process as similar to the receivers for simplicity, we choose a concentration of 20 μM arabinose to use for our initial experiments. This concentration was on the low end of bulk culture results. Initial experiments entailed a 50 min pulse of 20 μM arabinose given to the receiver bacteria. When the transmitter senses the arabinose it produces AHL, which in turn causes the transmitters to produce GFP. The fluorescent images are then processed and the relative fluorescence as a function of time is produced. One important finding with this first experiment, was the apparent plateauing of the relative fluorescence. With our transmitter bacterial construction, it was expected that when arabinose is no longer present in the media, the production of AHL would cease and lead to the fluorescence turning off. This initially appeared no to be the case experimentally, but after examining the AHL out that will be discussed in chapter 6, we realized that the transmitter bacteria produced AHL for a much greater time period in response to a 50 min pulse of arabinose than expected.

One possible area for this occurrence can be found in the affinity for the arabinose and AraC dimer formation. The rate of formation of the dimer is 8 orders of magnitude greater than the rate of disassociation [43]. This means that the arabinose is unlikely to leave the transmitter bacteria cell since any free arabinose in the cell will immediately form another dimer rather than leaving the cell. One way to combat this would entail decreasing the arabinose concentration so that eventually as the bacteria continue to divide, the arabinose would phase out. But since we were already at the lower limit of the detectible

range of arabinose, we decided to test another option. An alternative method to turning off the production of AHL was mentioned in the original transmitter construction paper [43], and exploited the bacteria's preference for glucose over arabinose. In the theory the bacteria would preferentially uptake the glucose which would then in turn inhibit the production of AHL. This was due to glucose decreasing cyclic amp levels, which are needed for the cap protein to bind to the DNA. The cap protein, is integral for both the p_C and p_{BAD} promoters, and without it AHL cannot be produced. To test this theory another transmitter experiment was conducted, but this time after the pulse of arabinose was given, the bacteria were given media with 20 μM glucose for the remainder of the experiment. A sample of these results are shown in Figure 28. The experiment was run 5 different times each with a minimum of 5 chambers per experiment. Although glucose was added, there was not difference in shut off time when compared to bacteria who were not given glucose. Although there is still possible room for improvement for shutting the transmitters off, this strain still proves useful since it does respond to the arabinose and produces the secondary signal AHL and eventually turns off. The production of GFP in the transmitters creates a conformation step that the bacteria are producing AHL, since AHL cannot be imaged. This will allow us to conduct communication studies between the transmitter and the receiver in the 2 node microfluidic chip.

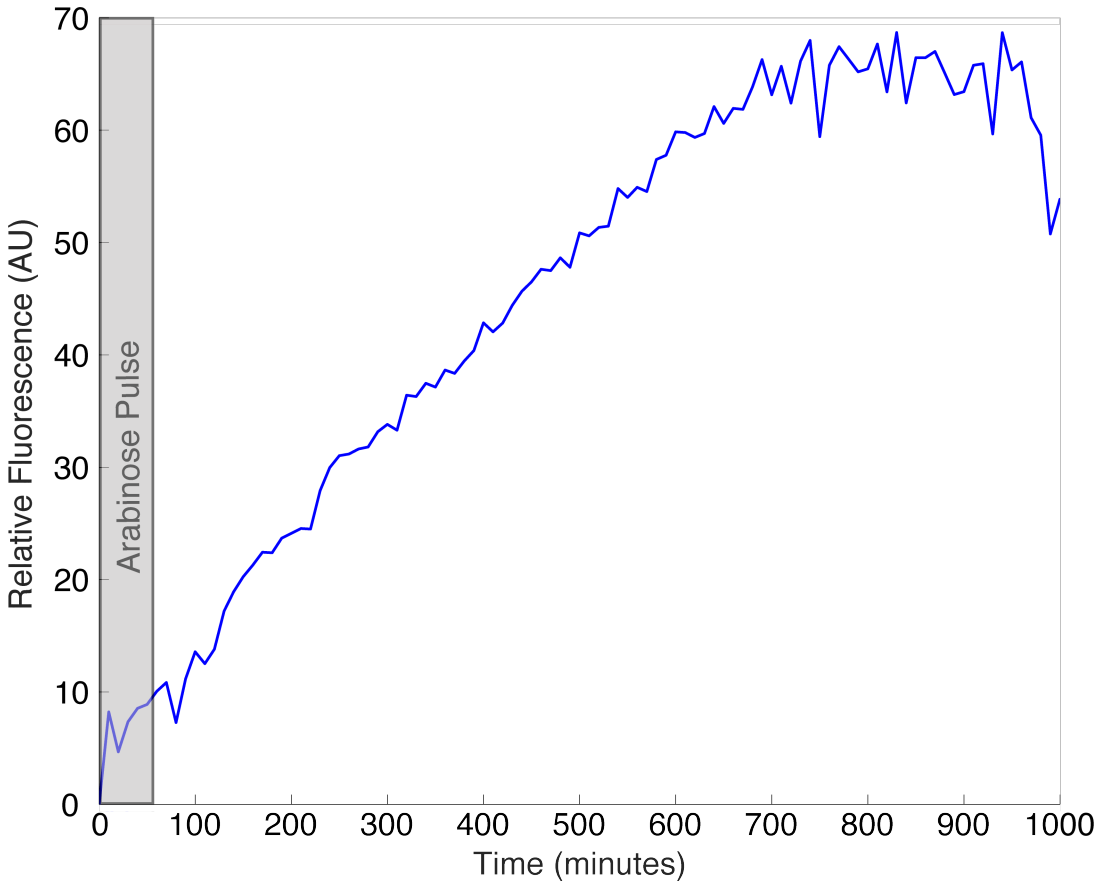

Figure 28: Transmitter bacteria were stimulated with a 50 min pulse of 20 μM arabinose followed by 20 μM glucose for the remainder of the experiment.

Another important aspect we wanted to test with the single node microfluidic device, was the growth rate comparison between the transmitter and receiver bacteria. To do this, transmitter bacteria were seeded into a single node chip while the receivers were seeded into a physically separated but adjacent chip. The chips were then placed on the heated microscope stage and imaged using bright light for a 24-hour growth period. For the duration of this growth experiment, the temperature and the flow rates were kept constant at 30°C and 75 μl/hour. Images were captured every ten minutes of chambers on both chips. The images were then compared after completion of the experiment. The time

period that was of most importance, was the time required for the bacteria population to fill the trapping chamber. Since initial seed count can effect this, we compared transmitter chambers and receiver chambers that contained similar initial seed count. The results showed that the transmitter and receiver bacteria grew roughly at the same rate with only a +/- 1.5 hour difference. This difference is easily manageable when transitioning to both population growing in the same microfluidic environment for the two node device communication experiments.

3.4 Conclusion

The single node microfluidic device was designed and fabricated, utilizing photolithography, PDMS casting, and plasma bonding. Two design iterations were created and tested, the first to examine the effects of chamber size, and the second to increase experimental output. These devices housed bacteria in small trapping chambers, while providing fresh media or chemical stimuluses and removing excess bacteria and waste. Experimental methods were developed to reduce complications such as contamination, air bubbles, and clogging.

The initial receiver experiments showed that chamber size did not affect the bacterial response, while the exposure time to the chemical stimulus AHL did impact the response. A 50 min pulse of AHL was given to the receiver bacteria while their GFP output was reordered using fluorescent imaging. This experiment was repeated to establish the duration of the response. This duration was key to establishing an improved encoding method in which the time between bacteria responses equated to bits of information. This work established the ability of the receiver bacteria to thrive in the microfluidic

environment, respond to chemical stimulus in a way that is easy to monitor, and that the response can be controlled in a manor by adjusting the input.

The transmitter bacteria strains tested lead to the final strain selection. The initial experimental results showed that the transmitter bacteria grow at the same rate as the receivers, are encoded for the same antibiotic resistance, and should theoretically be capable of culturing in a two node microfluidic device. The transmitters respond to arabinose, produce AHL, which in turn causes the production of GFP. We were able to stimulated the transmitter bacteria in the microfluidic environment and record their GFP output. With both strains tested in the microfluidic environment, we have established that the two node communication system will work in a co-cultured device, and we will have dynamic control of the network.

Chapter IV

RECEIVER MODELING

This chapter describes the modeling and validation of receiver bacterial gene expression in microfluidic environments. A series of generalized mass action equations were created to characterize the series of event that occur in the receiver bacteria when in the presence of AHL. This model allowed for the flexibility to adjust specific rates effected by the microfluidic environment to better capture the dynamics of the bacterial response. This model was tested on a range of concentrations, as well on prior work to test the validity. The model was then used to tackle the problem of addressing and was further validated by testing its ability to predict the output to multiple pulses. It was used in reverse to decode an AHL input, given in a series of 1's and 0's in a sequence. This model can be a valuable tool in predicting bacterial response in both bulk cultures or in the microfluidic system.

4.1 Bacteria Signaling Pathway

One of the common organisms used for biosensing is a genetically modified strain of *E. coli* that expresses genes from the quorum sensing, or autoinducer, system of *V. fischeri* [4]. In *V. fischeri,* the lactone AHL reversibly binds to the regulatory LuxR protein. This complex then binds to the promoter for the *LuxI* gene, inducing transcription. In genetically modified *E. coli*, the *luxI* promoter is engineered to control production of an unstable variant of GFP thus causing the bacteria to emit green fluorescence in the presence of AHL. The *E. coli* bacteria do not encode the genes to produce AHL, and thus act only

as reporters.

To create a model for the sequence of biological processes in which a population of genetically engineered reporter bacteria emit fluorescence in response to AHL stimulus, we first diagrammed the sequence of events that occur. Figure 29 shows a block diagram of the processes that occur in biosensing in *E. coli* with this LuxR system. Although this diagram is still a simplification of the signaling pathway from the literature [46], it illustrates reactions and chemical species not accounted for in previous modeling efforts and is generally applicable for both macro- and microfluidic environments.

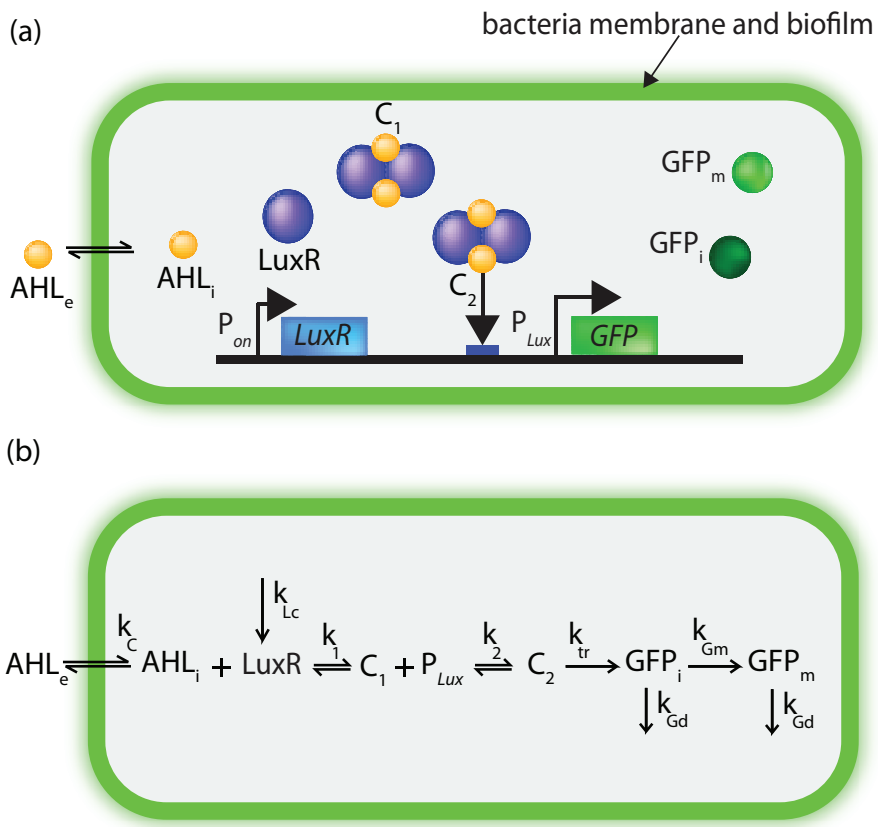

Figure 29: (a) The genetically engineered *E. coli* strain MG1655 has a LuxR signaling pathway that receives external AHL (AHLe) and produces mature GFP (GFPm). (b) In this signaling pathway, we illustrate the most significant biological molecules (e.g., AHLi, LuxR), complexes (denoted as C_n, where n is an integer), and gene sequences (e.g,. promoter P_{Lux}) with rates, k_i.

In this system, "external" AHL_e diffuses through the biofilm material surrounding the bacteria and subsequently across the bacteria membrane, becoming "internal" AHL_i at rate k_c. A constitutive promoter, P_{on}, drives the expression of the *luxR* gene that codes for the AHL receptor protein, LuxR. AHL_i and LuxR form a dimer complex (C_1), which reversibly binds to the *luxI* promoter sequence, P_{Lux}, forming complex C_2 that induces transcription and translation at rate k_{tr} of an unstable, immature variant of Green Fluorescent Protein (GFP_i). GFP_i folds into a mature fluorescent form GFP_m. Both GFP_i and GFP_m can degrade at rates k_{Gd} (See Figure 29).

4.2 Receiver Modeling

Our modeling method utilizes generalized mass action equations, GMA, based upon the chemical pathway shown in Figure 29 (b). Transcription and translation were represented as a b single species to simplify the model, while other biological processes affected by the microfluidic environment, such as diffusion of signal molecule AHL, and maturation of GFP, were kept accessible. The general form of a GMA system of ordinary differential equations is given by

$$\dot{X}_i = \sum\left(\pm k_i \prod X_j\right) \tag{1}$$

where $\dot{X}_i$ is the rate of change of a concentration of molecular species *I*, k_i is the corresponding rate constant, and X_j is a concentration of molecular species *j*. For the processes described in Figure 29, the following equations were determined to model the bacteria response:

$$\frac{dAHL_i}{dt} = k_c(AHL_e - AHL_i) - k_1 AHL_i^2 LuxR^2 + k_1 C_1, \tag{2}$$

$$\frac{dC_1}{dt} = k_1 AHL_i^2 LuxR^2 - k_1 C_1 - k_2 C_1 P_{Lux}, \tag{3}$$

$$\frac{dC_2}{dt} = k_2 C_1 P_{Lux} - k_2 C_2 - k_{tr} C_2, \tag{4}$$

$$LuxR = LuxR_T - 2C_1 - 2C_2, \tag{5}$$

$$\frac{dGFP_i}{dt} = k_{tr} C_2 - k_{Gm} GFP_i - k_{Gd} GFP_i, \text{ and} \tag{6}$$

$$\frac{dGFP_m}{dt} = k_{Gm} G_i - k_{Gd} GFP_m. \tag{7}$$

AHL_i and AHL_e are the concentrations of internal and external AHL, respectively; LuxR is the population of free LuxR, and $LuxR_T$ is the total amount of LuxR in the system; C_1 is the LuxR-AHL dimer; C_2 is the complex involving the dimer bound to the promoter sequence; GFP_i represents "immature" GFP, in its inactive, non-fluorescent form; and GFP_m represents mature, fully fluorescent GFP.

The rate constant k_c governs mass transfer through the bacteria membrane and biofilm. Nilsson [47] previously determined this rate of diffusion for membrane and biofilm separately; k_1 governs the association and dissociation of C_1; k_2 governs the association and dissociation of C_2; k_{Lc} represents the constitutive rate of production of LuxR and is is assumed to be equal to the degradation rate of LuxR; k_{tr} is the rate of protein production of GFP, encompassing transcription and translation; k_{Gm} governs GFP maturation; and k_{Gd} governs the rate of GFP degradation. Note that k_{Gd} is the same for both G_i and G_m, as GFP degradation proteases do not differentiate between the species. The vector **k** represents the set of rate constants $\mathbf{k} = (k_c\ k_1\ k_2\ k_{tr}\ k_{Gm}\ k_{Gd})$.

This system of ordinary differential equations was solved numerically in MATLAB using Euler's method. The set of initial values for the rate constants was based on literature as shown in Table 1. Rate constants $k_1$and k_2 were held fixed because they are processes that are independent of environment (e.g, oxygen concentration, biofilm) and thus literature values were assumed accurate, while k_c, k_{tr}, k_{Gm} and k_{Gd} were allowed to vary by up to one order of magnitude from literature values. To determine the quality of fit for each vector **k**, the sum of square errors (SSE) was calculated between the numerically approximated result and the experimentally measured fluorescence. SSE was minimized by iteratively adjusting **k** with an interior-point algorithm [48]. After a set of rate constants that

minimized SSE was found, their sensitivity was analyzed. Rate constants k_i were individually varied in increments of ±100%, ±10%, ±1%, ±0.1% while holding the others constant to create a vector $\mathbf{k}_n$ for which a new SSE was calculated. The difference in error between $\mathbf{k}$ and $\mathbf{k}_n$ was then plotted to determine the sensitivity of each rate constant. This showed which variables have the greatest influence on the model and therefore must be considered when adjusting for the microfluidic environment.

4.3 Results and Discussion

Figure 30 shows the relative fluorescence response of the bacterial populations in the microfluidic chambers to AHL stimuli of varying concentrations at constant 50 min duration. Figure 30 inset shows the amplitude of the relative fluorescence response to a 50 min pulse of AHL at concentrations from 10 μM to 30 μM (though 10 μM AHL did not elicit a response above the noise threshold (signal-to-noise ration greater than five [45]) and 30 μM approaches saturation). The relative fluorescence response data in Figure 30 is averaged across at least five trials at each concentration. For each concentration, experimentally and modeled, we determined threshold fluorescence, 95% of peak fluorescence, peak fluorescence, response delay, ramp-up time, response duration, and ramp-down time. Peak time averages 124.9 min for this range of concentrations. We measured an average absolute difference between the modeled and measured peak times for all concentrations as 17.1 min, or 14% error. Individually peak time averages (and absolute differences between modeled and measured were as follows: 79.8 min (22.6 min), or 28%, for 15 μM; 109.9 min (0.1 min), or 0%, for 20 μM; 170.0 min (32.8 min), or 19%, for 25 μM; 140.0 min (12.9 min), or 9%, for 30 μM. To our knowledge, no other reported

model for genetically engineered bacteria has the capability of predicting response peak time for time-varying stimuli. This feature of our model is important for applications in biosensing because the delay between stimulus and peak critically informs stimulus onset time.

Applications of engineered bacteria also involve communication networks [45], in which the response delay, ramp-up time, response duration and ramp-down time are important for data rate determination. Across all concentrations, we measured average (and absolute difference between modeled and measured) values as the following: response delay = 34.3 min (17.6 min), ramp-up time = 77.5 min (15.2 min), response duration = 344.54 min (114.5 min), and ramp-down times = 241.37 min (95.4 min). Corresponding errors range from 20%-52%. These errors are large, but represent the first modeling effort to date at capturing such dynamics of a bacterial population in a microfluidic environment. Communication schemes are being developed [45, 49, 50] that accommodate these errors, while further efforts are underway to improve repeatability (see inset) and modeling accuracy. Experimental data collection is painstaking, and thus this data represents a sampling of the linear regime over which this bacterial system operates.

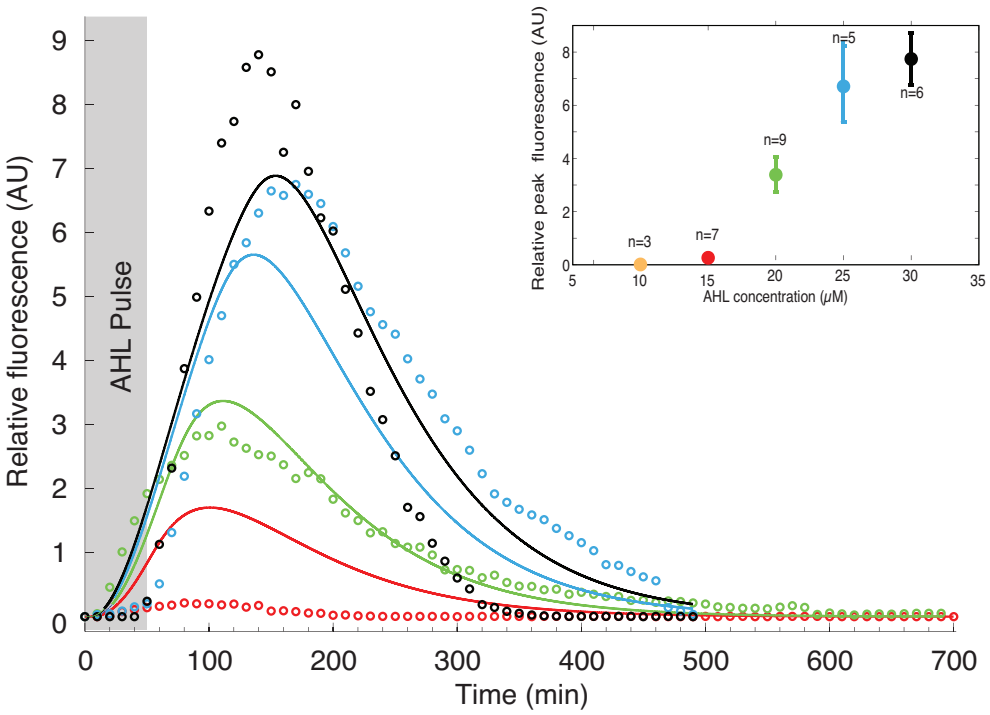

Figure 30: Modeled response (lines) overlaid with measured experimental data for the linear regime of AHL concentrations. All used a 50 min pulse of AHL (indicated by shaded area) and varying concentrations (inset). Inset shows peak amplitude of the averaged fluorescence response as a function of AHL concentration with standard deviation and number of trials.

Parameter sensitivity analysis was conducted to determine the rate constants with the greatest effect on the model fit. Rate constants of high sensitivity produced divergent SSE values. The GMA model had the highest sensitivity to the rate parameter for GFP maturation, k_{Gm}. The expression of over 200 genes in *E.coli* can be affected by oxygen concentration [25], and during the maturation of GFP, from immature GFP_i to mature GFP_m, a high amount of oxygen is needed [51] . The oxidation processes has been quantified and found to be rate limiting [52] and this has been quantified [53]. This shows the importance of adjusting this term to account for changes in the environment. Critically,

during maturation of GFP, from immature GFP_i to mature GFP_m, a high amount of oxygen is needed [51] and thus this term is very sensitive to the microfluidic environment.

For the constant flow rate in all experiments, shear stress is constant, thus biofilm thickness is constant, and thus oxygen diffusion rate is constant. We verified that by lowering the AHL diffusion rate, k_c, the modeled bacterial response was slowed as expected. Using parameter estimation, rate constants matching the kinetics of our system were determined, as shown in Table 1 (and used to generate the models of Figure 30). As previously mentioned, rate constants k_1 and k_2, are constant regardless of environmental factors (e.g., diffusion rate, oxygen concentration). AHL diffusion rate, k_c, was slowed from 3600 hr^{-1} to 254 hr^{-1}, a 93% change. This change accommodates dramatically slowed diffusion through the biofilm in addition to the bacteria membrane.

The GFP maturation rate, k_{Gm}, was decreased from 3.6 hr^{-1} to 1.8 hr^{-1}, a 50% change. This change has been suggested qualitatively in literature [51], but has not heretofore been quantified for a microfluidic environment. Constant k_{Gm} is rate-limiting [52], and our analysis confirms its sensitivity. Although it is not clear how the microfluidic environment can affect protein production rate (k_{tr}) and GFP degradation (k_{Gd}) rate, we note an increase in both in our model. Specifically, k_{tr} was found to increase by from 150 hr^{-1} to 1334 hr^{-1}. Some literature suggests that gene expression (e.g., k_{tr}) in *E.coli* can be affected by oxygen concentration [25], but this is not well understood and indicates an area of future study. In our model, rate constant k_{Gd} was found to increase by nearly 10x over published values [33]. GFP degradation is not commonly studied since most prior work focuses on constant rather than time-varying inputs. Some have assumed changes in k_{Gd} are negligible [10], and some have ignored this parameter altogether [9], while we report

here that it is critical and varies between the macro- and micro- environment. we also explored whether AHL degradation, due to bacteria consumption, should be included in the model. We found this effect was negligible, effectively zero, relative to the AHL mass transfer by diffusion through the bacteria membrane and biofilm (rate constant k_c).

Table 1: Published and best-fit modeled rate constants for the metabolic processes for AHL-mediated GFP expression in reporter bacteria in a microfluidic environment. Sources for published bulk (non-microfludic) rates are noted and whether these published values were adjusted in our model to accommodate for the changes due to the microfluidic environment.

Rate constant	Rate Description	Published bulk rate (hr^{-1})	Best-fit microfluidic rate (hr^{-1})	Adjusted	Source(s)
k_c	AHL diffusion	3600	254	yes	[47]
k_1	C_1 formation/dissociation	60	60	no	[32]
k_2	C_2 formation/dissociation	600	600	no	[32]
k_{tr}	Protein production	150	1334	yes	[32]
k_{Gm}	GFP maturation	3.6	1.8	yes	[32]
k_{Gd}	GFP degradation	4.15	39	yes	[33]

The generalizability of this model to other microfluidic experiments with genetically engineered bacteria can be seen by examining the work done by Meyer et al [10]. In their study, a similar microfluidic enviroment was used to predict relative fluorescence of GFP by *Pseudomonas pupida* IsoF biosensor strain in response to several external AHL concentrations, utilizing the Hill equation. To explore if our model was relevant to Meyer's data, we performed the following procedure. The published bulk rate values cited by Meyer were used to constrain our parameter estimation (See Meyer et al

[10] Table 1). As before, rate constants k_1 and k_2 were fixed, while k_c, k_{tr}, k_{Gm} and k_{Gd} were allowed to vary by up to one order of magnitude from initial values with parameter estimation using the same Equations 2-7 and again minimizing SSE by iteratively adjusting **k** with an interior-point algorithm.

In Figure 31, we present a comparison of Meyer's model to our GMA model. Meyer acknowledged that their model did not fully describe the shape of the kinetics for this bacteria population [10]. As shown in Figure 31, our model better captures the shape of the response at later times by accomodating rate constants that capture reduced oxygen concentration. Both the Hill model and our generalized mass action model are first order responses to Meyer's step input, while the measured response exhibits second order dynamics. The Hill model better captures early dynamics (e.g., 0-240 min), while the error over the entire time period is greatly improved with our model. The models were quantitatively compared by calculating mean squared error (MSE) between each model fit and the data from Meyer. The MSE for the Meyer model fit was 1.62×10^6 (AU), where our GMA model MSE was 1.28×10^4 (AU), a two order of magnitude improvement.

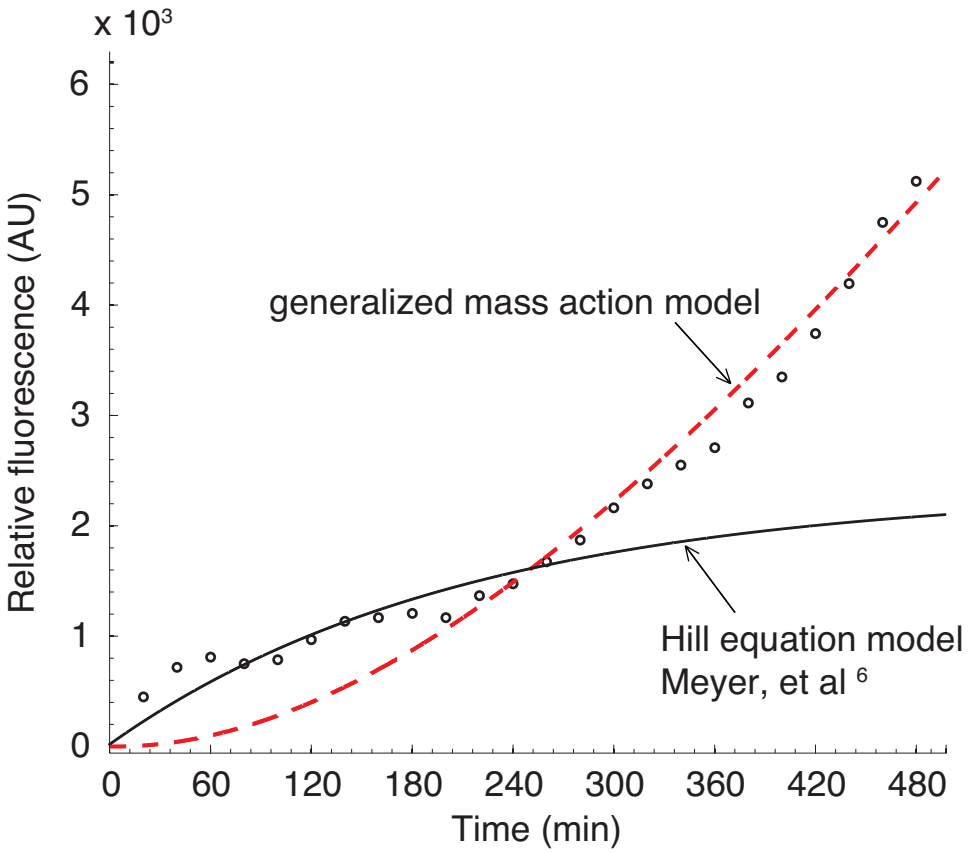

Figure 31: Data (circles) and model (solid line) reproduced from [10]. The generalized mass action model fit (dashed line) has an improved mean squared error over the duration of the experiment.

Although the model we have created captures the dynamic response of the receiver bacteria, there are simplifications and assumptions that deviate from the physical actions. The processes in the bacteria are incredibly complex and any model will have some simplifications. We examined areas that were simplified in previous modeling attempts that needed to be more complex to adapt to the microfluidic environment. Although we did add complexity to our model, there is still room for future exploration. The following details these key simplification areas.

We assumed in the case of the bound C_2 complex, that after transcription the complex would completely disassociate and the AHL would degrade shown in Equation 4. This was a simplification of the actual process in which C_2 would first unbind and become C_1, which could then disassociate, and AHL could degrade or diffuse out of the cell. In the case of k_1 and k_2, we assumed the rate constant for the forward reaction was equal to the rate constant for the reverse. This would not likely be the case biologically, and initially separate rate constants were included for the forward and reverse reaction were included in the model. When a sensitivity analysis was conducted, it was found that the model was insensitive to these rate constants. When the forward and reverse rate constants were assumed to be equal, the models fit was not impacted. These results lead to the decision to simplify the model.

In the characterization of the dimer formation equations 2 and 3, it suggests that all four components come together at once. In actuality, a single LuxR binds to a single AHL. Then this complex binds to another identical complex, forming a new complex with two AHLs and two LuxRs. By combining these steps, a squared term was created for both AHL and LuxR seen in Equations 2 and 3. This method of having a quadratic term to describe the dimerization of AHL and LuxR can be seen in literature, such as the work by Basu et al. [33]. If there was no simplification in this step, there would be a rate constant for a LuxR combining with an AHL, then a second rate constant with the complex squared.

If this change in characterizing the dimer formation where implemented, it could have an impact on the models ability to capture the dynamics of the bacterial response since the term order for that formation would decrease from fourth to second. Although this simplification exists in our current model, sensitivity analysis conducted suggests that the

impact the dimerization term has on the model fit is minimal when compared to the GFP maturation and degradation. Furthermore, the time required for dimerization is around 10 seconds [32], while the maturation of GFP is greater than 10 mins [54]. These insights suggest the model is dominated by the GFP maturation, and although undoing the dimer formation simplification could impact the model, it is thought that the impact would be minimal. Although this thesis work utilized the model above, the appendix section will provide an alternative set of mass action equations that could be implemented for future work that better captured the physical actions in the bacteria.

4.4 Encoding Data in Bacteria Signals

To take our model a step further, we worked with our collaborators in Sivakumar's lab to encode digital signals in bacterial communication and then later decipher the input using our generalized mass action model. In our system we used a digital signal consisting of ones (50 min pulse of AHL) and zeros (50 mins no stimulus).

Traditional bacterial biosensors, such as the multichannel biosensor metal detector [1], rely on a receiver bacteria for each chemical or metal of interests. They must sample each population in order to monitor the biosensor environment. This can be an inefficient method when scaled. To remedy some of the computational and monitoring burden, we created a system in which a single receiver population can give the same information as the many receivers required before. Theoretically this would be accomplished by utilizing multiple transmitter bacteria populations, each capable of detecting something different in the surrounding environment. Those populations would relay the message via a common secondary chemical signal to a single receiver bacteria population. The single receiver

bacteria population fluorescent output could then be monitored and analyzed. A more in-depth discussion of the methodology can be found in our collaborative work [55], but we will discuss it briefly here.

Addressing is traditionally used to identify or specify the destination. For e.g., in postal services and e-mails, address is used to find the receiver and for the receiver to identify the sender/source. In this work, we focus on source addressing, where a receiver utilizes the addressing mechanism to identify the source when identical and independent sources communicate to a receiver.

In this theoretical system our single receiver population deciphers a received signal, identifies the transmitter population and creates a timestamp. In order for the receiver population to differentiate between transmitter populations, each transmitter population would produce a different concentration of the secondary chemical (AHL) signal shown in Figure 32. These different concentration levels would be distinguishable by the receiver. The concentration levels would need to be tuned uniquely to ensure that a combination of any two transmitter concentrations would not equal a single transmitter concentration. For example, if population A sent an AHL concentration of 1 while population B sent a concentration of 3, population C cannot send a concentration of 4. This would lead to the receiver population inability to determine if population A and B sent a signal at the same time, or if population C sent a signal alone. Since we had determined the detectible range of concentrations for the receivers, shown previously in Figure 30, we were able to determine possible concentration levels.

With the transmitter side established, we shifted our focus to the receiver decoding. Using the generalized mass action model in reverse, we developed a means to input the

fluorescent response of the receivers, and output the original AHL (secondary chemical stimulus). Figure 32 shows a representation of this process.

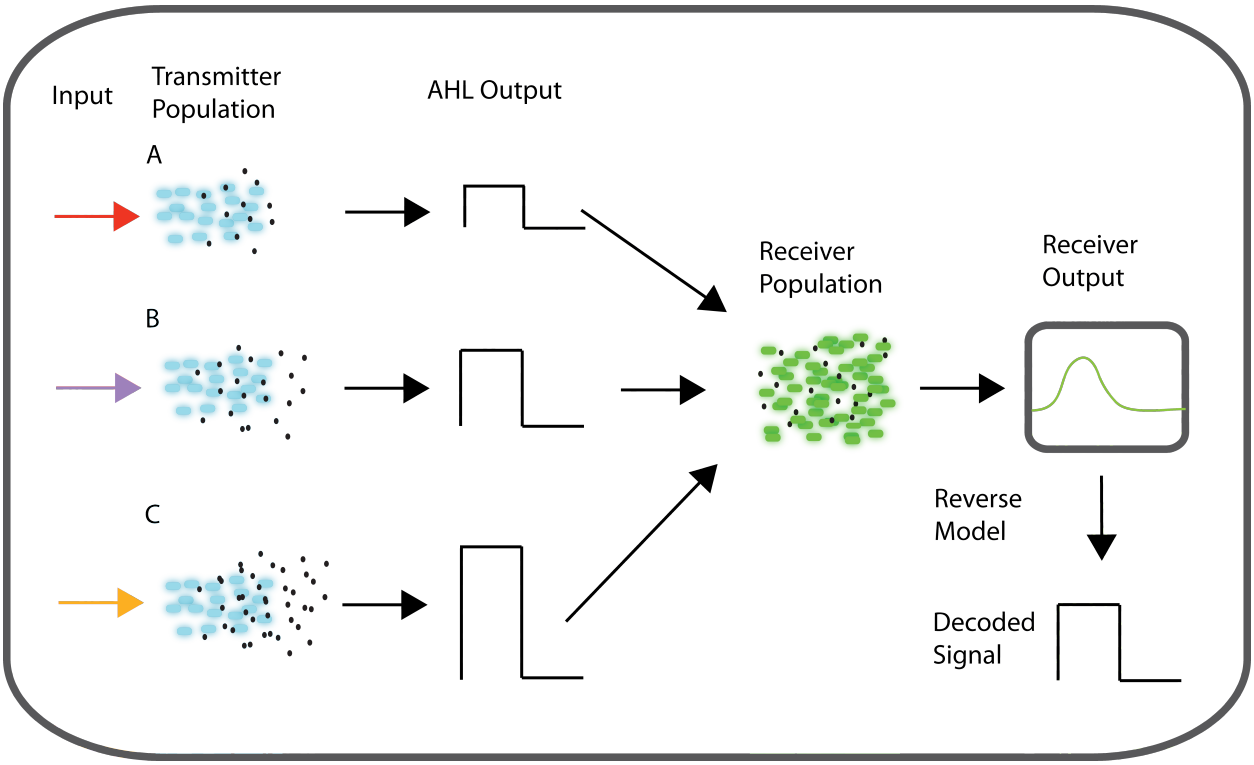

Figure 32: Illustration of bacterial addressing. Three different inputs are given to a transmitter bacterial population. Each transmitter bacterial population is responsible for detecting a specific input. The transmitter populations then produce a unique concentration level of AHL. This AHL it then given to the receiver bacteria. The receivers produce GFP in response to the AHL, creating a signal that can be inputted to the reverse model. The reverse model then decodes the signal and indicated which populations (A, B or C) sent the message and the associated time.

Since we had previously shown the ability of the receivers to detect varying concentrations of AHL with a single pulse and capture the dynamics with the model, we

wanted to test the model's capability with multiple pulses. As stated before, an "AHL pulse" is the duration and concentration over which the AHL was delivered to the bacteria chamber. Pulse durations of 50 minutes, that we have previously optimized, were used for "on" or "bit 1" state; while 50 minutes of no AHL equated to "off" or "bit 0" state.

For the following experiments a single concentration, 15 μM, was used to focus on the effects of multiple pulses. All digital sequences were tested by adjusting the first 10 bits followed by no AHL for the remainder of the experiment. We first tested the two extremes, all zeros and 1010101010, shown in Figure 33. Individual curves are shown in Figure 34, demonstrating = that although there is some variation in the amplitude, the features of the curves align. When no AHL is present, there should be no fluorescence. This was shown to be true both experimentally and with the model. With the 1010101010 sequence, the model closely captures the dynamics. Additionally, we tested other input sequences, one of with is shown in Figure 35. The digital input in this case was 1000100010. The model was able to capture the peak timing, which was critical for the decoding method.

In total the following input signals were tested: 1010101010, 1000100010, 1010000010, and 0000000000. The ability of the inverse model to decode the fluorescent bacterial output was found to have the following decoding efficiencies, respectively: 90%, 100%, 80%, 100%. Each tested sequence had a sample size of at least 4. These experiments are very time intensive and challenging due to the nature of bacteria. There are numerous factors that affect the bacteria's ability to process the AHL input and produce the GFP output. We have made great strides in controlling several of these factors such as temperature, population size and nutrients, by utilizing our microfluidic device, but several

factors remain out of our control. These uncontrollable factors can fluctuate and cause small variations in the bacterial response which can lead to lower decoding efficiencies. This is likely the cause for the 80% decoding efficiency of one sequence.

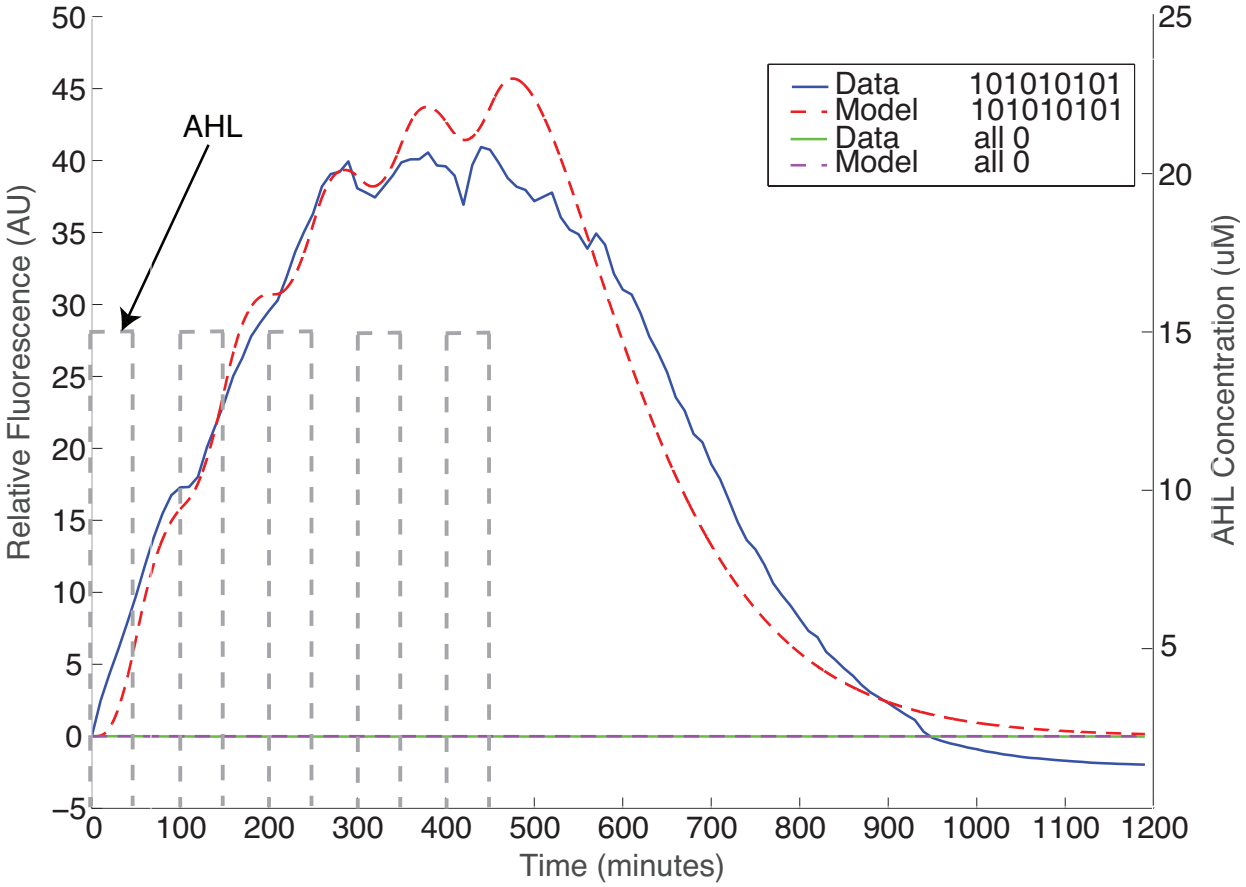

Figure 33: Experimental and model results for encoding a digital signal in the receiver bacteria. The two extreme sequences were tested.

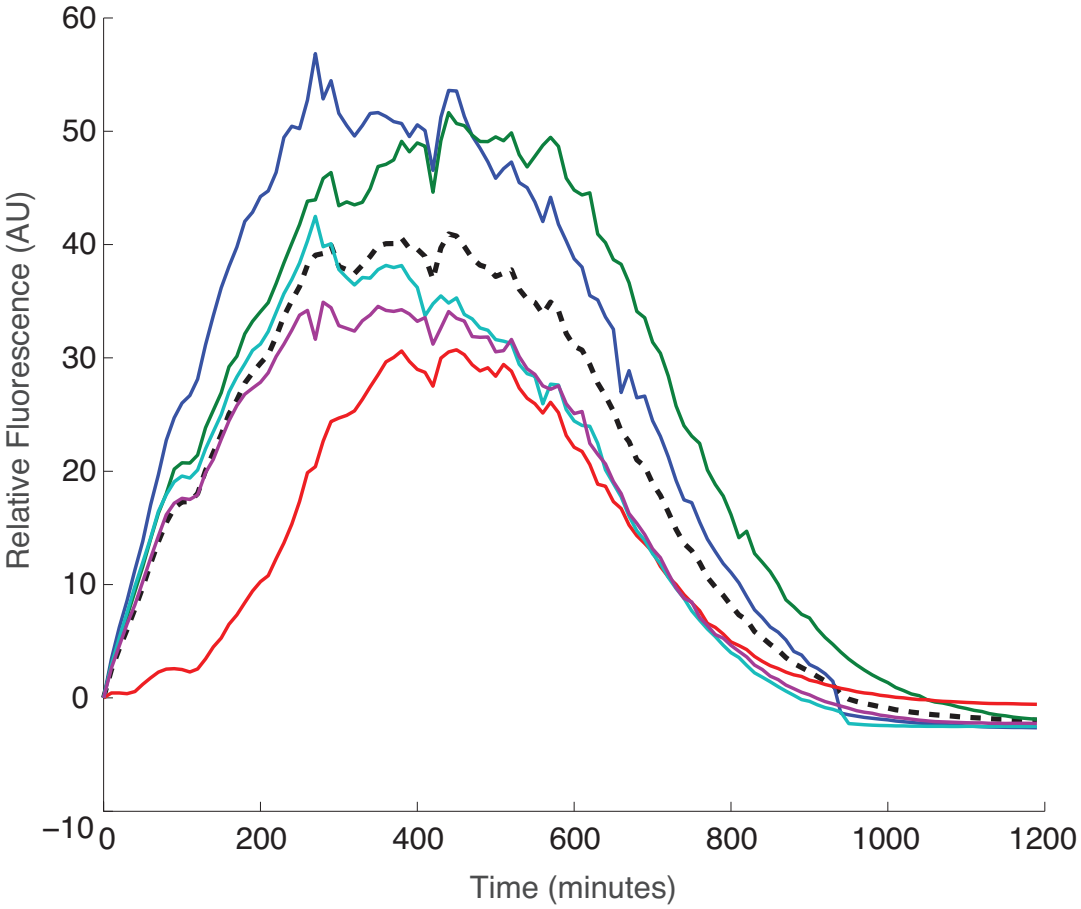

Figure 34: Individual curves used to obtain averaged curve (dashed line) demonstrating experimental variability. These are the results for the 1010101010 AHL input.

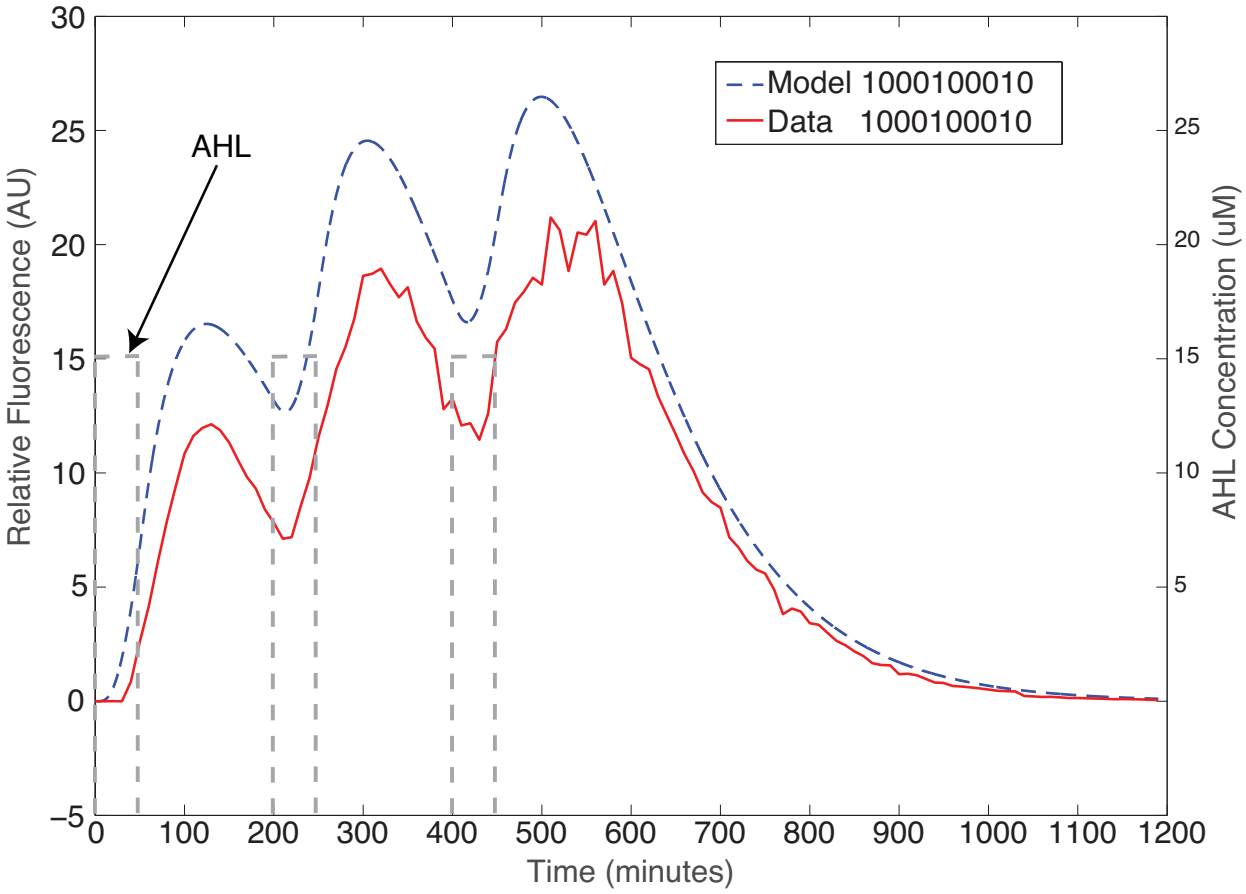

Figure 35: Experimental and model results for encoding a digital signal in the receiver bacteria. The two extreme sequences were tested.

4.5 Conclusion

Using a series of generalized mass action equations, we created a model that captures the dynamics of autoinducer-mediated bacterial gene expression, specifically AHL-mediated GFP expression, in reporter bacteria in a microfluidic environment. We subsequently fit that model to experimental data from both our laboratory and that of Meyer et al [10]. The model accurately captures the response peak time, with 14% error, and somewhat captures the response delay, ramp-up time, response duration, and ramp-down time for time-varying inputs across a range of input concentrations. The model is a

substantial improvement, as measured by mean squared error, over prevously reported models for time-constant inputs in microfluidic environments.

Four of the six rate constants involved in metabolic processes for AHL-mediated GFP expression in reporter bacteria were found to vary between the macro-environment and the micro-environment explored in this work. By relaxing assumptions made in prior modeling efforts, we were able to capture AHL diffusion rate changes, GFP transcription and translation rate changes, GFP maturation rate changes and GFP degradation rate changes. These rates changed due to increased biofilm formation in the microfluidic environment, which resulted in changes in oxygen and AHL concentration from what would be expected in bulk conditions. Most sensitively, GFP maturation is a sensitive, rate-limiting step and this rate is greatly affected by oxygen content.

The receiver bacteria were tested over an array of concentrations and with multiple pulses. This model is versatile: applicable to microfluidic or traditional macro-environments; it can be used with time varying (pulse) or constant (step) inputs. This model can serve as a valuable tool in understanding genetically engineered bacteria and improving biosensor design capabilities, opening the door for sensors that adapt to environmental dynamics and communicate with each other.

Chapter V

TWO NODE MICROFLUIDIC DEVICE

This chapter describes the design, fabrication, and testing of a two-node microfluidic system to house both sender and receiver bacteria population to enable stimulation and measurement of communication between the two populations. A porous monolith was developed inside a PDMS microfluidic channel. This monolith acted as a filter between the transmitter and receiver bacteria populations, that prevented cross contamination while allowing the diffusion of small molecules between them. This is the first microfluidic device to our knowledge that allows for the long term monitoring of bacterial communication in a microfluidic device with no cross contamination and dynamic control over inputs.

5.1 Two Node Device Design

To successfully house two separate populations of bacteria, they must be physically separated while allowing the diffusion of small molecules. Our first design constraint was that the two populations could not cross contaminate. If sender bacteria were to reach the receiver population and begin populating, the results from our receivers would be affected due to a possible local AHL production. As discussed in the background section, there have been three attempts so far to our knowledge to physically separate two populations of bacteria. The micro-ratchet structure [34] exploited the fact that their strain of bacteria often swim in one particular direction, to create essentially a maze for the bacteria to become trapped in. The small molecules were then free to diffuse across a series of

channels. This method led to significant cross contamination between the populations. It was clear from this and from our own experience that to keep the populations completely separated, a filter of some sort must be used. The two other groups mentioned before did in fact use filters to separate the populations. The first used a multi-layer PDMS device with a porous membrane sandwiched between two layers of PDMS [35]. This device was successful and listed no contamination, but there was no dynamic control (no flow) over inputs and the multilayers made imaging difficult. The third group housed bacteria in an alginate gel and separated them using chitosan membrane [36, 37]. Since the chitosan membrane was formed using a pH gradient, the geometry of the device is greatly limited. The alginate gel they used to house the bacteria was intended to hold the bacteria in place and act as a mock biofilm. This poses several issues some of which are the unknown effects on the bacterial growth, chemical stimulus production, and GFP production. Additionally, their experiments were limited to 12 hours after which point the bacteria outgrew the alginate gel and, from their own images, they appear to pass through the chitosan membrane.

When designing our two node microfluidic device, there were several filtering mechanisms we considered. Traditionally filters are integrated into the PDMS structure of the device, for example [56, 57]. Common filtering structures include pillars, angled ridges, and capillary channels. These features allow the separation of cells or particles by size and are created using the same photolithography techniques listed in section 3.2. Unfortunately, fabrication techniques limit the smallest achievable feature size to 1 μm. Since the size of our bacterial strains on average are 1 μm long and 0.5 μm in diameter,

they could easily pass through any PDMS filtering technique making this a nonviable option.

Next we considered integrating a porous membrane sandwiched between two layers of PDMS. The fabrication method can be challenging to ensure no leakage in the device. Additionally, for this to work the transmitter population and receiver population would have to be held in separate layers of the device making imaging very difficult. In our single node microfluidic devices, imaging is done through a very thin cover slip which allows ease of imaging. With a multi-layer device, we can still image one of the population types through the thin cover slip, but since the other population is located in a different layer of PDMS, imaging must be completed through a layer of PDMS. Although PDMS is optically transparent, there is a limitation on our microscope equipment z range. With our current equipment and fabrication difficulties, this option was deemed impracticable.

After many design considerations and examining the previous works, we decided on utilizing a porous monolith inside a PDMS design to act as a filter between the populations. The monolith will be a great tool because it can be patterned in any desired design since it is activated using UV light, and the pore size can be adjusted to the desired size by adjusting the poragen solution concentration. Once the filtering method was decided, the following list of design constrains were considered: constant flow of nutrients for both populations, reduced clogging potential, and maximizing AHL reaching the receiver population.

5.1.1 Microfluidic Design

Similar to our single node chip, we used trapping chambers to house the bacteria populations. A center monolith channel acted as a filter while two outer channels provided nutrients or a chemical stimulus for the senders. The constant flow of nutrients is critical not only for the health of the bacteria, but also to remove excess bacteria to maintain constant populations sizes for the duration of the experiment, and across all experiments. To maximize the amount of AHL that reaches the receivers while minimizing clogging potential, we used COMSOL modeling, shown in Figures 36, 37, and 38, to test several designs. We needed to minimize low velocity areas in the main channel because these areas would allow for unwanted bacterial growth that could eventually clog the device. Additionally, we utilized forced convection into the trapping chamber to reduce the amount of AHL diffusing into the sender channel.

There are two possible extremes, one maximizes the AHL diffusion from the transmitters to the receivers at the cost of low velocity dead zones, the other eliminates low velocity dead zones leading to extremely low AHL diffusion. We first tested these two extremes using COMSOL modeling and the results are shown in Figures 36 and 37. When the design benefits the elimination of low velocity dead zones, as shown in Figure 36, the percentage of AHL that can diffuse across to the receiver population is only 0.02%. Since this concentration retainment would result in a signal well below the detection limit of the receivers it would not be viable. The continuous flow in the channel adjacent to the trapping chamber essentially generates a constant zero concentration boundary condition. This in turn results in almost all AHL diffusing into the channel rather than diffusing across the monolith to the receivers.

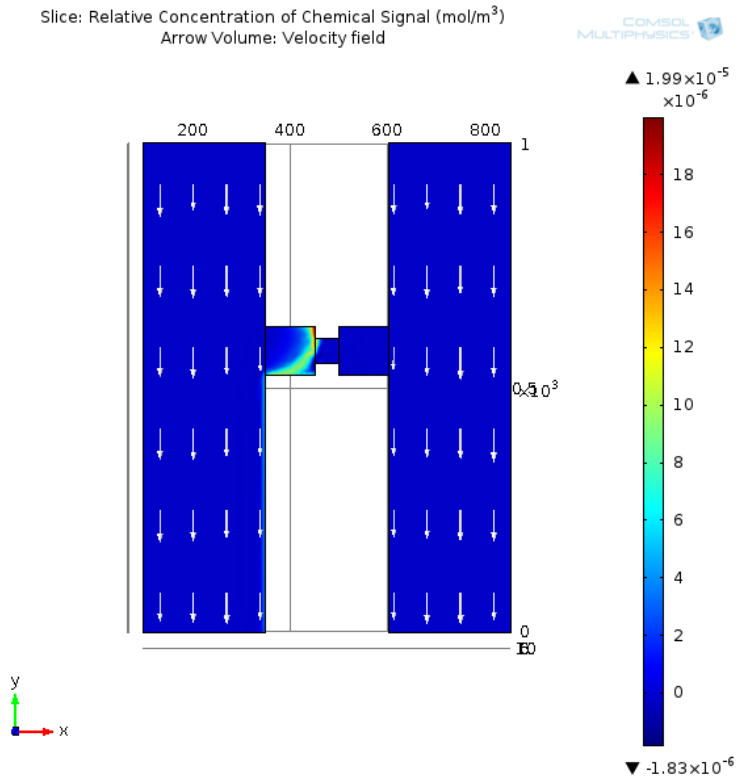

Figure 36: Two-node microfluidic chip COMSOL modeling for straight channels. The arrows represent the velocity fields and the color intensity represents the AHL concentration (blue low to red high).

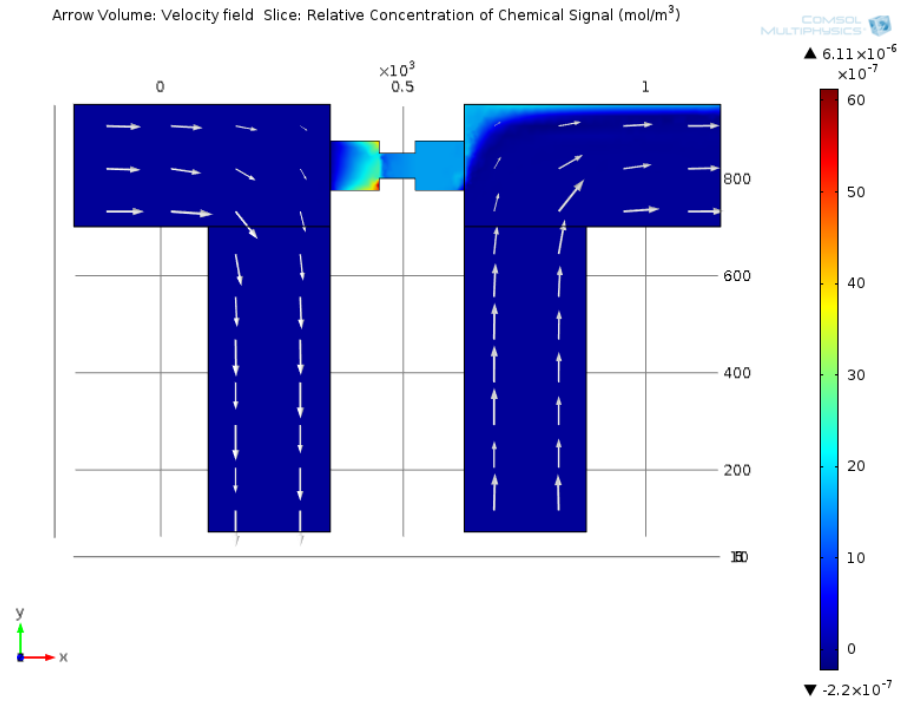

Figure 37: Two-node microfluidic chip COMSOL modeling for 90 degree channels. The arrows represent the velocity fields and the color intensity represents the AHL concentration (blue low to red high).

The design that maximizes AHL diffusion across the monolith, as shown in Figure 37, resulted in a highly 99.9% of the AHL concentration reaching the receiver population. Although these results suggest an extremely efficient design, low velocity fields are formed in the corners of the channels. These dead zones created ideal bacterial growth conditions, causing unwanted bacterial populations outside the trapping chambers, clogging the flow in the microfluidic device

(within 2-3 hours). This clogging prematurely ended the experiment terminating long term experimentation capabilities.

To balance these two extremes, we developed an angled channel shown in Figure 38. This design resulted in a detectable 30.6% of AHL reaching the receiver bacteria

population. Although there were lower velocity locations in this design, there were no true dead zones that would lead to unwanted bacterial growth. Since this design balanced between the two competing limitations, we chose it for all future chip design discussed in section 5.1.3.

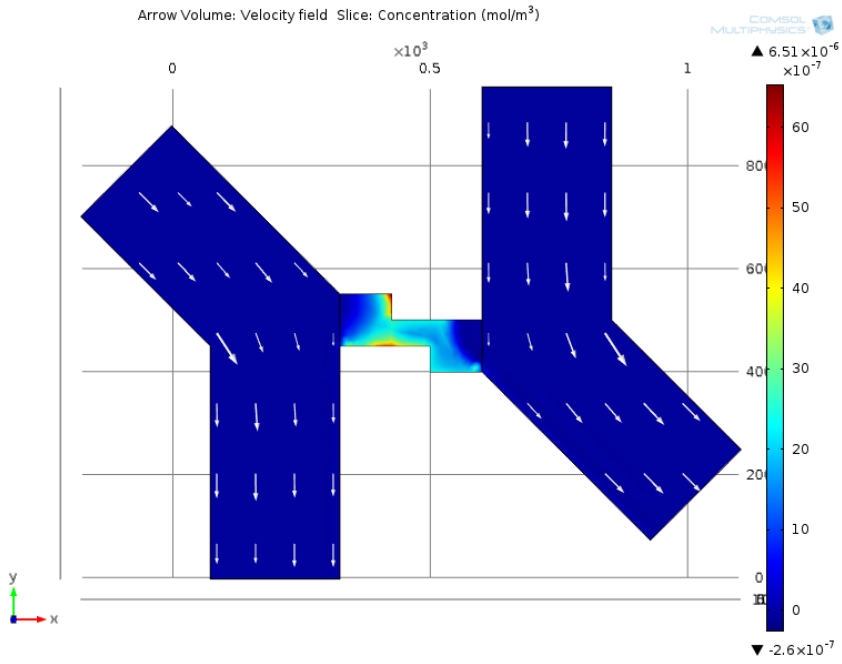

Figure 38: Two-node microfluidic chip COMSOL modeling for final design. The arrows represent the velocity fields and the color intensity represents the AHL concentration (blue low to red high).

5.1.2 AHL Diffusion Time

A crucial calculation moving forward to the two node bacterial communication experiments, is the time required for AHL to diffuse from the transmitter bacteria to the receiver bacteria. This diffusion time correlates to the delay between the start of the fluorescent output of the transmitters, and the start of the fluorescent output of the receivers. We will compare this diffusion time to experimental results in chapter six.

Although there are many factors that can effect this diffusion time such as miniscule convective forces and biofilm, we focus on the delay due to the monolith.

Normally, Fick's law of diffusion utilizes a diffusion coefficient that depends on size and shape of the molecule, interaction with the solvent, and viscosity of the solvent. This diffusion coefficient works when considering an unobstructed medium that the molecule is diffusing through. Since the AHL passes through a porous monolith, it was necessary to calculate an effective diffusion coefficient for the slowing effect the monolith would cause. This effective diffusion coefficient considers the size of the molecule and the size of the pores. The effective diffusivity (D_e) in porous medium is shown in equation 8.

$$D_e = \frac{D\varepsilon_t\delta}{\tau} \tag{8}$$

Where D is the diffusion coefficient in gas or liquid filling the pores (m^2s^{-1}), ε_t is the porosity available for the transport (dimensionless), δ is the constrictivity (dimensionless), and τ is the tortuosity (dimensionless). Porosity is a measure of the void (i.e. "empty") spaces in a material, and is a fraction of the volume of voids over the total volume measured between 0 and 1. Constrictivity is the ratio of the diameter of the diffusing particle to the pore diameter, and tortuosity is a property of curve being tortuous with a value between 1 and 2. All constants and their respective sources, when applicable, are shown in Table 2.

To calculate the constrictivity, we first needed to establish a radius for the AHL molecule. The Stokes radius, or a hydrodynamic radius, is the radius of a hard sphere that diffuses at the same rate as the solute of interest. Equation 9 represent the Stokes radius.

$$R_H = \frac{k_B T}{6\pi\eta D} \quad (9)$$

Where D is the diffusion coefficient in gas or liquid filling the pores (m^2s^{-1}), T is temperature (K), η is viscosity of the media, and k_B is the Boltzmann constant. The values listed in Table 2, were used to calculate the 3.88nm AHL radius. The constrictivity was then calculated by taking the ratio of the AHL radius to the monolith pore size, and was found to be 0.06. This was finally used to calculate the 1.335 $\mu m^2/s$ effective diffusivity of AHL.

The distance the AHL will travel through the monolith between the transmitters and the receivers is the width of the monolith fabrication channel, 75 μm. This distance combined with the effective diffusivity lead to the calculation of the diffusion time of 70.22 mins. This means we expect the transmitter bacteria to begin fluorescing, then close to 70 mins later, the receivers will begin to fluoresce. Comparison to experimental results will be shown in chapter six.

Table 2: Coefficients and calculated values for AHL diffusion through the porous monolith. Where applicable a source is provided and blank units equate to dimensionless parameter.

Symbol	Name	Value	Units	Source
D	AHL Diffusion Coefficient	43	$\mu m^2/s$	[58]
ε_t	Porosity	0.52		[59]
R_M	Monolith Pore Size	65	nm	[59]
R_H	Stokes Radius	3.88	nm	Calculated
k_B	Boltzmann constant	1.38E-23	m^2 kg /s^2 K^1	
T	Temp	303.15	Kelvin	
η	Viscosity of Media	8.01E-07	m^2/s	Equal to water
δ	Constrictivity	0.060		Calculated
τ	Tortuosity	1		Estimated
D_e	Effective Diffusion Coefficient	1.335	$\mu m^2/s$	Calculated
x	Monolith Width	75	μm	
t	Diffusion time through Monolith	70.22	mins	Calculated

5.1.3 Chip Design

After establishing the region of interest around the trapping chambers, the next step was to design the remainder of the chip. Our first design scaled the original pair of trapping chambers to an inline series with four sets of trapping chambers (shown in Figure 39). This would allow for multiple experiments to run simultaneously, increasing the sample size from one to four. On the left side of Figure 39, there are two inlet ports, one of which will supply the transmitter bacteria fresh nutrients while the other port supplies a chemical stimulus (arabinose). The middle port is used in the fabrication of the porous monolith. The far right port will supply the receiver bacteria with fresh nutrients, creating stable population sizes. In Figure 39 (b), the region around the trapping chambers is enlarged. On the left the sender channel is in direct fluidic contact with the sender chamber (which

holds the transmitter bacteria population). There is constant flow in the sender channel which both provides fresh nutrients and removes excess bacteria and waste, creating stable population sizes. The sender monolith channel is completely filled with porous monolith and creates a barrier between the sender chamber and receiver chamber. This monolith barrier will not allow bacteria to pass from one side to the other, but it will allow the diffusion of small molecules such as the secondary chemical stimulus AHL. There is no flow in this region. Similarly, the receiver channel is in direct fluidic contact with the receiver chamber (which holds the receiver bacteria population). Once again there is constant flow in the receiver channel which both provides fresh nutrients and removes excess bacteria and waste. The trapping chamber size is 100 μm x 100 μm x 5 μm, the chamber size previously optimized during the original single node chip testing, and the monolith channel is 75 μm width x 5 μm height.

We initially tested this design and had difficulty with the porous monolith forming throughout the monolith channel. This was due to the monolith washing out into the trapping chambers. We had positive results with the first set of trapping chambers having proper monolith formation which led us to redesign the overall chip. Although this is a brief summary, the full results will be discussed section 5.3.

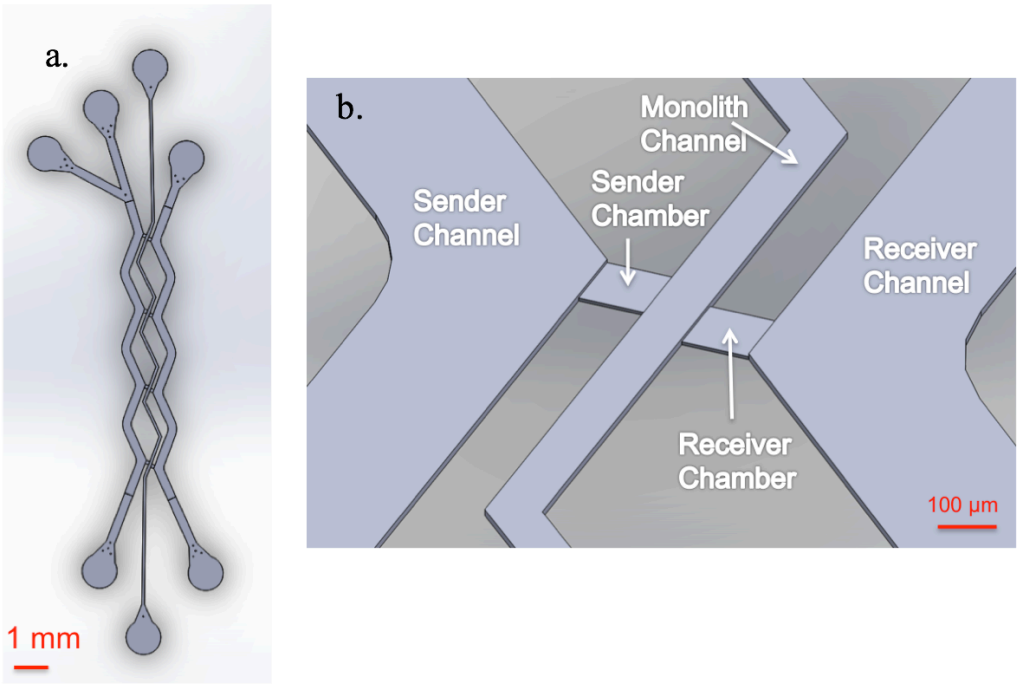

Figure 39: (a) illustrates the overall chip design of the first generation, and (b) zoomed in view of the chambers.

To combat the issues with our first generation microfluidic device, we redesigned it to have two pairs of trapping chambers in parallel. The overall device design can be seen in Figure 40 (a). Although the design appears complicated with the numerous ports, this was necessary in order to achieve parallel experimentation. The port locations had to be far enough apart so that when the metal connectors were added later for tubing, they did not cause collapsing of the PDMS channels. To reduce the number of ports, in thus the number of tubing connections, we tried to simplify the design by combining common channels. The very center port is a combination port for delivering fresh nutrients to the transmitter populations on both sides of the device. Similarly, the transmitter waste for both sides is combined into a common port. This simplification was achieved by mirroring the two halves of the chip. In this design transmitter flow channels reside in the inner portion, while

the receiver channels reside in the outer portion. As in the prior design both the transmitter and receiver channels provide fresh nutrients while removing excess bacteria and waste, creating stable population sizes.

In Figure 40, a zoomed in representation of the trapping chamber region is presented. The transmitter bacteria shown in blue resides in the left side trapping chamber. The transmitter produces the chemical stimulus AHL (shown as black dots), and the AHL is free to diffuse through the porous monolith (shown in gray) to the receiver bacteria (shown in green) in the right trapping chamber. The trapping chamber size is 100 μm x 100 μm x 5 μm, the chamber size previously optimized during the original single node chip testing, and the monolith channel is 75 μm across. The monolith channel height was increased to 10 μm. This increased the surface area of the porous monolith to anchor to the PDMS wall, while decreasing the possibility of the porous monolith solution washing out into the much shorter 5 μm trapping chambers. Since this design allowed correct formation of the porous monolith in the desired location without the washout issue of the previous generation, we chose this as our final design. The full results will be discussed in section 5.4.

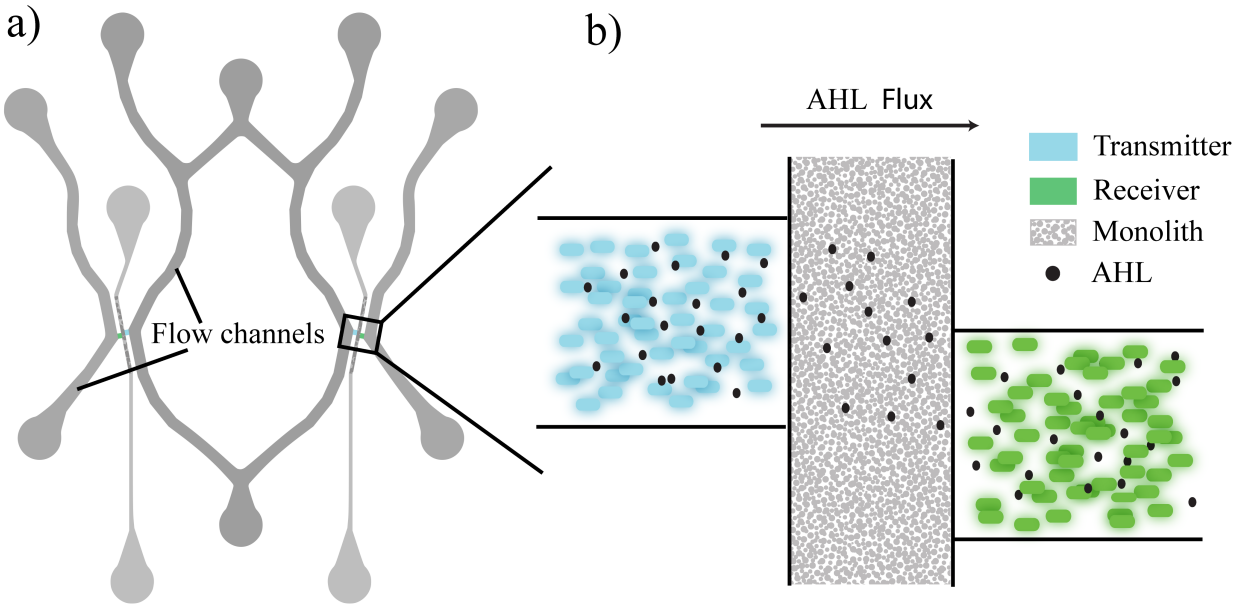

Figure 40: (a) Microfluidic chip design with flow channels and adjacent chambers shown (b) schematically. The bacterial populations grow in isolated chambers separated by monolith. AHL diffuses through the porous monolith from the transmitters to the receivers.

5.2 Monolith Fabrication Overview

The fabrication of the PDMS portion of the device used the same process explained in section 3.2. In this section we focus on the fabrication of the porous monolith inside the PDMS. Porous monoliths have seen a wide variety of uses such as chromatographic separation, solid-phase extraction, and for the extraction and enrichment of substances [60, 61]. Recently there has a movement to utilize porous monoliths in microfluidic devices for biological applications for the extraction and analysis of DNA from biological samples [62]. There are a wide variety of both porous monolith composition, and fabrication methods [63]. Although porous monolith fabrication is well established, there are several difficulties with fabrication in PDMS devices. The PDMS is hydrophobic which makes it

difficult to adhere the monolith to the surface of the PDMS, PDMS is oxygen permeable which quenches free radical polymerization [64], and the PDMS can absorb the solvents.

There are groups that have developed methods to fabricate porous monoliths inside PDMS [65-67]. All methods modify the surface of the PDMS to overcome these difficulties and allow the monolith to properly adhere to the PDMS structures. Hu et al. created an effective foundation for monolith formation in microfluidic channels by utilizing multiple monoliths consisting of either acrylic acid, poly(ethylene glycol) monomethoxyl acrylate, or poly(ethylene glycol) diacrylate monomers [65]. By preabsorbing a photoinitator into the PDMS before injection with the polymerization mixture a higher rate of polymerization was achieved as well as greater channel filling. This paper influenced the development of our PDMS surface modification. Burke et al. further advanced monolith formation in PDMS by utilizing a monolith consisting of a butyl methacrylate monomer and ethylene dimethacrylate crosslinker. Their method allowed for the formation of polymer entangled within the PDMS channel walls to aid in polymer formation and anchoring. Their monolith produced by this method was validated by being used to concentrate and subsequently mechanically lyse B lymphocytes. This paper also influenced the development of our PDMS surface modification methods. We used these methods in combination with [68] for the base of our first generation monolith fabrication method shown in Figure 41.

For our second generation monolith formation, we integrated the work by Araya-Farias et al. This work utilized a monolith consisting of a ethylene glycol methacrylate phosphate monomer and N,N′-methylene-bis-acrylamide crosslinker [59]. This method allows for a one-pot approach to simultaneously forming and anchoring the monolith to

the PDMS channel walls. This paper is the foundation of our current procedure for monolith formation without pretreatment shown in Figure 44.

5.3 First Generation Monolith

The first monolith protocol we fabricated and tested modified the surface of the PDMS to allow anchorage of the monolith to the PDMS. This process involved numerous steps that were very time intensive, and was extremly light sensitive. The overall method is illustrated in Figure 41. As a note, this protocol was only tested in a single node and the first generation two node chip.

5.3.1 Monolith Fabrication

A pictorial representation of the first generation monolith fabrication can be seen in Figure 41. First a chrome-plated glass mask (made in-house at Georgia Tech) was created that would block all UV light from the chip except for the area of the monolith channel. This allowed for precise monolith formation only in the desired areas while leaving the rest of the chip clear. The mask was then aligned under a microscope to the glass side of the microfluidic chip. The microfluidic chip was then put in the desiccator, vacuum set for 30 seconds, and left for 1 hour. Because PDMS easily allows permeation to oxygen, desiccation of the chip eliminates oxygen from entering the channels, and therefore prevents oxygen from restricting free radical polymerization. Next all reagents used to form the PDMS surface modification and monolith are prepared. Due to the extreme photosensitivity of the chemicals, all reagents were prepared and stored in 1.5 mL - black Eppendorf tubes. Reagent 1 consisted of 0.096 g 2,2'-dimethoxy-2-

phenylacetophenone (DMPAP, Sigma-Aldrich) in 1.5 mL of acetone. Reagent 2 was composed of 500 μL of methyl methacrylate (MMA, Acros Organics) and 428 μL of ethylene diacrylate (EDA, Sigma-Aldrich). Reagent 3 was prepared in a 1 mL portion by combining 600 μL of a 1:1 ratio of methanol:2-propanol, 144 μL of butyl methacrylate (BuMA, Sigma-Aldrich), 286 ethylene dimethacrylate (EDMA, Sigma-Aldrich), and 0.0044 g of DMPAP.

Reagents 1 and 2 are responsible for the PDMS modification. When Reagent 1 is introduced into the channels of the microfluidic chip, it forms radicals on the surface of the PDMS that allows for initiation of polymerization [65, 66]. Acetone is used because it is known to swell and have a high permeability to PDMS, which assists the pre-absorption of Reagent 2 into the channel walls. The surface modification solution, Reagent 2, is then absorbed into the PDMS and polymerizes upon radiation with 365 nm UV light. The new surface modification polymer is intertwined within the PDMS, and allows for the monolith to be firmly affixed to the channel walls.

After all reagents are created, the microfluidic chip was removed from the desiccator and placed into a blacked-out box to eliminate premature photoreactivity of the chemicals. Next, 0.3 μL of Reagent 1 (DMPAP in acetone) was injected into the chip. The ports were sealed off and the chip was left untouched for 1 minute to allow diffusion of the monomers into the PDMS. Deionized water was then flushed through the chip for 15 seconds, followed by two more rinses of DI water to ensure elimination of undiffused monomers. Immediately following, Reagent 2 (50% MMA and 50% EDA by weight) was injected into the chip (0.2 mL in 20 seconds). The ports were sealed and the chip was left untouched for 1 minute. Reagent 2 was flushed again through the port, and left for 1 minute

after being sealed. The chip was then exposed to 365 nm UV radiation from a handheld UV lamp (Spectroline, ENF-280C, 60Hz, 115 V, 0.20 A) for 40 seconds. Methanol was then quickly flushed through the chip for about 5 seconds to eliminate any unreacted monomers. Reagent 3 was injected into the chip (0.2 μL), and the top of the chip was sealed for 1 minute. The chip was then placed under the UV lamp (365 nm) for 45 minutes to allow polymerization of the porous monolith. 0.1 μL of methanol was subsequently flushed through the chip to wash away any un-polymerized monolith solution.

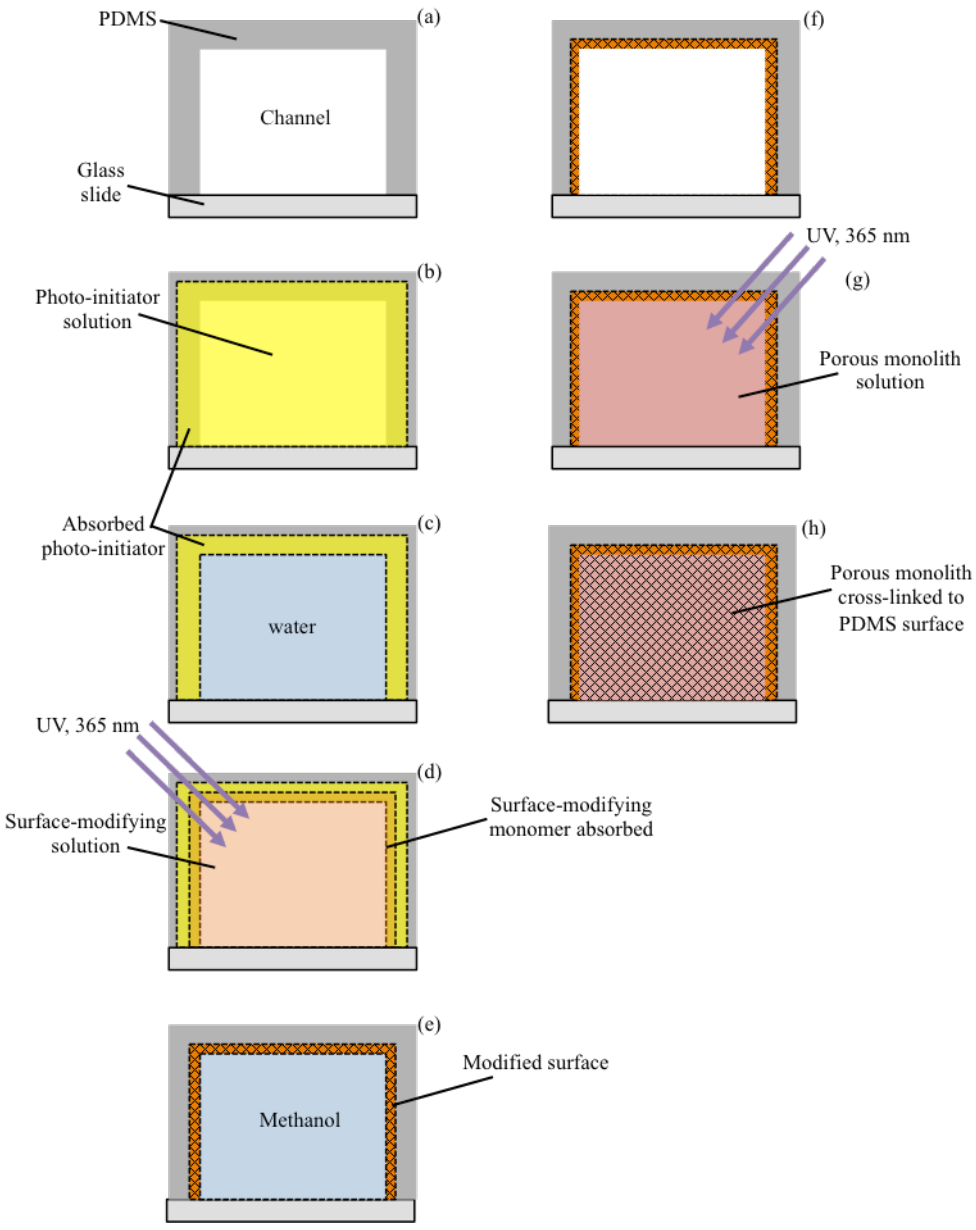

Figure 41: A graphic representation of the surface-modification technique within a micro-fluidic channel (a) A PDMS micro-channel attached to a glass slide. (b) Photo-initiating solution is flushed and subsequently absorbed into the walls of the PDMS micro-channel. (c) Unabsorbed photo-initiating solution is washed away with water. This step is repeated twice. (d) Surface-modifying solution is flushed into the channel and the monomers are absorbed into the micro-channel walls. The channel is irradiated with UV light (365 nm). (v) The channels are flushed with methanol to remove unreacted monomers (f) The micro-channel with modified walls. (g) The solution of the porous polymer monolith is introduced into the micro-channel. It is then irradiated with UV light (365 nm) to induce polymerization of the monolith. (h) The porous monolith is now cross-linked to the surface of the PDMS. Finally, methanol is flushed slowly through the channels to eliminate any unpolymerized monomers.

5.3.2 Monolith Testing

There were a few major concerns with the utilization with the porous monolith that required initial testing. The monolith pore size had to be fabricated to ensure free diffusion of AHL while preventing bacteria passage. Additionally, the monolith could not be toxic or inhibitory to the bacteria's growth and communication.

First we tested the monolith's ability to filter the bacteria population by creating a monolith plug in the main channel of the single node microfluidic chip. For ease of testing, this was done by using a glass cover slip with electrical tape to create a makeshift mask that allowed only a small portion of the channel to polymerized. Once the chip was fabricated, we injected a strain of *E-coli* that is constitutively produced GFP, making them always fluorescent. This allowed us to easily see if the bacteria could infiltrate the monolith and pass through to the other side. In Figure 42, the experimental results are presented. The monolith plug is located on the left had side of the channel. The direction of the flow is from the right to the left, and the bacteria were injected from the right hand side. As demonstrated, the bacteria collected at the facade of the monolith with no penetration. This confirmed our theory that the monolith pore size was small enough to prevent bacteria passage.

Next, we tested the ability of AHL to freely diffuse across the porous monolith. Once again, this was done by creating a monolith plug in the main channel of the single node microfluidic chip. This time our receiver bacteria were placed on the right hand side of the plug while the direction of flow was from left to right. The receiver bacteria were given 24 hours to create a stable population on the façade of the monolith. After the 24-hour growth period, AHL was injected into the left side of the microfluidic device (opposite

of the bacteria population). We imaged the receiver bacteria population over time to record their production of GFP in response to the AHL diffusing across the porous monolith. We were pleased to see the receiver bacteria produced GFP similarly to the one node receiver experiments. Not only did this show that AHL can freely diffuse through the monolith, but also the monolith was nontoxic to the bacteria.

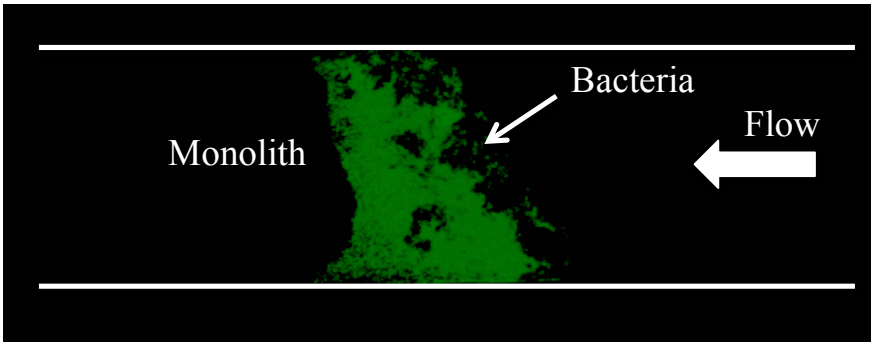

Figure 42: The porous monolith formation shown to the left of the green bacteria prevents the bacteria from continuing further along the channel. The direction of flow is from right to left.

After establishing the validity of the monolith as a filtering mechanism, we proceeded to form the monolith in the first generation two node microfluidic device. To accomplish this, we utilized a chrome plated glass mask that allowed us to polymerize the porous monolith in the monolith channel between the two trapping chambers. Figure 43 demonstrates our first attempt at forming the porous monolith inside the 2-node microfluidic chip. In the monolith channel, the dark substance seen is the monolith formation. Note the formation is not uniform throughout the channel, but the monolith is in the desired location. Furthermore, the trapping chambers are free of any excess monolith debris. Although this pair of trapping chambers had the correct formation, the subsequent

pair of trapping chambers did not have complete monolith formation. This rendered the chip unusable, because the transmitter bacteria and receiver bacteria could cross contaminate due to their motility.

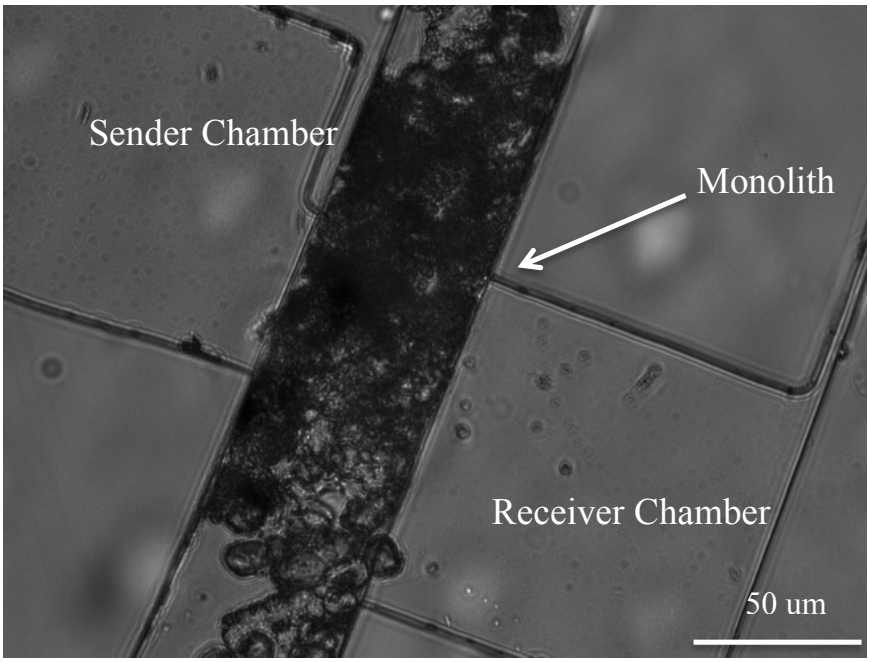

Figure 43: First generation monolith formation between the trapping chambers in the first generation 2-node microfluidic device. Although there was full formation in this section, there was no proper formation in other key areas.

A major obstacle that led to inconsistences during experimentation was attributed to the extreme sensitivity of the polymer solutions to all light sources forcing us to work in darkness. Since a dedicated dark room was unavailable, any and all light leakage led to partial chemical structures forming during the initial steps, which in turn prevented proper monolith formation. The chemicals used to form this particular monolith were exceptionally hazardous both for respiratory and contact, and required a fume hood. This made working in the dark potentially disastrous for the user. These issues combined with

the numerous failed attempts at resolving the incomplete monolith formation, we conducted an intensive literature review to determine other possibilities. Since the practice of creating a porous monolith inside a PDMS device is very challenging, there are very few research groups working to solve this problem. Fortunately, a new group in the field emerged in late 2015 providing us with a more robust and streamlined method utilizing a new set of chemicals [59]. This method reduced the fabrication time from 4-5 hours to 1.5-2 hours, and allowed the use of red light during the process enabling us to see. Furthermore, the chemicals used were less hazardous reducing the risk factor to a more acceptable range.

5.4 Second Generation Monolith

Because the fabrication of porous monoliths within PDMS is so difficult, as previously discussed, research is constantly being conducted in order to reduce the number of steps and processes required to fabricate the monolith. In this section, the newest and most efficient microfluidic design has been adapted to a novel method of porous polymer fabrication in PDMS in one simultaneous synthesis step. This process was adapted from [59], and our contributions and modifications will be reviewed bellow. This method is advantageous because it allows for the synthesis of the polymer monolith along with the simultaneous anchorage of the polymer in the PDMS microchip.

5.4.1 Monolith Fabrication

The monolith solution consisted of 2-(methacryloxy)ethyl phosphate monomer (EGMP, 12.8% w/w), N,N'-methylenebis(acrylamide) crosslinker (BAA, 9.8% w/w), 2,2-dimethoxy-2-phenylacetophenone photoinitiator (DMPA, 1.8% w/w), and porogenic

solvents composed of N,N-dimethylformamide (DMF, 7.3% w/w), 1-dodecanol (DDC, 24.3% w/w), and dimethylsulfoxide (DMSO, 44.0% w/w). This reaction mixture is vortexed to mix and left to sit at room temperature for ~2 hr to ensure complete mixing and is then injected into the device's inlet ports. A SMT solder-paste stencil steel mask is aligned prior to injection such that the monolith channel of the device is exposed to incident light while masking the flow channels and bacterial chambers as shown in Figure 44. The device and mask is then irradiated with 365 nm light (12 min, 1.5 mW/cm2, UL-2000L Crosslinker). Following UV exposure, the device is manually flushed with 30% v/v methanol in DI water to remove unreacted monomers and stored in DI water at -4 degrees Celsius.

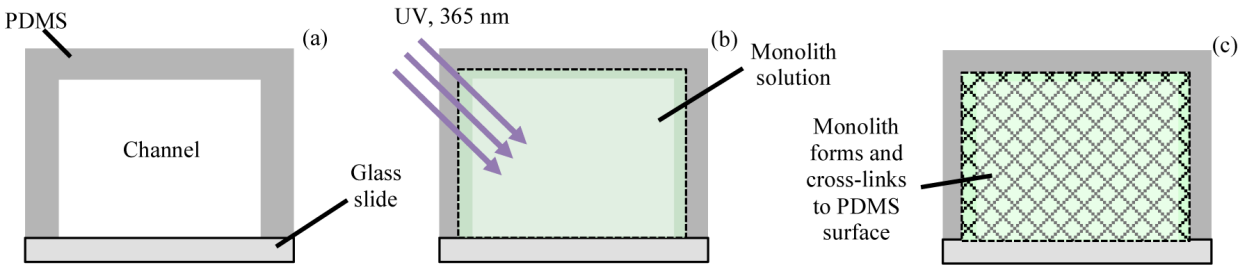

Figure 44: Polymer monolith synthesis process within a microfluidic channel. (a) A PDMS microchannel attached to a glass slide is filled with a liquid phase polymer solution and (b) lithographically polymerized in defined regions with UV light (365 nm). (c) The resulting monolith is cross-linked to the PDMS. Adapted from [59].

5.4.2 Monolith Masks

The monolith is UV initiated, which means the formation can be dictated using a mask. The mask works essentially as a filter, where a desired pattern is integrated in the design. UV light can pass through the mask in key regions, will the remaining areas are

shielded from UV exposure. This masking technique is very common for photolithography, therefore it was adapted for our use. In all cited monolith publications [59, 64, 66, 68], desired areas were either not masked at all, or they were masked simply by placing electrical tape in regions the monolith was not desired. Although this technique works and was tested during the initial experimentation with our work, it is greatly limited to inaccurate and large features. To have better control on the regions exposed to the UV light, we explored a variety of mask options.

The first mask material we attempted to use was a Mylar mask from Infinite Graphic. Mylar is an inexpensive, simple, and fast fabrication. Essentially a transparency sheet is printed on using a special ink. Places with no ink are clear and easily allow the UV light to pass through, while inked areas should block the UV light. The mask blocked the entire chip except for the monolith fabrication channel. Ideally only the monolith channel would contain formed monolith while the remainder of the chip remained clear. When we tested the Mylar mask, we noticed substantial monolith formation in all regions of the chip. After some investigating it was found that the 365nm wave length we were using, was on the cusp of what was transmissible through the inked Mylar. Unfortunately, this made this mask material no longer an option.

Next more traditional photolithography materials were selected for testing. Chrome plated glass masks are used in a variety of MEMS fabrication. The glass provides a sturdy substrate for the chrome mask. Chrome has zero UV transmission making it an excellent mask material. Just as before a detailed pattern can be incorporated in the plated chrome to expose regions to the UV light, while shielding the remainder of the chip from the UV. We utilized the Georgia Tech cleanroom facility and mask fabrication team to create our glass

and chrome masks. The cleanroom regularly uses soda lime glass because it is less expensive than other glass material such as quartz. Checking the emission spectrum of soda lime glass, shown in Figure 45, it can be seen that at 365nm it would be expected that UV passes through. Because of this reason we choose to test the soda lime glass and chrome mask. Unfortunately, we found that the monolith sporadically and incompletely formed in the monolith channel when the soda lime mask was used. Although the transmission spectrum in Figure 45, indicates 365nm transmission, this can vary depending on manufacture tolerances and defects in the glass. This means in some cases the transmission may actually be in the ramp up region allowing some UV light to pass through, but not enough to correctly form the monolith.

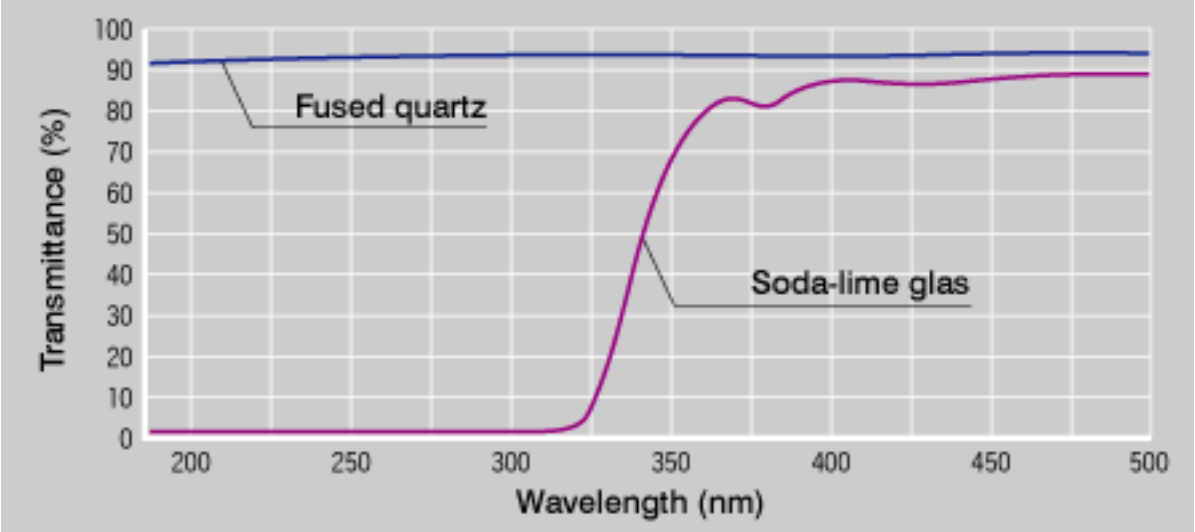

Figure 45: Transmission spectrum for soda-lime glass and fused quartz glass. Figure provided by SK Electronics company.

Since there where transmission issues with the soda lime glass mask material, we choose to try the more reliable quartz glass and chrome mask. As can be seen in Figure 45,

quartz allows great transmission over the desired 365nm region. This would suggest that UV light can easily pass through. The quartz and chrome mask were tested on the final two node chip design with the final monolith formula. As mentioned in the previous section detailing the monolith methods, there is a step indicated as the UV radiation step. Since it is unclear how the required radiation time is determined from the original methods paper, [59], this step required a lot of fine tuning. The results and testing methods will be discussed in more detail in section 5.4.3. Briefly, a variety of experimental tests were conducted to determine the ideal radiation time. It proved to be incredible difficult with the quartz glass masks. The masks were purchased from Telic company and were 0.09" thick. This thickness was believed to cause some transmission issues that were challenging to overcome. We tested three mask conditions (quartz, electrical tape, and no mask), in a variety of experimental conditions. We were able to successfully and reliably form monolith in the microfluidic chip when no mask was used and when a simple mask made out of a coverslip and electrical tape was used. We had very inconsistent, but some monolith formation in the monolith fabrication channel when the quartz mask was used. This inconsistency and the pressure of time, lead to the development of a final mask material.

The final mask selection eliminated any material between the UV light source and the microfluidic chip. We utilized a 75 μm thickness stainless steel sheet that was laser cut by the Stricklin Company. Although the mask was very thin, it was easy to use and the features held up for repeat uses. One major drawback to this mask, was the difficulty in aligning the mask to the chip features. Alignment was conducted under a microscope, where the mask was maneuvered on the glass side of the microfluidic device using tweezers

and taped in place using scotch tape. If the mask was misaligned along the channel wall, the PDMS surface area available for the monolith to adhere to, would be greatly decreased. This would leave only the top of the channel, and one side wall of the channel for the monolith to attach. To minimize this miss alignment issue, the mask was widened slightly over the area of the monolith fabrication channel between the trapping chambers. This mask allowed the UV light to reach the monolith fabrication channel and correctly polymerize the monolith, while preventing polymerization in the remainder of the device. For these reasons, the stainless steel mask was our final mask selection.

5.4.3 Optimization

The development of the monolith protocol required a wide array of optimization experiments to create ideal formation. Although monoliths have been utilized for a wide array of applications, the integration in PDMS microfluidic systems is still an area in early development. The main hurdles for properly forming the monolith in PDMS microchannels are oxygen and irradiation time. Mentioned earlier, oxygen can restrict free radical polymerization and prevent proper monolith formation. Additionally, the amount of time the monolith is exposed to the UV light can affect the formation of the monolith. If not exposed enough the formation will be incomplete, and if the monolith is over exposed then the structure can collapse. This section will discuss the optimization of the second generation monolith formation in the microfluidic device.

One of the first things tested was the effect of oxygen during the production of the monolith. There are two main ways oxygen can integrate and impact proper formation: during the mixing of the monolith solution and bubbles entering the channels during injection. There are a few ways to remove oxygen introduced to the monolith solution

during the mixing process: desiccating, vac-n-bac, and purging. The first method was tested by placing the monolith solution in a glass desiccator for one hour. This solution was then injected into the microfluidic chip and irradiated under the UV light. The control for this was created using a solution that sat for the same amount of time, but was not degassed. Figure 46 shows the trapping chamber region of two chips, the first did not undergo degassing while the second did. Both chips were irradiated for 10 mins and no masks were used. The image of the non-degassed chip presents highly irregular formation or in some areas no formation. In comparison, the desiccated chip shows more uniform formation throughout. This demonstrated the need for a degassing step. Although there was uniform formation with the desiccated chip, there was still room for improvement.

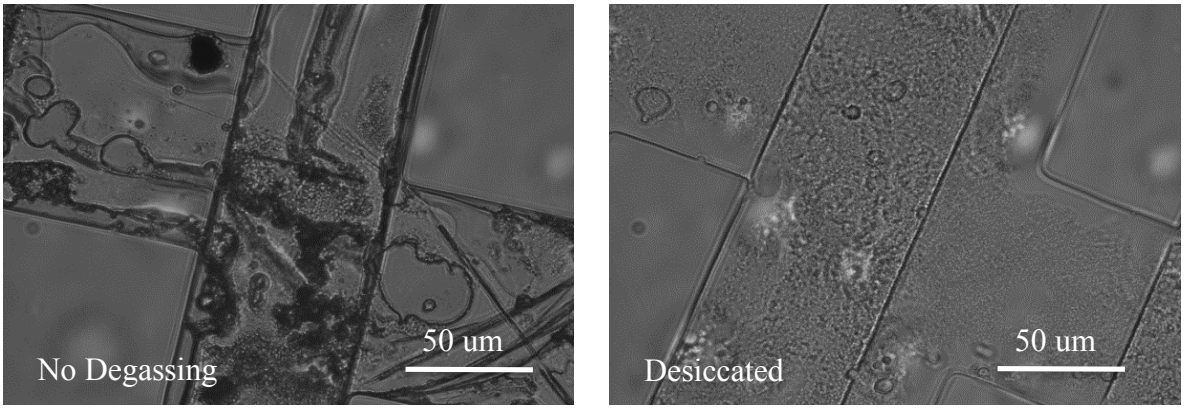

Figure 46: Images of the trapping chamber region of microfluidic chips with monolith formation under (left) no degassing, (right) degassed utilizing a desiccator.

The next degassing method tested was a method referred to as vac-n-back, a common practice used in chemistry. This entailed using a small glass chamber attached via tubing to both a vacuum and a nitrogen tank. The vial of monolith solution is placed in the glass chamber, and a pressure release valve was integrated in the top. In short intervals, first oxygen is first removed with the vacuum and then nitrogen gas is pumped in. This

oxygen removal and nitrogen replacement is repeated 15 times to insure all oxygen is replaced. Figure 47 (right) shows an image of a chip tested with the vac-n-back method. It can been see from this image that the monolith is more consistent than the previous method and resulted in ideal monolith formation.

Figure 47 demonstrates the impact of air bubbles. Although the solution is degassed, when injecting the solution into the microfluidic device small air bubbles can become trapped. In Figure 47 (left) arrows indicate air bubbles trapped in the device. This is the only difference between the two chips. It can be seen that proper monolith formation occurs when no bubbles are present, while the left side is highly irregular and no complete formation. To eliminate this issue, we implemented a degassing step for the microfluidic chip as well to ensure no oxygen remained and impeded the monolith formation.

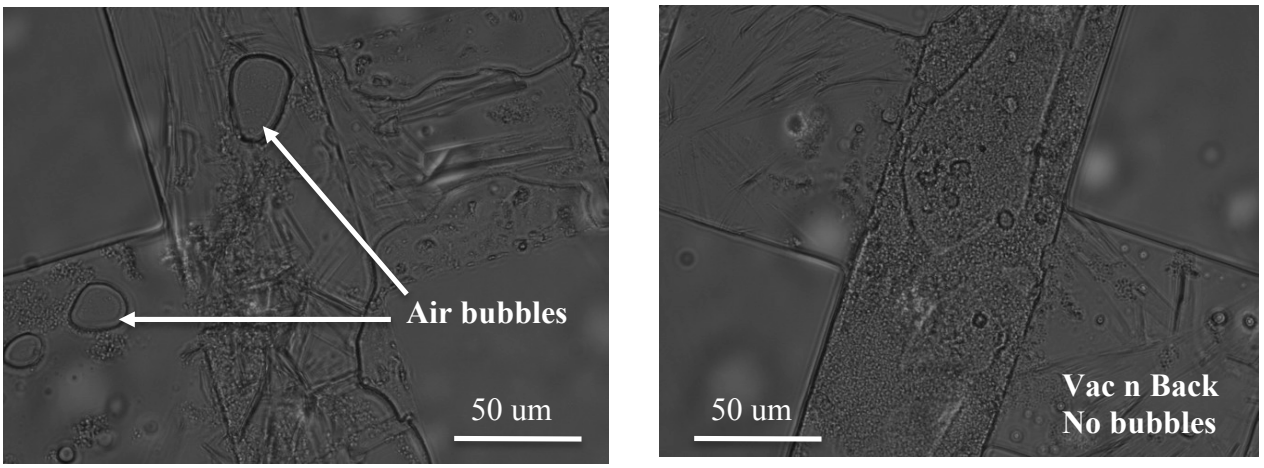

Figure 47: Images of the trapping chamber region of microfluidic chips with monolith formation degassed utilizing Vac n Back (left) bubbles from injecting prevent proper monolith formation, (right) no bubbles are present a monolith properly forms.

5.4.4 Results and Discussion

The second generation monolith was tested in a very similar manner to the first generation. A monolith plug was formed in the single node microfluidic device to determine if the pore size would suit our needs. Initially, a bacterial strain that constitutively produces GFP was injected on one side of the monolith plug to confirm the bacteria could not pass through the pore size. Figure 48 demonstrates that even under flow, the proper monolith formation acts as a filter and prevents the bacteria from passing through. The channel does contain monolith debris that detached from the main plug and is noted in the image. What is important here is that the bacteria were not able to enter the fully formed monolith region indicated by the dash line.

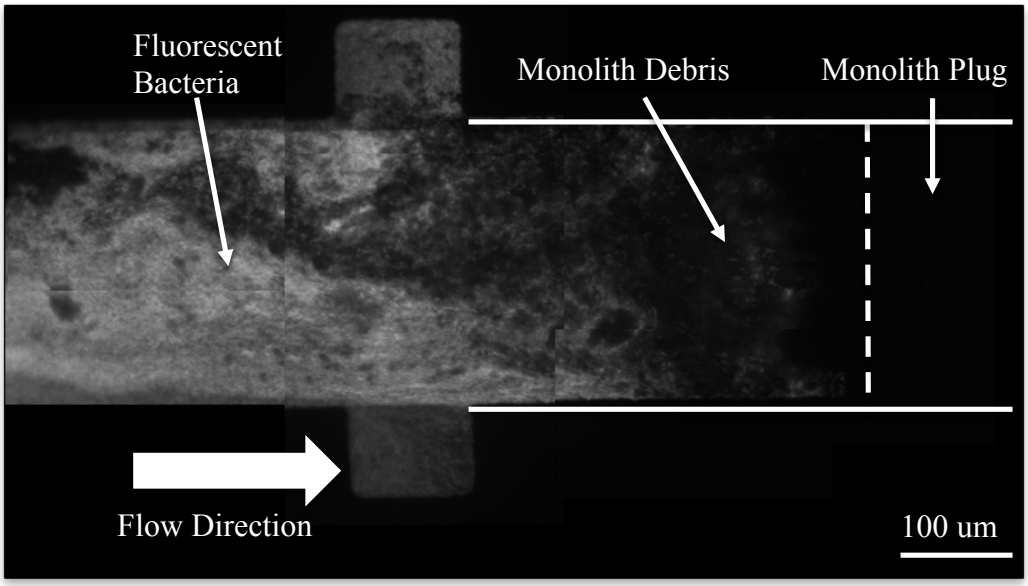

Figure 48: Second generation monolith plug was formed in the single node device and bacteria that constitutively produce GFP were flown through the chip. Since the plug was roughly created, there is some monolith debris that can be seen among the bacteria.

Next the AHL diffusion through the monolith was tested by placing the receiver bacteria on one side of a monolith plug and placing AHL on the other side. Since it was established that the monolith pore size was small enough to prevent bacteria contamination, we needed to verify that the AHL would easily diffuse through. Fluorescent images were captured of the receiver bacteria population that was grown on one side of the monolith plug after AHL was injected on the opposite side of the chip. Figure 49 is the results of this experiment. After the AHL was injected, it diffused through the porous monolith and reached the receiver bacteria population. The receivers then began producing GFP, which correlates to the relative fluorescence level. This experiment confirmed that the AHL was free to diffuse through the second generation monolith. Overall both of these experiments demonstrated the monolith would effectively act as a filter between the transmitter and receiver bacteria for communication studies.

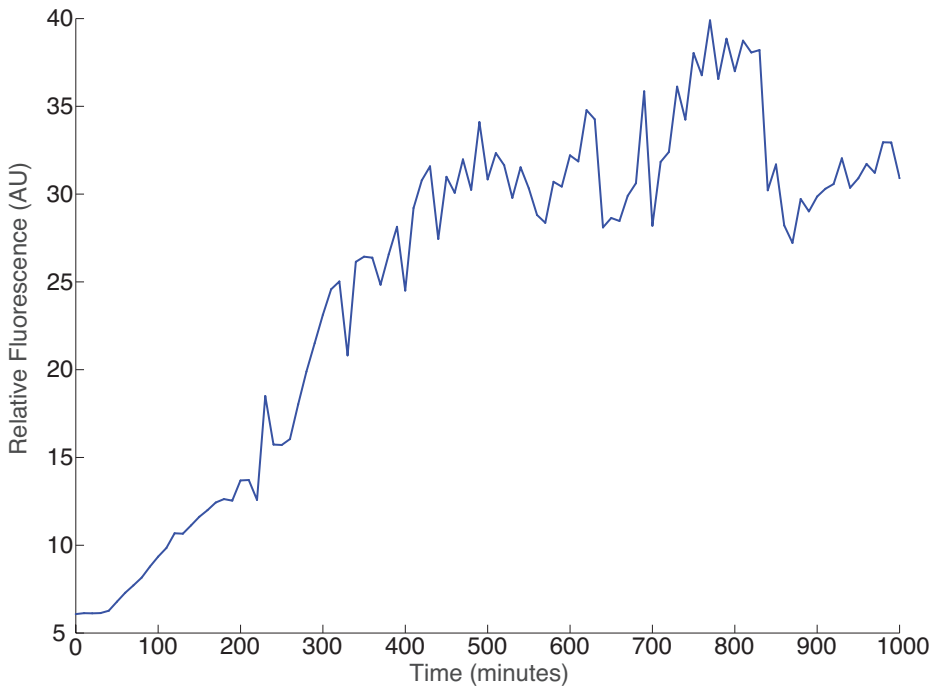

Figure 49: A monolith plug was placed in the single node microfluidic device with receiver bacteria on one side and AHL on the other. The relative fluorescence over time was captured to see if AHL could successfully diffuse through the monolith. Since the fluorescence increases over time, this proves the monolith can effectively act as a filter between the population without hindering communication.

After extensive iterations to optimize the fabrication methods and masks, we were able to successfully form proper monolith in the fabrication channel of the second generation microfluidic device. Figure 50 is an example of the final monolith formation. The image shows proper monolith formation in a chip filled with DI (deionized) water. The monolith creates a barrier between the two trapping chambers to prevent bacteria traveling from one side to the other and cross contaminating the populations, while still allowing AHL to diffuse across. Although there is some monolith debris in the trapping chamber, it is minimal and will still allow the bacteria to create a stable population. This device will be used to study bacterial communication between the transmitter and receiver bacteria populations under dynamic inputs.

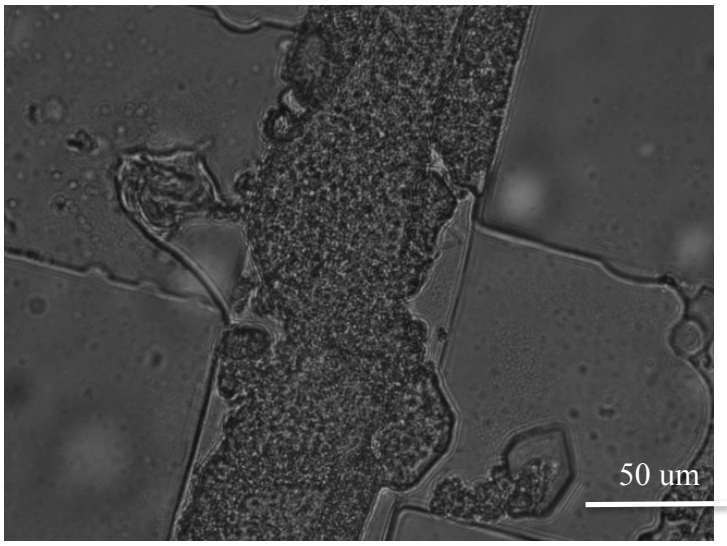

Figure 50: Proper monolith formation in the second generation two node microfluidic device.

After creating proper monolith in the channels, we noticed that if left at room temperature, the monolith would form large cracks where bacteria could potentially cross through. To address this issue, the chip was stored in DI water to ensure the monolith does not dry out and crack, and refrigerated to slow the degradation of the monolith. Even with these conditions, the monolith had a limited shelf life of 2 weeks. This could pose an issue in the future when trying to scale experimental output. Additional optimization on storage conditions could be conducted in the future to slow the degradation of the monolith.

5.5 Conclusion

We designed a microfluidic device capable of separately housing both the transmitter and receiver bacteria population while allowing diffusion of small molecules for bacterial communication. This was accomplished by creating a porous monolith filter between the two bacteria populations that would prevent cross contamination while

allowing AHL to freely diffuse. Initially the region around the trapping chambers was optimized to reduce low velocity regions while maximizing AHL diffusion between chambers. Once this was completed, the remainder of the chip was first designed to have several pairs of chambers in a series. This design failed due to monolith washout, and led to our second generation design with two pairs of chamber in parallel. This device was successful and was chosen as our final design.

The formation of the monolith inside the PDMS channels proved to be a very difficult process to optimize. An initial monolith fabrication technique was used to first modify the surface of the PDMS which then would allow the monolith to anchor to the walls of the channel. This method was very complicated, sensitive, and dangerous to work with. This led us to the development of our final monolith fabrication methods which was proven to successfully prevent bacteria from passing through while allowing AHL to diffuse through. Once the monolith methods were developed, properly forming it in the two node microfluidic device was challenging. Several masks were created and tested until a final mask material proved to be effective. The mask was used in conjunction with the second generation monolith in the two node device to create a usable microfluidic chip to study the communication between the receiver and transmitter bacteria.

Although we have made great strides in creating this unique microfluidic system, there is still room for future developments. There are numerous factors that affect the formation of monoliths in PDMS channels, and it could take years to resolve all the issues to make this a more reliable method of device fabrication. The main take away is that only a handful of groups have been successful in forming monolith in PDMS, and none of those have attempted controlling the formation through a small feature mask. Additionally,

monoliths have never been used to separate bacteria populations before. We were the first to our knowledge to create a microfluidic system that allows dynamic control of inputs, long term experimentation, and no cross contamination.

Chapter VI

AHL extraction and quantification

This chapter describes the methods, results and discussion of AHL extraction and quantification. We developed an AHL extraction method and utilized mass spectrometry and liquid chromatography to quantify the AHL. The AHL extraction method was tested against known quantities of AHL to determine the validity of the method. From this data a calibration curve was created that related the output of the mass spectrometry results to concentrations of AHL. Finally, we were able to collect the AHL produced by the transmitter bacteria in response to arabinose and plot the concentration as a function of time.

6.1 AHL Extraction

With the receiver population we were able to quantify the output response of the bacteria through imaging which allowed us to model the bacterial response. In order to model the sender bacteria, we needed a method to quantify the output of the sender population. Additionally, with our two node device design, there will be some loss of AHL and from what we learned in aim 2, the microfluidic device could affect the sender bacteria's ability to produce AHL. This led to a need to quantify the AHL concentration at varying times throughout the testing process. The gold standard for measuring AHL is to do a bioassay. In this method the AHL solution is given to a bacterial strain with fluorescent output, and compared to a standard curve created by giving the same bacterial population known quantities of AHL. Although this method can give a ballpark range of the AHL

concentration, we looked for a more quantitative method. We adapted the methods used by Kannappan et al. [69] and [70] to quantify AHL which uses liquid chromatography mass spectrometry. One major hurdle with this method is it requires the isolation of the AHL and extraction.

To test the different extraction and quantification methods, a set of sample standards were created. Six clean 1.5 mL microcentrifuge tubes were set up on a rack, and 1 mL of 15% methanol 85% DI water was added to each of the tubes. A 100 μM concentration standard was made by adding 10 mM AHL to the first microcentrifuge tube with methanol. The previous step was then repeated with the respective amount to make 75 μM, 50 μM, 25 μM, 10 μM and 1 μM standards. All the standards were vortexed for 10 seconds and 500 μL of the resulting solution was transferred to mass spec vials using a 1 mL pipettor. The standards were labeled and turned in for liquid chromatography mass spectrometry with the rest of the samples. To produce the reference standards, N-Hexanoyl-L-homoserine lactone was purchased from Sigma-Aldrich.

Extracted standards were prepared in 2XYT media with known AHL concentrations introduced. A 100 μM concentration standard was made by adding 10 mM AHL to the first microcentrifuge tube with 1ml of media. Then this was repeated with the respective amount to make 75 μM, 50 μM, 25 μM, 10 μM and 1 μM extracted standards. All the standards were vortexed for 10 seconds before undergoing the extraction process.

To extract the AHL, the media solution was transferred into a sterile centrifuge tube and subsequently centrifuged for 10 minutes at 10,000 rpm. The supernatant was transferred to another centrifuge tube, and the pellet of bacterial cells was discarded. The filtrate was then mixed with ethyl acetate (2:1 ratio) and incubated for 15 minutes. Once

transferred to a separatory funnel and allowed to sit for 5 minutes, two immiscible layers, ethyl acetate (organic) and aqueous, were present. The two layers are separated due to the density difference, and can be seen in **Figure 51**. The top layer is the organic (less dense), while the bottom layer is the aqueous (denser) layer. The organic layer was collected in a sterile container, and the aqueous layer was extracted twice.

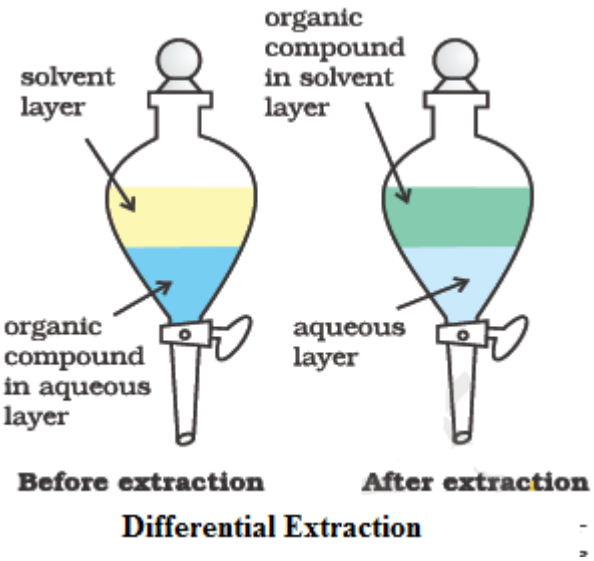

Figure 51: Illustration of a separatory funnel showing the separation by density. Figure from Wikipedia.

Next a rotary evaporator was used to collect the AHL solid from the ethyl acetate solvent. **Figure 52** is an illustration of a rotary evaporator which works by lowering the pressure which in turn lowers the boiling point of the solvent. This allows for steady and delicate evaporation that does not denature the AHL. The rotary evaporator consists of a motor that rotates a flask containing the sample. A round bottom flask is used for more uniform heating of the sample. The vacuum lowers the pressure in the system while the

water bath (set to 37°C) heats the sample flask. The lower boiling point allows the solvent to evaporate at a lower temperature and the vapor travels to the cold trap. The cold trap cools and condenses the vapor, which then falls and collects in the collection reservoir. The solid AHL remains behind in the sample flask and is re-suspended later in methanol.

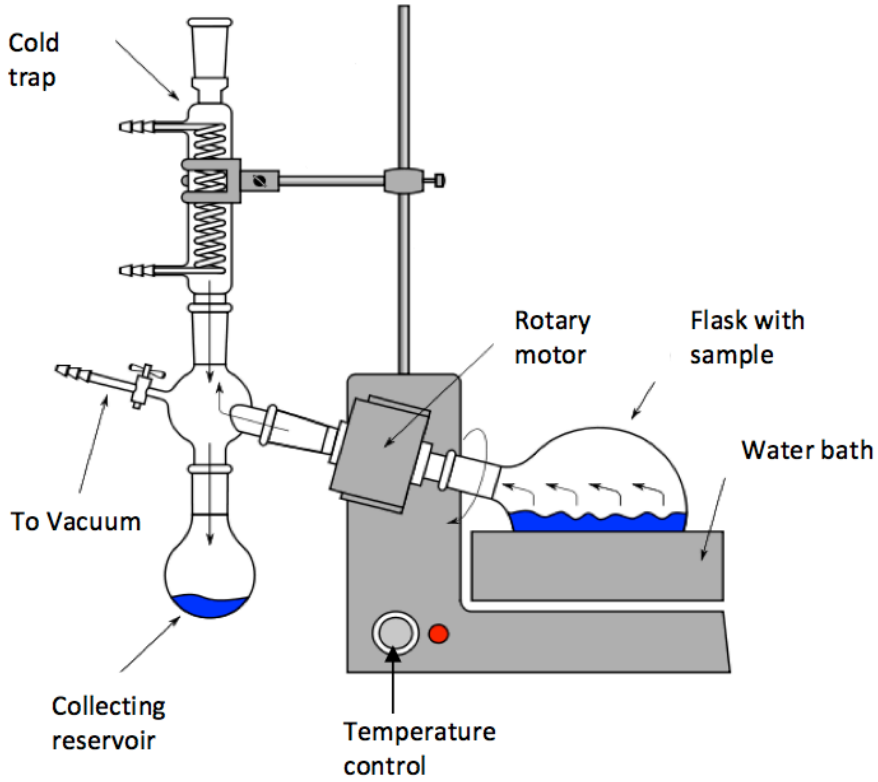

Figure 52: Illustration of a rotary evaporator. The water bath gently heats the sample under vacuum. This allows the liquid to vaporize and travel to the cold trap where it condenses and falls to the collection reservoir. The solid sample remains in the sample flask where it can be collected. Figure from Wikipedia

For our experiments, the AHL ethyl acetate sample was transferred into a 100 mL round bottom flask. Next the flask was attached to the rotary evaporator using a clamp, submerged in the 37°C water bath, and the rotary evaporator was started. The pressure of

the rotary evaporator system was slowly dropped until the pressure reached 80 mbar, and then left until all solvent has evaporated and the solid AHL remains. Next everything was turned off and the AHL was re-suspended in the 15% methanol solution. The samples were then stored at -60 °C until they could be analyzed using liquid chromatography mass spectrometry.

6.2 AHL Quantification

Liquid chromatography and mass spectrometry provide a way to quantify the purified AHL sample. All quantification methods were conducted in the Georgia Tech core facilities. Generally speaking, column liquid chromatography is a technique used to separate a sample into its individual parts based on interactions. As the liquid mobile phase passes through the column, components in the mobile phase interact to varying degrees with the solid stationary phase. Molecules of interest in the mobile phase are separated based on their differing physicochemical interactions with the stationary and mobile phases. Once the sample is properly separated, mass spectrometry quantifies the AHL. This is done by ionizing chemical species and sorting the ions based on their mass to charge ratio. AHL has a unique mass to charge ratio which allows the AHL to be quantified. It is important to note that the extraction process is necessary due to this liquid chromatography and mass spectrometry method. When AHL samples are tested in media, the resulting data contains too much cross talk (other ions containing the same mass to charge ratio as AHL), making AHL quantification impossible.

There are two different quantification methods that were conducted. The first liquid chromatography mass spectrometry (LC-MS) method was performed by a Micromass Quattro LC with a Gemini C18 Column. For each sample, 20 µL was injected onto the

column, at a flow rate of 200 μL/min. The capillary voltage was 3.5kV and the cone voltage was 20V, with nitrogen as the nebulizing (90 L/hr.) and desolvation gas (600 L/hr., 250 °C). Three multiple reaction monitoring (MRM) transitions were conducted with the mass spectrometer. The 214 ion was the precursor for all such transitions, and argon was used as the collision gas at a pressure of 2.2×10^{-4} mbar. For the transition from 214.0 to 112.8, the cone voltage was 30V, and the collision energy was 20V. For the 214.0 to 101.9 transition, the values were 30V and 15V respectively, and the values for the 214.0 to 70.9 transition were 30V and 25V. For each transition, the dwell time was 0.25 seconds.

To test the validity of this method, an experiment was conducted where known quantities of AHL were directly quantified, and known quantities of AHL that went through the AHL extraction method and then quantified were compared. The efficiency of the extraction method could then be evaluated. With this method, the results showed a 85%-95% AHL loss during the extraction process. Although initial thoughts pointed toward the extraction method causing the issue, it turned out that the quantification method was not accurate enough to detect the re-suspended AHL. Since this was an unacceptable efficiency we looked to develop a more accurate quantification method.

The second quantification method utilized a more sensitive mass spectrometer in order to detect the very small quantities of AHL being produced by the bacteria. LC-MS was performed using a ThermoFisher Scientific LTQ Orbitrap XL ETD, a high performance, hybrid linear ion trap and orbitrap mass spectrometer, which was interfaced with a liquid chromatography separation. This machine has several advantages over the Micromass Quattro LC. Orbitrap technology allows for higher resolution mass analysis and higher mass accuracy over standard linear ion traps by tangentially injecting ions into

the orbitrap to form oscillating rings around the center electrode, which ultimately become trapped in an electrostatic field. Axial oscillation frequency is then related to mass to charge ratio using a Fourier transform. This quantification method was much more sensitive, and was able to detect AHL concentrations as low as 1 μM, allowing for the generation of a calibration curve for AHL extracts.

6.3 Results

All results discussed in this section utilized the final AHL extraction and quantification methods. Figure 53 shows a typical output from the mass spectrometry data. There are two main ways to quantify the results, peak value and peak integration. Since small variations can occur in the separation time, peak integration provides a more reliable quantification and was used for all mass spectrometry data analysis. One of the first things tested was the efficiency of the final extraction and quantification method.

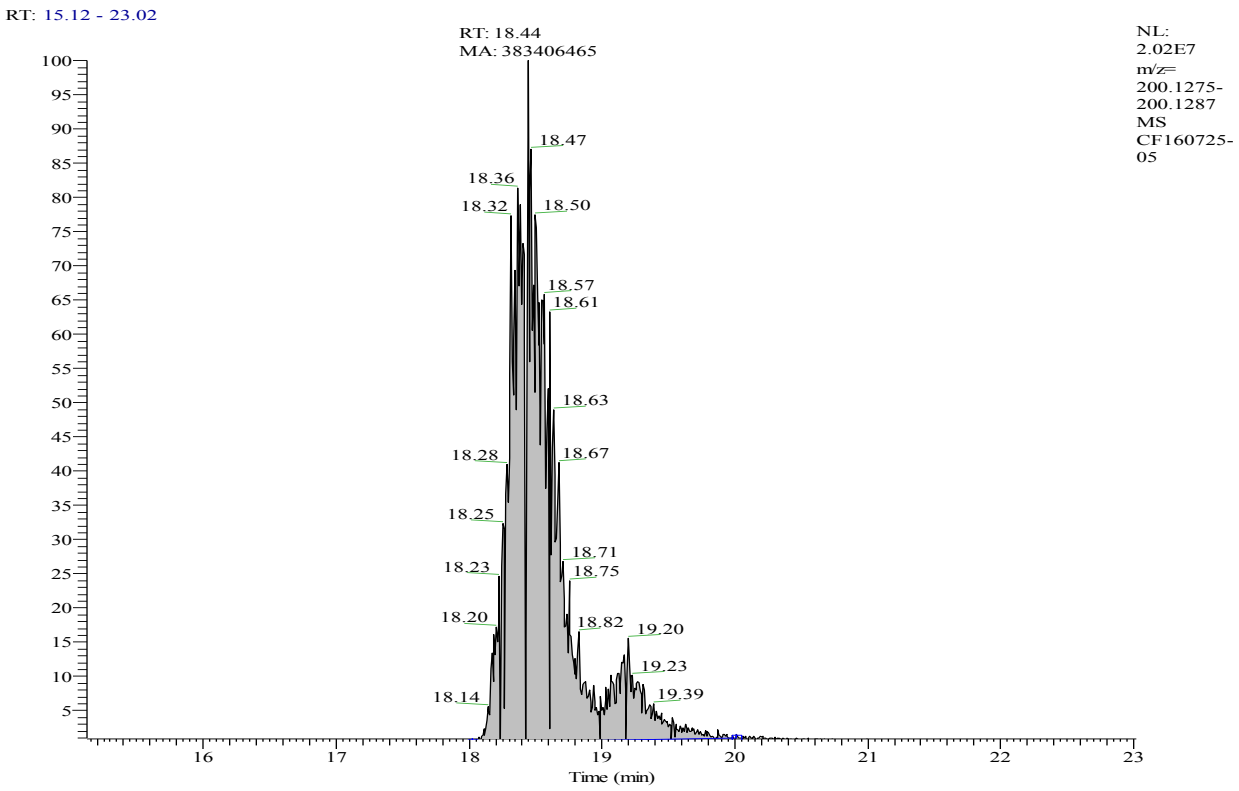

Figure 53: Example mass spectrometry result from a 25 μM AHL quantification peak. The integral of the peak is taken to quantify AHL.

As discussed in the methods section previously, AHL standard were created with known concentrations of AHL in 15% methanol. Extracts were created by using known concentrations of AHL in media that then underwent the extraction method and re-suspended in 15% methanol. Figure 54 confirms both the ability to quantify the AHL, and that the extraction method creates minimal loss. The following AHL concentrations were tested: 100 μM, 75 μM, 50 μM, 25 μM, 10 μM and 1 μM. The standards were repeated seven times and the extracts were repeated six times. The linear fit shown as a dashed lines and the corresponding R^2 values are displayed. The AHL retention efficiency of the extraction method on average was above 90% for the range of concentrations. This proved

that AHL extraction and quantification were possible to determine the output of the transmitter bacteria.

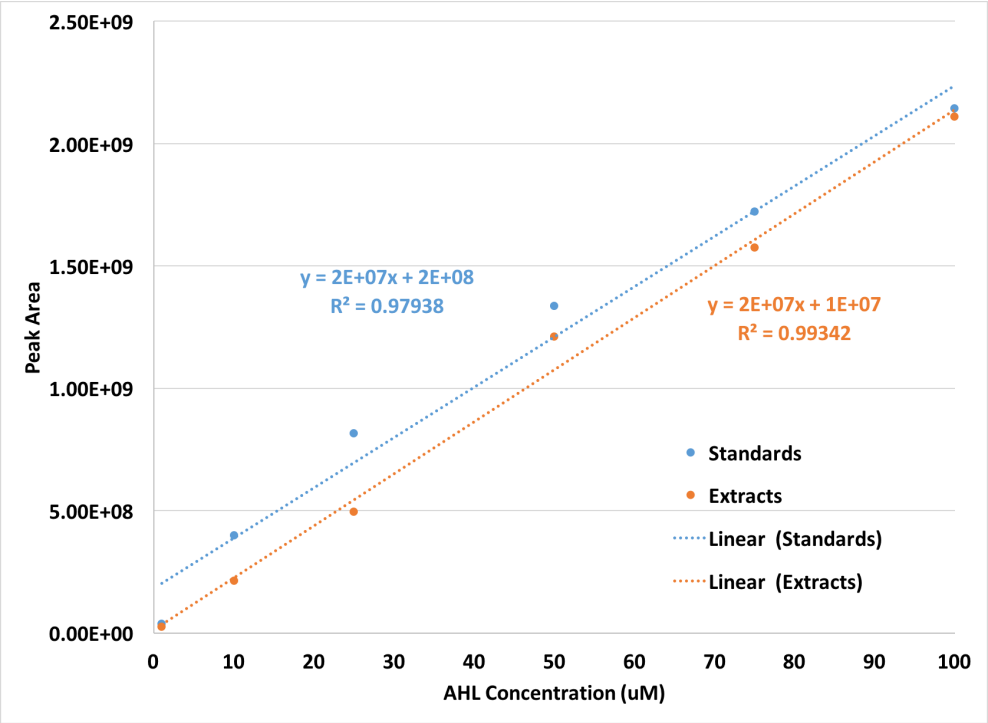

Figure 54: Concentrations of AHL (standards) were compared to samples that have undergone an extraction method (extracts), with the aid of liquid chromatography and mass spectrometry to show ability to quantify AHL produced by transmitter bacteria populations. Dashed lines represent a linear fit, and the corresponding R^2 values are displayed.

One of our ultimate goals was to establish the AHL output of the transmitter bacteria which would allow us to accurately model the transmitter dynamics. Since the AHL extraction and quantification had to be conducted offline, the only way to capture the dynamics was to collect bacteria output over small time segments. There was concerns that taking too small of a time segment would increase AHL loss. This was due to the extraction process, specifically the rotary evaporator step. To test this theory an experiment was

conducted to determine the percent yield as a function of sample volume size. A 5ml solution of 25 µM AHL solution in 2xYT solution was divided up into the following sample volumes: 500 µl, 250 µl, 100 µl, 50 µl and 20 µl. To calculate the percent yield, all volume samples were compared to the 25 µM AHL standard. Figure 55 is the final result of this experiment, where an exponential fit (shown with dotted line) and the corresponding R^2 value is displayed. This showed that as we decreased the sample volume, the percent yield greatly increased. For this reason, we decided that 500 µl was the minimum acceptable sample volume.

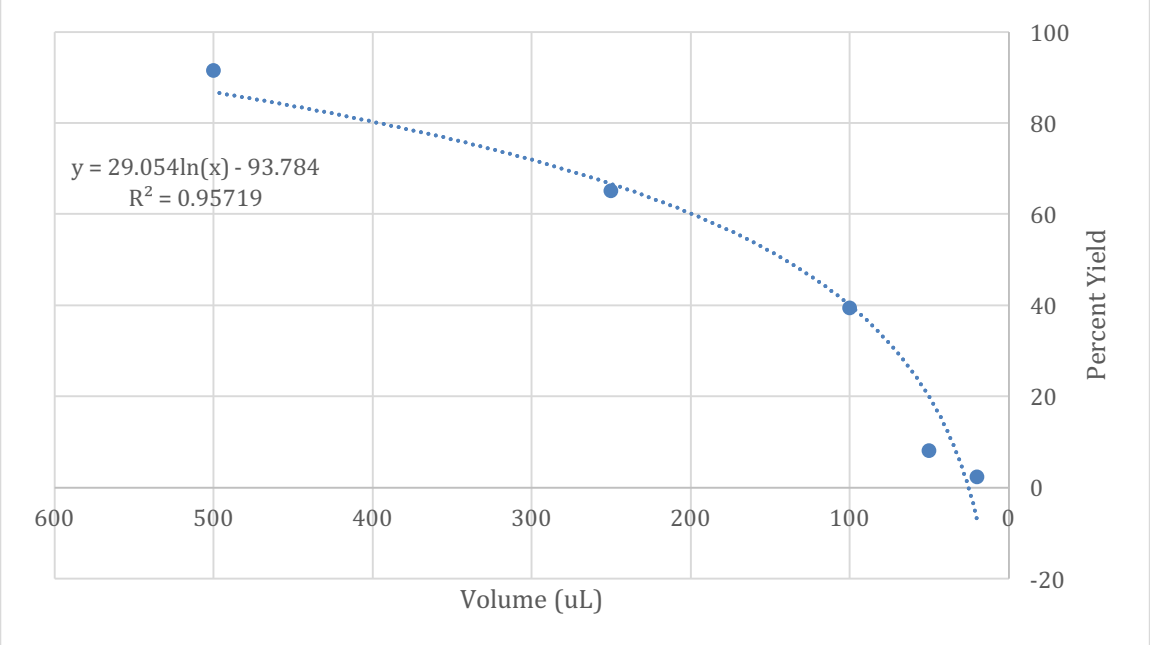

Figure 55: A range of different volumes all with an AHL concentration of 25 µM. The dotted line represents an exponential fit displayed with the R^2 value.

6.4 Transmitter AHL Output

After establishing the methods for extracting and quantifying the AHL, we measured the transmitter AHL production over time. We were able to determine the local AHL concentration in the trapping chambers at 30 minute intervals, and correlate it to the bacterial fluorescent response. These results are essential in understanding the communication between transmitter and receiver bacteria.

6.4.1 Experimental Methods

Transmitter output experiments were conducted in the second generation single node microfluidic device described in section 5.4. The transmitter bacteria were injected into the microfluidic chip through an inlet port. The bacteria were placed on the heated microscope stage and given fresh media via a syringe pump and tubing. Once the bacteria had completely filled the trapping chambers, 20 μM arabinose in media was injected in the chip for 50 minutes. The remainder of the experiment consisted of media with no arabinose.

The waste port of the chip was connected, through tubing, to a syringe on a syringe pump. The pump was withdrawing at the same rate as the media pumps were infusing. The tubing was long enough to ensure that the output would remain in the tubing. Essential the tubing was used to maintain the time segmented collections for the duration of the experiment so collection did not have to be taken every 30mins for 10 hours straight. Although there is some minimal diffusion that occurs in the tubing, this is a sufficient enough collection method. After the experiment was completed, the output/waste pump was switched to infuse and the 30 min time segments were collected. Since the flow rate of 350 μl/hour is really slow, and we saw that a minimum volume was need biased on the volume experiments previously, we ran this experiment 8 times to collect enough volume

per time segment. That meant that each time segment concentration would be the average over 8 total chips each containing 14 trapping chamber. The time segments output collections then underwent the extraction and quantification methods to determine the AHL production.

6.4.2 Results and Discussion

The transmitter AHL output over a 10-hour experiment was collected every 30 minutes. This was repeated 8 times and the time segmented outputs were combined over the 8 experiments. The results are shown in Figure 56, with the AHL concentration for each 30-minute time segment. The AHL concentration was determined by taking the area under the curve of the mass spectrometry data, correcting for volume changes, and comparing to the extraction calibration curve above using a linear fit. Since there is constant flow, the volume of the microfluidic chip output was much greater than the volume of the trapping chambers. To determine the correct concentration, the final mass spec count per 1 ml needed to be adjusted to determine AHL count of the trapping chambers. Once this was calculated, the AHL count values were compared to the calibration. A linear fit, with a R^2 value of 0.993, was used on the extraction calibration to determine the AHL concentrations for the different time segments.

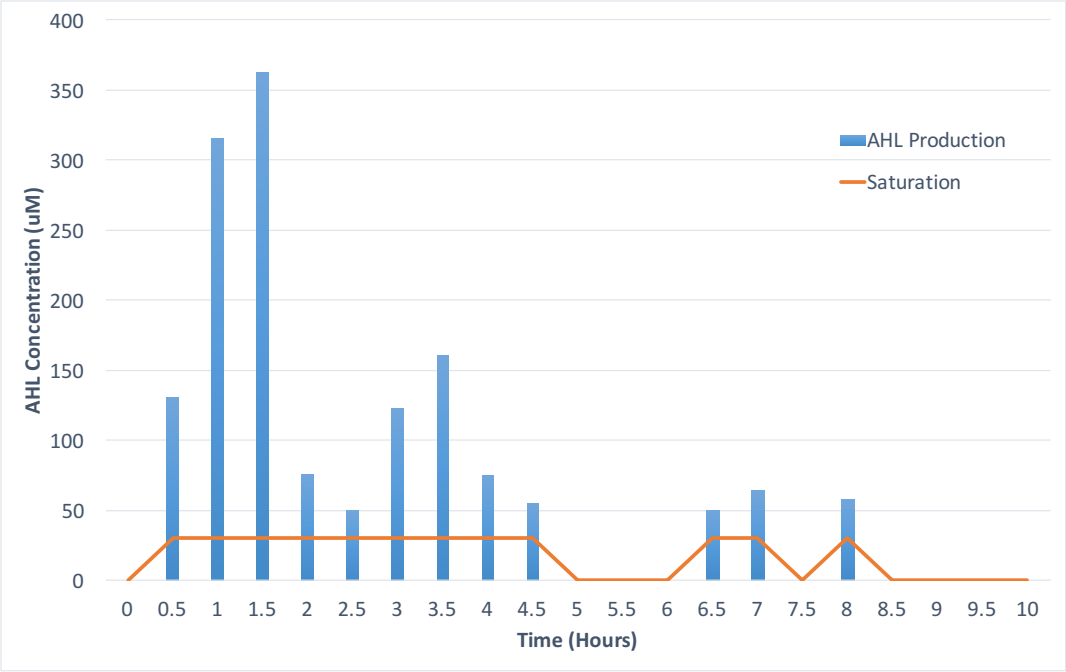

Figure 56: Transmitter AHL output as a function of time. The output was collected in 30 min segments, extracted and quantified using LCMS. Values were then compared to extract calibration curve to obtain AHL concentrations.

It can be seen in Figure 56 that the AHL concentration first increases in response to the 50 min pulse of 20 μM arabinose, and then begins decreasing. One important note, we found in earlier experiments that the saturation point of the AHL to GFP circuit is around 30 μM. This means that any concentration above 30 μM does not elicit additional GFP production. The orange line represents what the bacteria see essentially, a constant concentration or step function. Since the receiver bacteria do not turn off until roughly 600 mins or 10 hours after the removal or AHL, it would make sense that the transmitter bacterial response would not stop fluorescing until around the 18-hour mark.

6.5 Conclusion

A method for extracting and quantifying the small molecule produced by the transmitter bacteria, was developed. The AHL extraction method utilized a separation funnel and a roto-evaporator to gently remove AHL from media containing nutrients, bacteria, and waste. This method isolated the AHL in solid form with minimal AHL loss/degradation. This extraction method was compared to synthetic AHL in the mass spectrometry and liquid chromatography quantification method. This validated the extraction method and created a calibration curve for the methods. This allowed the the time segmented AHL output of the transmitter bacteria to be quantified, giving huge insight to the intermediate step in the bacterial communication system developed.

Chapter VII

Two Node Molecular Communication

This chapter describes the methods, results and discussion of molecular communication between transmitter and receiver bacteria in the two node microfluidic device. A transmitter bacteria population and a receiver bacteria population were separately housed in the same microfluidic device with a porous membrane between them. The transmitters were stimulated with arabinose, and the cascade of communication from both the transmitters and receiver bacteria were captured. We were successful in dynamically stimulating and recording bacterial communication in the microfluidic system for an extended period of time.

7.1 Experimental Methods

All two node molecular communication experiments were performed in the second generation microfluidic device (section 5.1) with the second generation monolith formula (section 5.4). After chip and monolith fabrication, the microfluidic chip is prepped for experimentation. All monolith fabrication ports were first plugged using stainless steel wire equivalent to 25 gage needle to insure no contaminates could enter. Next the microfluidic chip was flushed with DI water using a syringe to washout any PDMS or other debris in the main channels. The chip is the filled with 2XYT media, containing ampicillin, via a syringe and placed under a UV light for serialization. This was to ensure that any contaminant strains of bacteria did not proliferate. Next the transmitter bacteria were

loaded via a syringe into an inlet port on one side of the chip, while the receivers were loaded on the opposite side of the chip.

Once the chip was ready, it was placed on the heated microscope stage where it would remain for duration of the experiment. To provide fresh nutrients to the bacteria, 2XYT media was filled in 10 ml syringes with Tygon tubing attached. The opposite end of the tubing had a 25 gauge metal connector that was inserted into the PDMS ports. On the transmitter side of the chip, an arabinose and 2XYT media solution was connected via tubing and syringe to provide the stimulus for the transmitter bacteria. Waste collection lines were filled with media, and connected to an empty syringe on one end and connected to waste ports on the other end. Figure 57 illustrates what the different ports where used for during fabrication and experimentation for the two node microfluidic device.

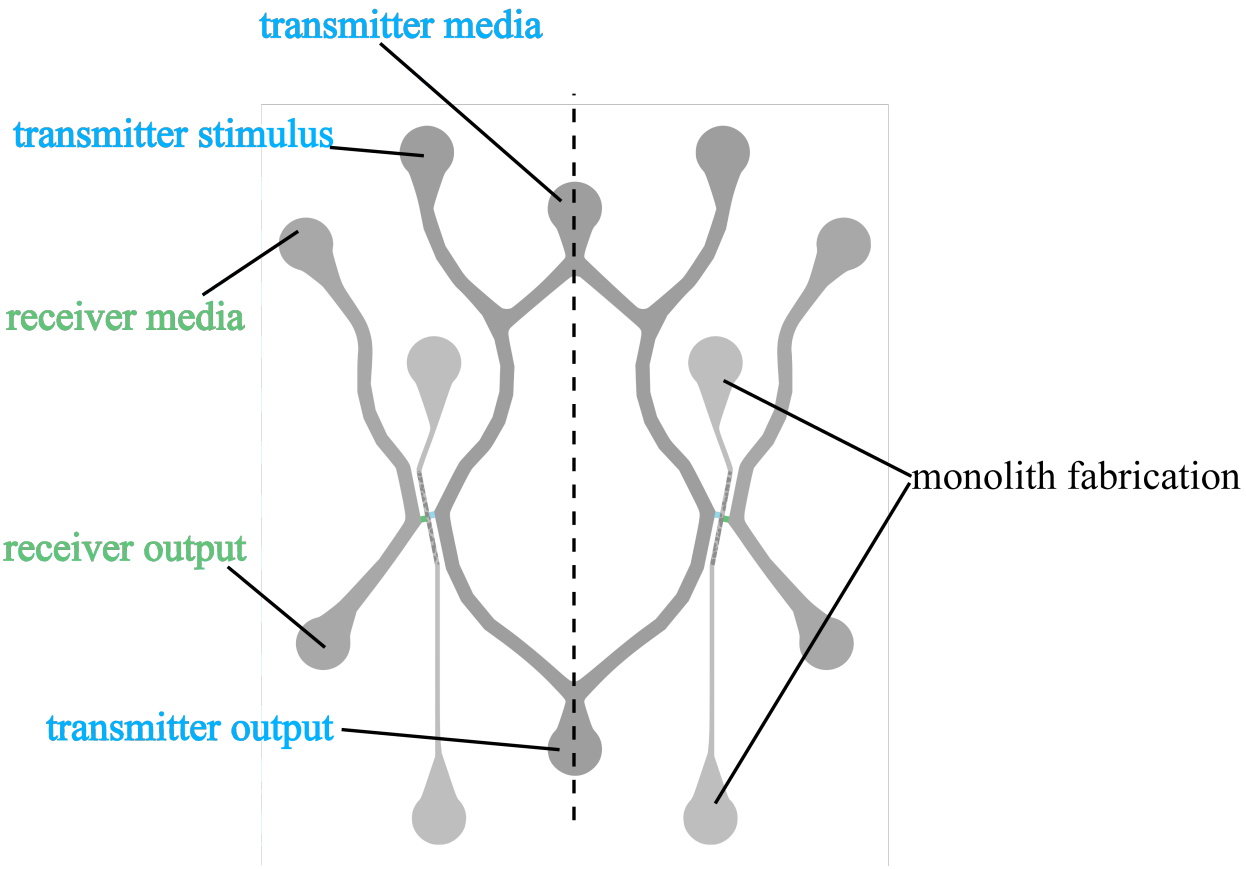

Figure 57: Two node microfluidic device with port use labeled. The ports are mirrored over the dashed line.

A total of 4 syringe pumps were used to ensure independent and complete over flowrates. One pump was used to control the flow of media for the transmitters, while another pump was used to control the flow of media for the receivers. The third pump was used to control the flow of the chemical stimulus, arabinose. The final pump was used to collect the waste output from the transmitter bacteria and from the receiver bacteria. During the growth phase, the two media pumps were set at a low flowrate(75 μl hour-100 μl/hour), while the waste just collected in a small falcon tube and no arabinose was given. The temperature was kept between 28°C and 30°C while monitoring for over growth. The

bacteria populations were allowed to grow for 24 hours to ensure they completely filled the trapping chambers.

Once the bacteria populations were stable, the communication experiment was started. The arabinose pump was set to 10 μl/hour and ran for a total of 50 mins. The media pumps kept a constant 350 μl/hour flow rate, while the waste collection pump was programed to insure it was withdrawing at the same rate as the other pumps were infusing. The temperature was maintained at 30°C for the duration of the experiment. Both the transmitter and receiver bacteria populations were fluorescently imaged every 10 min using a 20x objective and CCD camera on an upright Nikon microscope.

7.2 Results and Discussion

The fluorescent response of both the transmitter and receiver bacteria were captured over time, after the transmitters were given a 50 min pulse of arabinose. Figure 58 is the results of this experiment, in which the fluorescent output of both the transmitter bacteria population and the receiver population were imaged every 10 mins. The arabinose causes the transmitters to begin producing AHL. This AHL then causes the transmitters to produce GFP, which correlates to relative fluorescence. The AHL produced by the transmitter, will diffuse across the porous monolith to the receiver population, will lead to the receivers producing GFP.

In section 5.1.2., it was estimated that it would take 70 mins for the AHL to diffuse through the porous monolith. To compare this to experimental results, we established the time between when the transmitters began fluorescing and when the receivers began fluorescing. The start of fluorescence was established using a thresholding method. When

the relative fluorescence went above 10% of the maximum fluorescence, and did not cross back below that level, that was considered the start. The time between the transmitter and receiver fluorescent start was found to be 78 mins. This correlates well to expected diffusion time. Although there can be additional factors besides diffusion that play apart in the AHL travel time, the diffusion time is the most dominate.

In addition to the delay time, we looked into the theoretical concentration of AHL that would elicit the response from the receiver bacteria. To do this we utilized the reverse receiver model to determine the AHL input and found it to be 8.5 μM AHL. This means that roughly 8.5 μM AHL diffused through the monolith and reached the receiver bacteria. This is the right order of magnitude expected from our COMSOL models and transmitter AHL quantification results. Although the experiment ends at 1200 mins, we plan on running for longer in future experiments to see both bacteria populations return to the off state. Despite this we already surpassed previous attempt's two node experimental times, with a 24-hour growth period followed by 20-hour communication period.

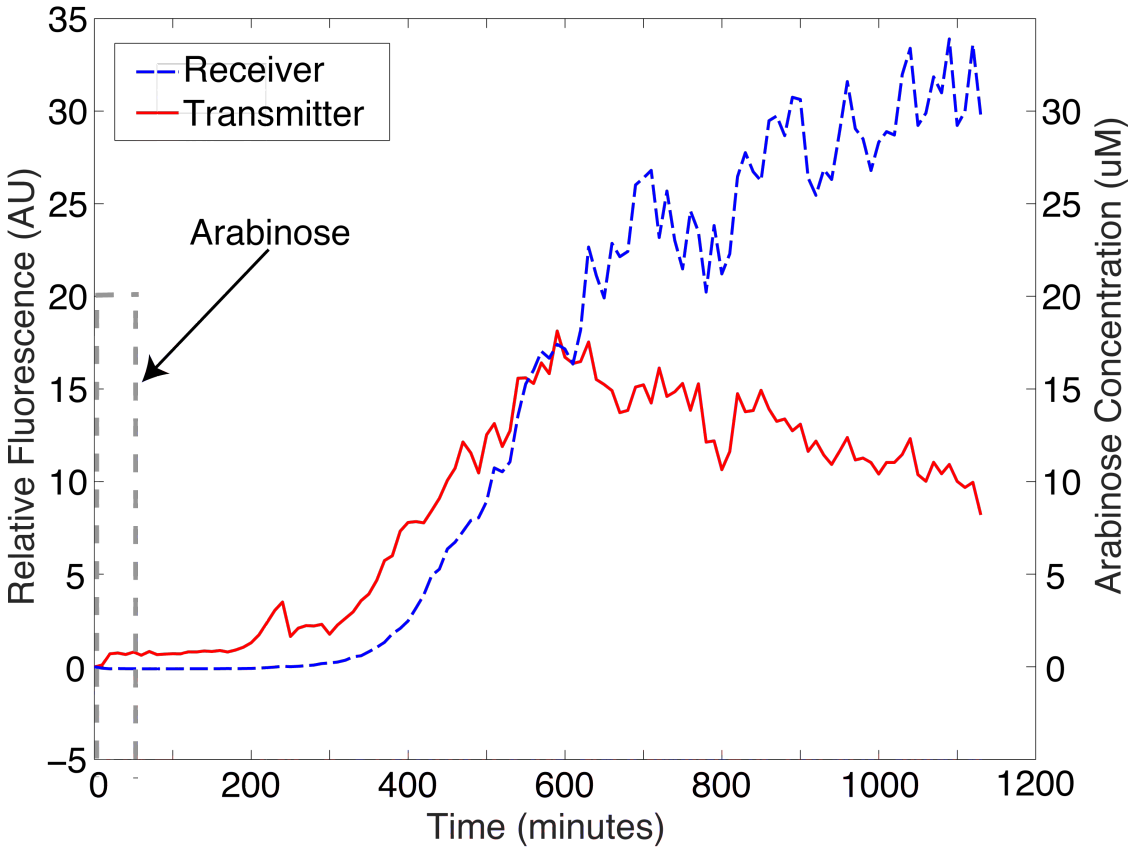

Figure 58: Bacterial communication results. A 50 min pulse of 20 μM arabinose was given to the transmitter bacteria. The Transmitters produced AHL which in turn caused them to produce GFP. This AHL diffused across the porous monolith to the receiver bacteria population who, in response, produced GFP.

7.3 Conclusion

We successfully house both the transmitter and receiver bacteria, physically separated, in the same microfluidic deceive. The two node communication network was monitored using fluorescent imaging every 10 mins. The results were consistent with calculated predictions, and are the first long term two node dynamic bacterial communication on a microfluidic device. This work will open the door for studying bacterial communication networks in a controlled environment.

Chapter VIII

CONCLUSION AND FUTURE DEVELOPMENT

8.1 Conclusion

Biosensors exploiting communication within genetically engineered bacteria are becoming increasingly important for monitoring environmental changes. Recently these sensors have miniaturized towards microfluidics due to the greater control they provide over things such as the population density and dynamic inputs. In Chapter 1 of this thesis, we briefly touched on two main applications for biosensors that would benefit from multi-strain intercellular bacterial signaling. For monitoring toxins in water or soil, these sensors can be used to reduce testing cost by pairing down a large number of samples to only a few that need additional costly testing. Another application for this type of multi-strain sensor, is studying the unique intercellular bacterial signaling that occurs in the human digestive system. If the communication balance in the microbiome was better understood through small scale studies in microfluidics, it could lead to personalized medicine that impacts the communication networks rather than mass killing bacterial strains. Although great strides have been made to study a single strain of bacteria in a microfluidic device, there is still a need to be able to study two populations of bacteria communicating with one another before these applications can be pursued. Creating a microfluidic system capable of housing two populations of bacteria while allowing dynamic stimulation and communication monitoring could enable a new field of bacteria biosensors.

As stated in Chapter 2, two bacterial strains were developed in conjunction with the Hammer lab. The transmitter bacteria, in response to arabinose, would produce AHL and

in turn produce GFP. The receiver bacteria would, in response to AHL, would produce AHL. Both these strains allowed ease of monitoring through fluorescent imaging. Next we designed, fabricated, and tested multiple microfluidic devices to house bacteria populations and monitor their biological responses. In Chapter 3, we demonstrated the ability to house a single bacteria population in a microfluidic device for several days while maintaining population size, nutrient levels, waste removal, and stimulus control. We studied the effects that AHL pulse widths had on the receiver GFP response, as well AHL concentration and chamber size. We also studied the transmitter bacteria response in the microfluidic system in the presence of arabinose.

Once we had established the fluorescent output of the receiver bacteria, we sought to create a mathematical model that would accurately predict the GFP output of the receiver bacteria given the AHL input. In Chapter 4, it was discussed the impact the microfluidic environment can have on the bacteria's ability to respond, and how traditional bulk culture models may be too simplified to adapt to these changes. We developed a generalized mass action model that accurately captured the dynamic response of the receiver bacteria. This model was tested with multiple AHL concentrations, with multiple pulse inputs, and was used as a decoding method.

Although three other groups have attempted to house two bacteria populations on the same microfluidic device, they each have their strengths and weaknesses. In Chapter 5 of this thesis, we developed a microfluidic platform capable of housing two bacteria populations to study the bacterial communication with dynamic control of inputs, long-term experimentation, and no cross contamination. This is the first of its kind to our knowledge. We integrated a porous monolith inside the microfluidic device to create a filter

between the bacteria populations. Forming monoliths inside PDMS is incredibly difficult and has never been utilized with micron scale mask to form filters between cells. In addition to monitoring the fluorescent output of the transmitter bacteria, we also developed an accurate way to extract and quantify AHL in Chapter 6. This gave us the opportunity to see the intermediary step between transmitter and receiver bacteria, that would not normally be possible with traditional bioassays.

Finally, in Chapter 7 both transmitter and receiver bacteria were housed on the same microfluidic device and the intercellular bacterial signaling was recorded. The transmitters were initial stimulated via a pulse of arabinose, which led to the production of AHL, which stimulated the transmitters to produce GFP. The AHL also diffused through the porous monolith to the receivers who in turn produced GFP. Previous two node microfluidic systems allowed for experiments that lasted for ten hours or less. In our case we were able to house a single node bacteria population for three and a half days, and a two node system capable of housing the bacteria for two days. This work can serve as a valuable tool in understanding genetically engineered bacteria and improving biosensor design capabilities, opening the door for sensors that adapt to environmental dynamics and communicate with each other.

8.2 Original Contributions

In summary, we developed a novel microfluidic device capable studying bacterial communication between two populations. The single node microfluidic device developed was unique in the ability to conduct long term experiments (lasting three or more days). The communication limitations of receiver *E. coli* bacteria were established and

contributed to three collaboration papers that developed methods for encoding and decoding information in the bacterial signals. Although modeling bacteria response has been conducted before, we did find the short comings of having an over simplified model due to the implications of the microfluidic environment on bacteria signaling. A generalized mass action model was created that accurately predicted the response of the receiver bacteria to AHL. This model was utilized as a decoding tool in collaborative studies.

This work was the first of its kind to integrate a porous monolith inside a PDMS microfluidic channel using a photo mask to pattern the formation. This is also the first to our knowledge to utilize a porous monolith to isolate bacteria populations in a PDMS microfluidic chip. We successfully created a two node microfluidic device that housed both the transmitter and receiver bacteria while monitoring their communication. Previous works have had a few of the following characteristics, but only our system captures them all: experimentation time lasting two days, the ability to give a stimulus and remove a stimulus, maintain consistent population size, waste removal and collection, ability to clearly image all populations, no cross contamination, and free diffusion of small molecules between populations.

8.3 Future Development

This work has made great strides and laid the foundation for future work studying bacterial communication. There is initial work that will be done to continue the basic science development and study of bacterial communication. This will be followed by future development focusing on using the knowledge developed for a specific health application.

8.3.1 Initial Future Development

The development of the receiver model was successful in this work at predicting the bacterial response. For future work, we look to develop a similar model with the transmitter bacteria. We will utilize generalized mass action equations to characterize the processes in the transmitter bacteria, starting with external arabinose and ending with external AHL. We have already made significant progress in characterizing the transmitter bacteria, which will lay the foundation for the model development. The AHL extraction and quantification allows us to see the production of AHL as a function of time. Refinement of the process will capture a more intricate and dynamic transmitter response. With known input and output, the model creation can begin.

In addition to the model development, further refinement of the monolith fabrication will be conducted. This will allow us to gather more bacterial communication data using the two node microfluidic device. After the collection of this data, a full communication model can be compared to experimental data. This model will contain the transmitter bacteria, diffusion delay, and the receiver bacteria. This will be a valuable tool for a wide range of applications, from encoding and decoding information, to future health studies between bacteria populations.

Although the tools we have developed will be very valuable moving forward, there are still a few areas that could be improved to increase the reliability of the studies. The fabrication of the monolith can be improved through some additional experiments to study the implication of the feature size, and the rinsing of the excess monolith. Additionally, since the oxygen is critical to the bacterial communication, adding oxygen to the media through a bubbling technique, could improve signal to noise of the bacterial signals.

Increasing the reliability of both the device fabrication and the bacterial signal will allow for more complex studies in the future.

8.3.1 Application Development

For longer term development, this project will begin focusing on an application for the knowledge we have gained thus far. Currently we are writing a grant for microfluidic modeling and measurement of bacterial communication in the human gut. We will design a microfluidic device that will allow us to take a subset of the vast GI tract microbiome to enable a fundamental understanding of the intercellular signaling between these bacterial populations. This will be done utilizing the same techniques discussed in this thesis work. We can utilize this knowledge to our advantage in order to understand the how the symbiotic relationship between these bacterial species reaches stability or is disrupted. We will engineer a novel microfluidic device that can sustain three isolated bacterial populations, while permitting communication via diffusion of chemical signal molecules. This microfluidic device will allow us to dynamically control experimental inputs and outputs which will allow us to manipulate, monitor, and measure communication.

After understanding, fundamentally, the symbiosis of the GI tract bacterial subset, we can engineer a synthetic bacterial modulator to disrupt the stability of the system. This is advantageous because it is known that some bacterial strains are incredibly harmful to human health. Being able to regulate the population size or chemical output of a particular, harmful, bacterial species by manipulating its communication network to our advantage can change the balance of the microbiome. Ultimately, this can lead to personalized treatment for individuals suffering from GI tract disorders.

APPENDIX A

In this thesis work a generalized mass action model was created to predict the response of the receiver bacteria. Assumptions and simplifications were made that deviated from what is happening physically in the cell. Specifically, the dimerization of AHL and LuxR could have an impact on the model. Figure 59 represents a proposed system to characterize the receiver bacteria. This differs from the previous model in that an AHL and a LuxR first combine to form complex C_1. This C_1 binds to another C_1 to form a dimer C_2. The C_2 complex is then bound to the DNA and forms the C_3 complex. Equations 10 through 16 then represent the new updated generalized mass action equations associated with this system. Moving forward, this new series of equations would be used to model the receiver bacteria.

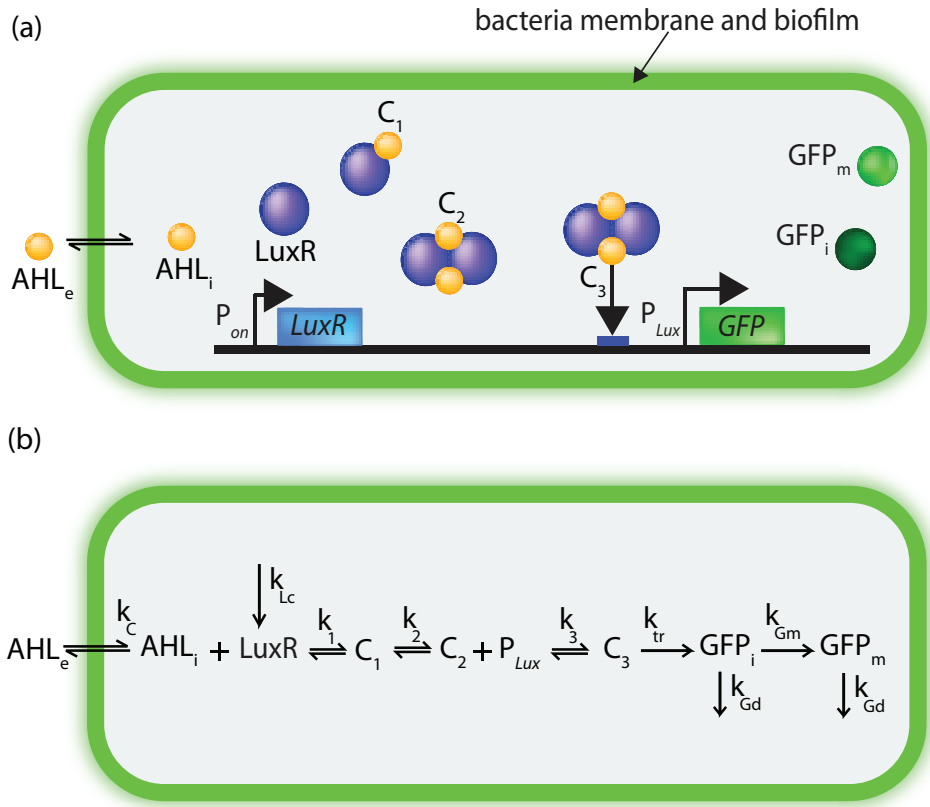

Figure 59: Future receiver model that can be implemented. In this model the dimer formation is more biologically correct than model used in this work.

$$\frac{dAHL_i}{dt} = k_c(AHL_e - AHL_i) - K_1 AHL_i LuxR + K_1 C_1, \quad (10)$$

$$\frac{dC_1}{dt} = K_1 AHL_i LuxR - K_1 C_1 + K_2 C_2 P_{Lux} - K_2 C_1, \quad (11)$$

$$\frac{dC_2}{dt} = K_2 C_1 - K_2 C_2 P_{Lux} + K_3 C_3 - K_3 C_2 P_{Lux}, \quad (12)$$

$$\frac{dC_3}{dt} = K_3 C_2 P_{Lux} - K_3 C_3 - k_{tr} C_3, \quad (13)$$

$$LuxR = LuxR_t - C_1 - 2C_2 - 2C_3 \quad (14)$$

$$\frac{dGFP_i}{dt} = k_{tr} C_2 - k_{Gm} GFP_i - k_{Gd} GFP_i, \text{ and} \quad (15)$$

$$\frac{dGFP_m}{dt} = k_{Gm} G_i - k_{Gd} GFP_m. \quad (16)$$

PUBLICATIONS

1. Austin, C. M., Stoy, W., Su, P., Harber, M. C., Bardill, J. P., Hammer, B. K., & Forest, C. R. (2014). Modeling and validation of autoinducer-mediated bacterial gene expression in microfluidic environments. *Biomicrofluidics*, *8*(3), 034116.

2. Krishnaswamy, B., **Austin, C. M**., Bardill, J. P., Russakow, D., Holst, G. L., Hammer, B. K., ... & Sivakumar, R. (2013). Time-elapse communication: Bacterial communication on a microfluidic chip. *Communications, IEEE Transactions on*, *61*(12), 5139-5151.

3. Bicen, A. Ozan, **Caitlin M. Austin**, Ian F. Akyildiz, and Craig R. Forest. "Efficient Sampling of Bacterial Signal Transduction for Detection of Pulse-Amplitude Modulated Molecular Signals." *IEEE transactions on biomedical circuits and systems* 9, no. 4 (2015): 505-517.

4. Krishnaswamy, Bhuvana, **Austin Caitlin**, Jian Yubing, Patel Sagar, Perdomo Jorge, Forest Craig, , Hammer Brian and Sivakumar Raghupathy. "*ADMA*: Amplitude-Division Multiple Access for Bacterial Communication Networks" under review in IEEE Transactions on Communications

REFRENCES

1. Charrier, T., et al., *A multi-channel bioluminescent bacterial biosensor for the on-line detection of metals and toxicity. Part II: technical development and proof of concept of the biosensor.* Anal Bioanal Chem, 2011. **400**(4): p. 1061-70.
2. Stocker, J., et al., *Development of a set of simple bacterial biosensors for quantitative and rapid measurements of arsenite and arsenate in potable water.* Environ Sci Technol, 2003. **37**(20): p. 4743-50.
3. Siddiqui, M.F., et al., *Targeting N-acyl-homoserine-lactones to mitigate membrane biofouling based on quorum sensing using a biofouling reducer.* Journal of Biotechnology, 2012. **161**(3): p. 190-197.
4. van der Meer, J.R. and S. Belkin, *Where microbiology meets microengineering: design and applications of reporter bacteria.* Nature Reviews Microbiology, 2010. **8**(7): p. 511-522.
5. Miller, M.B. and B.L. Bassler, *Quorum sensing in bacteria.* Annual Review of Microbiology, 2001. **55**: p. 165-199.
6. Nealson, K.H. and J.W. Hastings, *Bacterial bioluminescence: its control and ecological significance.* Microbiol Rev, 1979. **43**(4): p. 496-518.
7. Engebrecht, J., K. Nealson, and M. Silverman, *Bacterial Bioluminescence - Isolation and Genetic-Analysis of Functions from Vibrio Fischeri.* Cell, 1983. **32**(3): p. 773-781.
8. Lei, Y., W. Chen, and A. Mulchandani, *Microbial biosensors.* Analytica Chimica Acta, 2006. **568**(1-2): p. 200-210.
9. Whitaker, R.D., et al., *Single cell time-resolved quorum responses reveal dependence on cell density and configuration.* J Biol Chem, 2011. **286**(24): p. 21623-32.
10. Meyer, A., et al., *Dynamics of AHL mediated quorum sensing under flow and non-flow conditions.* Phys Biol, 2012. **9**(2): p. 026007.
11. Groisman, A., et al., *A microfluidic chemostat for experiments with bacterial and yeast cells.* Nat Methods, 2005. **2**(9): p. 685-9.
12. Tothill, I.E., *Biosensors developments and potential applications in the agricultural diagnosis sector.* Computers and Electronics in Agriculture, 2001. **30**(1-3): p. 205-218.
13. Rodriguez-Mozaz, S., et al., *Biosensors for environmental applications: Future development trends.* Pure and Applied Chemistry, 2004. **76**(4): p. 723-752.
14. Tecon, R. and J.R. van der Meer, *Bacterial biosensors for measuring availability of environmental pollutants.* Sensors, 2008. **8**(7): p. 4062-4080.
15. Kotula, J.W., et al., *Programmable bacteria detect and record an environmental signal in the mammalian gut.* Proc Natl Acad Sci U S A, 2014. **111**(13): p. 4838-43.
16. Sun, J. and E.B. Chang, *Exploring gut microbes in human health and disease: Pushing the envelope.* Genes Dis, 2014. **1**(2): p. 132-139.
17. West, C.E., et al., *The gut microbiota and inflammatory noncommunicable diseases: Associations and potentials for gut microbiota therapies.* Journal of Allergy and Clinical Immunology, 2015. **135**(1): p. 3-14.
18. Guinane, C.M. and P.D. Cotter, *Role of the gut microbiota in health and chronic gastrointestinal disease: understanding a hidden metabolic organ.* Therap Adv Gastroenterol, 2013. **6**(4): p. 295-308.
19. Park, A., et al., *Effect of shear stress on the formation of bacterial biofilm in a microfluidic channel.* BioChip Journal, 2011. **5**(3): p. 236-241.

20. Vieira, H.L., P. Freire, and C.M. Arraiano, *Effect of Escherichia coli morphogene bolA on biofilms.* Appl Environ Microbiol, 2004. **70**(9): p. 5682-4.
21. Stewart, P.S., *Diffusion in biofilms.* Journal of Bacteriology, 2003. **185**(5): p. 1485-1491.
22. Lawrence, J.R., G.M. Wolfaardt, and D.R. Korber, *Determination of Diffusion-Coefficients in Biofilms by Confocal Laser Microscopy.* Applied and Environmental Microbiology, 1994. **60**(4): p. 1166-1173.
23. Bryers, J.D. and F. Drummond, *Local macromolecule diffusion coefficients in structurally non-uniform bacterial biofilms using fluorescence recovery after photobleaching (FRAP).* Biotechnology and Bioengineering, 1998. **60**(4): p. 462-473.
24. Charati, S.G. and S.A. Stern, *Diffusion of gases in silicone polymers: Molecular dynamics simulations.* Macromolecules, 1998. **31**(16): p. 5529-5535.
25. Losen, M., et al., *Effect of oxygen limitation and medium composition on Escherichia coli fermentation in shake-flask cultures.* Biotechnology Progress, 2004. **20**(4): p. 1062-1068.
26. Hill, A.V., *The mode of action of nicotine and curari, determined by the form of the contraction curve and the method of temperature coefficients.* J Physiol, 1909. **39**(5): p. 361-73.
27. Michaelis, L. and M.M. Menten, *The kinetics of invertin action. 1913.* FEBS Lett, 2013. **587**(17): p. 2712-20.
28. Horn, F. and R. Jackson, *General Mass Action Kinetics.* Archive for Rational Mechanics and Analysis, 1972. **47**(2): p. 81-&.
29. Leveau, J.H. and S.E. Lindow, *Predictive and interpretive simulation of green fluorescent protein expression in reporter bacteria.* J Bacteriol, 2001. **183**(23): p. 6752-62.
30. Zucca, S., et al., *Characterization of an inducible promoter in different DNA copy number conditions.* BMC Bioinformatics, 2012. **13 Suppl 4**: p. S11.
31. Garde, C., et al., *Quorum Sensing Regulation in Aeromonas hydrophila.* Journal of Molecular Biology, 2010. **396**(4): p. 849-857.
32. Weber, M. and J. Buceta, *Dynamics of the quorum sensing switch: stochastic and non-stationary effects.* BMC Syst Biol, 2013. **7**: p. 6.
33. Basu, S., et al., *A synthetic multicellular system for programmed pattern formation.* Nature, 2005. **434**(7037): p. 1130-1134.
34. Park, S., et al., *Microfabricated ratchet structure integrated concentrator arrays for synthetic bacterial cell-to-cell communication assays.* Lab Chip, 2012. **12**(20): p. 3914-22.
35. Nagy, K., et al., *Interaction of Bacterial Populations in Coupled Microchambers.* Chemical and Biochemical Engineering Quarterly, 2014. **28**(2): p. 225-231.
36. Luo, X., et al., *Biofabrication of stratified biofilm mimics for observation and control of bacterial signaling.* Biomaterials, 2012. **33**(20): p. 5136-43.
37. Luo, X., et al., *Distal modulation of bacterial cell-cell signalling in a synthetic ecosystem using partitioned microfluidics.* Lab Chip, 2015. **15(8)**: p. 1842-1851.
38. Engebrecht, J., K. Nealson, and M. Silverman, *Bacterial bioluminescence: isolation and genetic analysis of functions from Vibrio fischeri.* Cell, 1983. **32**(3): p. 773-81.
39. Sambrook, J., D.W. Russell, and J. Sambrook, *The condensed protocols from Molecular cloning : a laboratory manual*. 2006, Cold Spring Harbor, N.Y.: Cold Spring Harbor Laboratory Press. v, 800 p.
40. Blattner, F.R., et al., *The complete genome sequence of Escherichia coli K-12.* Science, 1997. **277**(5331): p. 1453-62.
41. Andersen, J.B., et al., *New unstable variants of green fluorescent protein for studies of transient gene expression in bacteria.* Appl Environ Microbiol, 1998. **64**(6): p. 2240-6.

42. Danino, T., et al., *A synchronized quorum of genetic clocks.* Nature, 2010. **463**(7279): p. 326-30.
43. Schleif, R., *AraC protein, regulation of the l-arabinose operon in Escherichia coli, and the light switch mechanism of AraC action.* FEMS Microbiol Rev, 2010. **34**(5): p. 779-96.
44. McDonald, J.C., et al., *Fabrication of microfluidic systems in poly(dimethylsiloxane).* Electrophoresis, 2000. **21**(1): p. 27-40.
45. Krishnaswamy, B., et al., *Time-Elapse Communication: Bacterial Communication on a Microfluidic Chip.* Ieee Transactions on Communications, 2013. **61**(12): p. 5139-5151.
46. Dunlap, P.V., *Quorum regulation of luminescence in Vibrio fischeri.* J Mol Microbiol Biotechnol, 1999. **1**(1): p. 5-12.
47. Nilsson, P., et al., *Kinetics of the AHL regulatory system in a model biofilm system: How many bacteria constitute a "quorum"?* Journal of Molecular Biology, 2001. **309**(3): p. 631-640.
48. Byrd, R.H., M.E. Hribar, and J. Nocedal, *An interior point algorithm for large-scale nonlinear programming.* Siam Journal on Optimization, 1999. **9**(4): p. 877-900.
49. Akyildiz, I.F., et al., *Monaco: Fundamentals of Molecular Nano-Communication Networks.* Ieee Wireless Communications, 2012. **19**(5): p. 12-18.
50. Pierobon, M. and I.F. Akyildiz, *Capacity of a Diffusion-Based Molecular Communication System With Channel Memory and Molecular Noise.* Ieee Transactions on Information Theory, 2013. **59**(2): p. 942-954.
51. Tsien, R.Y., *The green fluorescent protein.* Annual Review of Biochemistry, 1998. **67**: p. 509-544.
52. Craggs, T.D., *Green fluorescent protein: structure, folding and chromophore maturation.* Chemical Society Reviews, 2009. **38**(10): p. 2865-2875.
53. Iizuka, R., M. Yamagishi-Shirasaki, and T. Funatsu, *Kinetic study of de novo chromophore maturation of fluorescent proteins.* Analytical Biochemistry, 2011. **414**(2): p. 173-178.
54. Iizuka, R., M. Yamagishi-Shirasaki, and T. Funatsu, *Kinetic Study of De Novo Chromophore Maturation of Fluorescent Proteins.* Biophysical Journal, 2011. **100**(3): p. 486-486.
55. Krishnaswamy, B., Austin Caitlin, Jian Yubing, Patel Sagar, Perdomo Jorge, Forest Craig, , Hammer Brian and Sivakumar Raghupathy, *ADMA: Amplitude-Division Multiple Access for Bacterial Communication Networks*. 2016: IEEE Transactions on Communications.
56. Ji, H.M., et al., *Silicon-based microfilters for whole blood cell separation.* Biomed Microdevices, 2008. **10**(2): p. 251-7.
57. Gossett, D.R., et al., *Label-free cell separation and sorting in microfluidic systems.* Analytical and Bioanalytical Chemistry, 2010. **397**(8): p. 3249-3267.
58. Schwarz-Schilling, M., et al., *Chemical communication between bacteria and cell-free gene expression systems within linear chains of emulsion droplets.* Integrative Biology, 2016. **8**(4): p. 564-570.
59. Araya-Farias, M., et al., *A new strategy for simultaneous synthesis and efficient anchorage of polymer monoliths in native PDMS microchips.* Polymer, 2015. **66**: p. 249-258.
60. Namera, A., et al., *Monolith as a new sample preparation material: Recent devices and applications.* Journal of Separation Science, 2011. **34**(8): p. 901-924.
61. Deng, J.P., et al., *Developments and new applications of UV-induced surface graft polymerizations.* Progress in Polymer Science, 2009. **34**(2): p. 156-193.
62. Vazquez, M. and B. Paull, *Review on recent and advanced applications of monoliths and related porous polymer gels in micro-fluidic devices.* Analytica Chimica Acta, 2010. **668**(2): p. 100-113.

63. Svec, F., *Porous polymer monoliths: Amazingly wide variety of techniques enabling their preparation.* Journal of Chromatography A, 2010. **1217**(6): p. 902-924.
64. Bedair, M.F. and R.D. Oleschuk, *Fabrication of porous polymer monoliths in polymeric microfluidic chips as an electrospray emitter for direct coupling to mass spectrometry.* Analytical Chemistry, 2006. **78**(4): p. 1130-1138.
65. Hu, S.W., et al., *Surface-directed, graft polymerization within microfluidic channels.* Analytical Chemistry, 2004. **76**(7): p. 1865-1870.
66. Burke, J.M. and E. Smela, *A novel surface modification technique for forming porous polymer monoliths in poly(dimethylsiloxane).* Biomicrofluidics, 2012. **6**(1): p. 016506.
67. Rohr, T., et al., *Surface functionalization of thermoplastic polymers for the fabrication of microfluidic devices by photoinitiated grafting.* Advanced Functional Materials, 2003. **13**(4): p. 264-270.
68. Kim, J.-Y., S.-I. Chang, and D. O'Hare, *Integration of monolithic porous polymer with droplet-based microfluidics on a chip for nano/picoliter volume sample analysis.* Nano Convergence, 2014. **1**(1): p. 1-5.
69. Kannappan, S., et al., *Extraction and detection of quorum sensing N-acyl homoserine lactones from shrimp pathogen Vibrio harveyi and antagonistic effect of terrestrial plants against its growth.* Extraction, 2013. **7(26)**: p. 3275-3284.
70. Kim, Y.W., et al., *MALDI-MS-Based Quantitative Analysis for Ketone Containing Homoserine Lactones in Pseudomonas aeruginosa.* Analytical Chemistry, 2015. **87**(2): p. 858-863.